TID-2508 (Del.)

NUCLEAR SCIENCE AND TECHNOLOGY

Volume 1A, Issue 3

December 1955

Photostat Price $18.30

Microfilm Price $6.00

Available from the
Office of Technical Services
Department of Commerce
Washington 25, D. C.

696-001

NUCLEAR SCIENCE AND TECHNOLOGY

A Journal Devoted to the Science and Technology of Nuclear Reactors and to Related Subjects

379-380

Contents

Special Announcement

With the numerous changes brought about by the new declassification guide, the question of need for a classified journal within the Atomic Energy Commission naturally arises. This question will be examined carefully during the coming months, and it is sufficient to say at this time that the journal of *Nuclear Science and Technology* will continue to be published at least through 1956.

In the interest of expediting publication and of minimizing certain classification, compartmentalization, and similar problems, the journal will be published only as a "Secret" journal on a bimonthly schedule during this coming year, with each item being given its appropriate classification. Those papers which can be extracted for distribution to "L" cleared persons will be reproduced separately and almost simultaneously with each journal issue. Such published extracts from the journal will be available, as are the present "Gray Area" documents.

The question of continuance of a classified journal merits your consideration and attention since the Editors depend upon the readers of the journal to guide its policies. If you have interest in seeing the journal continue beyond 1956, kindly address your comments before Apr. 1, 1956, to the Editors at Oak Ridge National Laboratory, P. O. Box P, Oak Ridge, Tennessee, Attention: NST.

J. A. Lane, Editor

W. H Sullivan, Managing Editor

NEUTRON-INDUCED FISSION CROSS SECTION OF U^{238} FROM 0.5 TO 4.0 MEV NEUTRON ENERGY

R. W. LAMPHERE

Oak Ridge National Laboratory

June 17, 1955

ABSTRACT

The fission cross section of natural uranium has been measured from 500 kev to 4.0 mev neutron energy using protons from the Oak Ridge 5-Mv Van de Graaff to bombard a tritium-gas target. Neutron energy spread varied from 60 to 100 kev for most points. Data were corrected for the U^{235} present in natural uranium in order to get the cross section of U^{238}. With the energy spread present in the neutron beam, no minimums were found, but there are a few features worthy of note.

The U^{238} cross-section curve has a much longer low-energy "tail" than either U^{234} or U^{236} The cross section is of the order of 0.4 millibarn at 500 kev. It gradually rises to 17 millibarns at 950 kev, remains constant to 1.05 mev, rises to 40 millibarns at 1.16 mev, remains constant to 1.23 mev, and then rises in a normal manner to 0.54 barn at 2.0 mev and to 0.58 barn at 3.0 mev. At about 3 mev the cross section begins to increase more rapidly with energy, reaching 0.65 barn at 4.0 mev.

Results are believed to be good to 6 per cent.

1. INTRODUCTION

The fission cross sections of natural uranium and U^{238} have been measured by others,[1–4] but it seemed advisable to have an independent check by another laboratory. Consequently, several foils of natural uranium and of U^{235} were made, and a simple comparison type experiment was performed by which the cross section of natural uranium was found as a ratio to that of U^{235}. The U^{235} cross section has been carefully determined[5] by comparison with the (n,p) scattering cross section over the energy range 400 kev to 1.6 mev and has been extended to higher energies by means of the long-counter method.[3] These results were used to get the U^{238} cross section from the comparison experiment. [The work cited in reference 3, summarizing the Los Alamos Scientific Laboratory (LASL) work on fast fission cross sections, shows the points taken from references 3 and 5 on U^{235}. These points are plotted in Fig. 8 of Report LA-1714. From looking at this figure, one would be inclined to take $\sigma_f^{U^{235}}$ to be about 1.30 barns in the region around 2 mev. Figure 3 of this article is based on the points shown in references 3 and 5 but is consistent with Report LA-1714, within the stated limits of accuracy.]

Classification Note: The classification of this article does not apply to all illustrations.

2. PROCEDURE

The experimental procedure is essentially the same as that followed in finding the U^{234} and U^{236} cross sections.[6,7] Foils were prepared which contained about 4.0 mg of natural uranium plated over a 1-in.-diameter circular area on 0.002-in.-thick nickel backing. These were carefully compared with very thin foils containing only 0.200 mg of natural uranium on a 1-in.-diameter circular area to find an equivalent weight, W′, which is always less than 4.0 mg by an amount proportional to the counting loss due to absorption and bias setting, as described in reference 7. Similar foils were made from pure U^{235}. The heavy foils of natural uranium and of U^{235} were placed back to back in the comparison chambers.

By use of the 8-foil chamber shown in Fig. 5 (this one was not used in any of the previous work cited in the references), the counting rate was increased by a factor of about 2.6 over that obtained with the 2-foil chamber shown in Fig. 4. The chamber was mounted in the neutron beam from the Van de Graaff so that the first pair of foils subtended a half angle of 15 deg as seen from the gas target. The foils were mounted in pairs, always with a natural-uranium foil back to back with a U^{235} foil. All eight foils used in this chamber had previously been tested to find the radial distribution of uranium on them. This was done by successively masking concentric areas with thin aluminum foil and alpha counting the unmasked portion. The specific activities from four approximately equal concentric areas were measured for each of the eight foils. A variation of ±10 per cent was found in some cases. When they were placed in the chamber, they were matched so that, as far as possible, foils with closely similar distributions were placed back to back. This reduced the error that can arise when foils with different radial deposition densities are compared in the neutron beam from a Van de Graaff. The error arises from the fact that the neutron intensity falls off with the angle measured from the 0-deg (beam) axis.[8] The correction for this effect was calculated to be −0.1 per cent for neutrons of 2.5 mev. In the case of the 2-foil chamber, foils were selected which had essentially the same radial distribution so that the correction was negligible.

The ratios of the W′ values for the four pairs of foils used in the big chamber differed slightly. It is necessary, therefore, to calculate the ratios of the neutron fluxes at the four positions in the chamber in order to determine a properly weighted over-all figure for the mass ratio of the natural uranium to U^{235}. This calculation involves simple integrations to get $\overline{r^{-2}}$ for each position since the neutron source is a line rather than a point source. Because these calculations are simple, they will not be discussed in detail. Since the front pair of foils subtends a half angle of 15 deg, it is clear that the average angle for all the foils will be less. It turns out to be 12.9 deg, properly weighted for flux density and W′ variations over the four positions.

Owing to the relatively fast count rate obtainable with the 8-foil chamber, points were taken very close together over the entire curve. The inelastic-scattering correction turned out to be greater than that for the 2-foil chamber. This is discussed in Sec. 5.

As is shown in Table 1, the low-energy portion of the curve was investigated with a spiral counter also. This counter contained 117 mg of pure U^{238} (except for 6.1 ppm of U^{235}). It was mounted at 10 deg to the beam axis and at a distance so that it subtended a half angle of 5.7 deg about the 10-deg line. A long counter of conventional design was placed at 10 deg on the opposite side of the beam axis and at a distance so that it subtended a like half angle as seen from the gas cell. A normalization point was taken to 0.84 per cent statistics at a neutron energy of 2.03 mev, and the U^{238} cross section was taken to be 0.540 barn from the work done with the 2- and 8-foil counters. The long-counter response was assumed to be independent of neutron energy down to 420 kev, and it was used as a flux monitor. Thus, for any neutron energy between 2.03 mev and 420 kev, the ratio of spiral- to long-counter counts served to determine the U^{238} cross section by simply dividing this ratio by the ratio at the normalization point and then multiplying by 0.540 barn.

Since a spiral counter has no observable plateau, it is important to monitor the gain of the amplifier in the counting channel very carefully. A check for gain changes was made by returning to the normalization point after all data had been taken. Six hours was required to

Table 1 — Data Taken To Determine the Fission Cross Section of U^{238} Vs. Neutron Energy

E_n, mev	σ_f, barns	Statistics, %	Counter*	E_n, mev	σ_f, barns	Statistics, %	Counter*
0.42	0.0001	72	S	1.18	0.041	4.4	S
0.49	0.0003	51	S	1.19	0.041	3.2	8
0.57	0.0007	32	S	1.20	0.041	4.4	S
0.61	0.0016	22	S	1.21	0.041	3.2	8
0.64	0.0012	25	S	1.22	0.038	4.5	S
0.68	0.0012	25	S	1.23	0.041	3.2	8
0.70	0.0012	25	S	1.24	0.044	4.2	S
0.70	0.0013	18	8	1.25	0.045	3.1	8
0.72	0.0019	20	S	1.26	0.048	4.0	S
0.74	0.0022	19	S	1.27	0.042	3.1	8
0.74	0.0021	13	8	1.28	0.050	4.0	S
0.76	0.0023	18	S	1.29	0.056	2.8	8
0.78	0.0034	15	S	1.30	0.063	3.6	S
0.78	0.0021	14	8	1.31	0.064	2.6	8
0.79	0.0030	16	S	1.32	0.078	2.3	S
0.81	0.0049	12	S	1.33	0.079	2.4	8
0.81	0.0039	10	8	1.34	0.084	3.1	S
0.83	0.0047	13	S	1.35	0.090	2.2	8
0.85	0.0072	10	S	1.36	0.105	2.8	S
0.85	0.0059	8	8	1.37	0.109	2.0	8
0.87	0.0073	10	S	1.38	0.134	2.5	S
0.89	0.0096	9	S	1.40	0.139	1.8	8
0.89	0.0082	7	8	1.40	0.157	2.3	S
0.91	0.012	8	S	1.41	0.171	1.7	8
0.93	0.014	7	S	1.42	0.180	2.2	S
0.93	0.013	6	8	1.44	0.211	1.5	8
0.95	0.017	7	S	1.46	0.240	1.4	8
0.95	0.017	5	8	1.48	0.290	1.3	8
0.97	0.016	7	S	1.49	0.251	0.34	2
0.97	0.017	5	8	1.50	0.315	1.0	8
0.98	0.016	7	S	1.52	0.346	0.86	8
0.99	0.016	5	8	1.54	0.345	1.4	8
1.00	0.017	7	S	1.57	0.360	1.0	8
1.01	0.016	5	8	1.58	0.380	1.4	8
1.02	0.017	7	S	1.58	0.354	0.9	2
1.03	0.017	5	8	1.61	0.390	1.4	8
1.04	0.017	7	S	1.63	0.406	1.4	8
1.05	0.019	4.7	8	1.65	0.412	1.4	8
1.06	0.018	7	S	1.67	0.431	1.4	8
1.07	0.021	4.5	8	1.69	0.429	1.4	8
1.08	0.022	6	S	1.71	0.433	1.4	8
1.09	0.022	4.4	8	1.74	0.452	1.5	8
1.10	0.028	5	S	1.76	0.467	1.5	8
1.11	0.026	4.0	8	1.78	0.473	1.5	8
1.12	0.028	5	S	1.80	0.482	1.5	8
1.13	0.027	4.0	8	1.83	0.492	1.5	8
1.14	0.035	4.7	S	1.85	0.513	1.5	8
1.15	0.034	3.5	8	1.87	0.519	1.5	8
1.16	0.041	4.4	S	1.89	0.493	1.5	8
1.17	0.036	3.4	8	1.91	0.529	1.5	8

*S, spiral counter; 2, 2-foil counter; 8, 8-foil counter.

Table 1 — (Continued)

E_n, mev	σ_f, barns	Statistics, %	Counter*	E_n, mev	σ_f, barns	Statistics, %	Counter*
1.93	0.533	1.5	8	2.85	0.533	1.5	8
1.96	0.539	1.5	8	2.91	0.562	1.5	8
1.98	0.518	1.5	8	2.96	0.570	1.5	8
2.01	0.538	1.5	8	2.99	0.578	0.48	8
2.02	0.536	0.9	2	2.99	0.580	0.34	2
2.03	0.528	1.1	8	3.00	0.573	0.7	2
2.05	0.542	0.34	2	3.01	0.575	1.5	8
2.05	0.539	1.5	8	3.06	0.573	1.5	8
2.06	0.544	0.48	8	3.11	0.581	1.5	8
2.07	0.548	1.1	8	3.16	0.592	1.1	8
2.10	0.548	1.5	8	3.22	0.602	1.1	8
2.12	0.560	0.6	8	3.27	0.602	1.5	8
2.14	0.557	1.5	8	3.28	0.592	0.48	8
2.16	0.549	1.5	8	3.29	0.594	0.34	2
2.19	0.557	1.5	8	3.31	0.600	0.9	2
2.21	0.552	1.5	8	3.32	0.598	1.5	8
2.24	0.569	1.5	8	3.38	0.600	1.5	8
2.26	0.552	1.5	8	3.43	0.617	1.5	8
2.30	0.555	0.8	8	3.49	0.610	1.5	8
2.30	0.571	0.7	2	3.53	0.613	0.48	8
2.34	0.568	0.44	8	3.54	0.615	0.34	2
2.34	0.568	0.34	2	3.54	0.617	1.5	8
2.39	0.557	1.1	8	3.59	0.616	0.7	2
2.44	0.553	1.1	8	3.60	0.622	0.9	8
2.48	0.574	1.5	8	3.65	0.623	1.5	8
2.50	0.570	1.1	8	3.71	0.630	1.5	8
2.55	0.574	1.1	8	3.77	0.651	1.5	8
2.60	0.564	1.1	8	3.81	0.634	1.1	8
2.65	0.566	1.1	8	3.88	0.657	1.5	8
2.69	0.570	0.7	2	3.95	0.660	1.5	8
2.70	0.577	1.1	8	4.03	0.653	1.5	8
2.71	0.576	0.34	2	4.10	0.670	1.5	8
2.71	0.578	0.34	8	4.18	0.670	1.5	8
2.75	0.579	1.1	8	4.25	0.665	1.5	8
2.80	0.570	1.1	8				

* S, spiral counter; 2, 2-foil counter; 8, 8-foil counter.

take all the data, and the spiral-counter counts at the normalization point for a fixed long-counter count were 113.9 and 111.3 scales of 64 at start and finish, respectively. The average of these figures was used in the calculations.

The discriminator setting that would just eliminate noise (no counts in a 5-min interval) was found, and all data were taken with a setting 1.5 times this. Occasional checks for noise were made during the course of the work, but none was observed.

As a check against possible loss of uranium from the foils, they were alpha counted immediately upon being received and again after completion of all experimental work. A comparison of these counts showed that no uranium had been lost during the course of the work.

3. RESULTS

Figure 1 shows the U^{238} cross section up to 4 mev, and Fig. 2 shows the low-energy tail. For comparison the cross sections of U^{234} and

U^{236}, as reported in reference 6, are also shown in Fig. 1. Below 500 kev the U^{238} cross section becomes too low to be measured by the methods used in this work.

Table 1 lists all the U^{238} data, and Fig. 3 shows the U^{235} cross section that was used in the computations. Three types of counters were used: a spiral counter of conventional design[9] made from depleted uranium (U^{238}); a 2-foil counter (shown in Fig. 4); and an 8-foil counter (shown in Fig. 5). Statistics vary quite widely from point to point, and, for this reason and because of the close spacing of the points, they are not indicated on the curves of Fig. 1. However, points with much better than average statistics are circled. Neutron energy spread varied from 60 to 100 kev for most points taken with the 2- and 8-foil counters, and this variation is indicated by the little triangles along the base of the figure. The spread was somewhat less for points taken with the spiral counter, varying between 30 and 40 kev.

Agreement of the data taken with the various counters is generally good, except where the cross section is changing sharply with energy. Lack of agreement here is felt to be due to uncertainty in average neutron energy, arising from uncertainty in the composition of the gas, tritium and sometimes a little air, in the gas target. A little trouble was experienced with air leaking into the gas cell. Since at the same time there was a slow loss of tritium through the nickel entrance foil, it was not possible to determine the composition of the gas from the pressure alone. Because air has roughly five times the stopping power of tritium, the effect of a 30 per cent admixture of air into the 3-cm-long gas cell with 0.5-atmosphere total pressure of gas would result in a decrease of 25 kev in average neutron energy at 1.5 mev, and also, of course, in a greater energy spread. For example, this would account completely for the discrepancy between the curve and the point at 1.49 mev, and, consequently, this point, although shown, was not considered in drawing the curve. This effect was considered to be much smaller for most points, about ±10 kev, and, in view of the very tight schedule of other work for the Van de Graaff, it was decided not to do this part of the work over.

Table 2 shows a comparison of some of the measurements made over the past five years. The results given in Report AECU-2040 are for natural uranium, and they have been corrected for the U^{235} contribution. Report ORNL-1458 lists the ratio of U^{238} to U^{235} cross sections, and the points listed for this reference in Table 2 have been converted using the U^{235} cross section shown in Fig. 3.

Table 2 — Comparison of U^{238} Cross-section Measurements

Report	σ_f, barns			
	2.0 mev	2.5 mev	3.0 mev	4.0 mev
AECU-2040[1]	0.41	0.47	0.51	0.58
LA-1495[3]	0.51	0.51	0.51	0.51
ORNL-1458[2]	0.49	0.53	0.54	0.58
LA-1714[4]	0.54	0.55	0.55	0.56
This work	0.54	0.57	0.58	0.65

Table 3 — Estimate of Errors

Source	Standard deviation, %
Foil weight	0.7
Inelastic scattering	0.5
Statistics	0.3
Room scattering	0.2
Foil nonuniformity	0.1
Foil separation	0.1
Beam momentum	0.1
Gain changes	0.1
Systematic error	1.0
Ratio error	1.4
$\sigma_f^{U^{235}}$	5.0*
$\sigma_f^{U^{238}}$	5.2

* Estimated by B. C. Diven and R. L. Henkel of LASL to be 6 per cent from 400 to 700 kev, 4 per cent from 700 kev to 2 mev, and 5 per cent from 2 to 4 mev.

4. ESTIMATE OF ERRORS (Table 3)

4.1 Fission Cross Section of Monitor Foil

The fission cross section of U^{235} used to get the results given here is that shown in Fig. 3, which is a copy of a curve submitted by R. L. Henkel of LASL, based on work summarized in reference 4. The standard error is estimated to be 3.5 per cent.

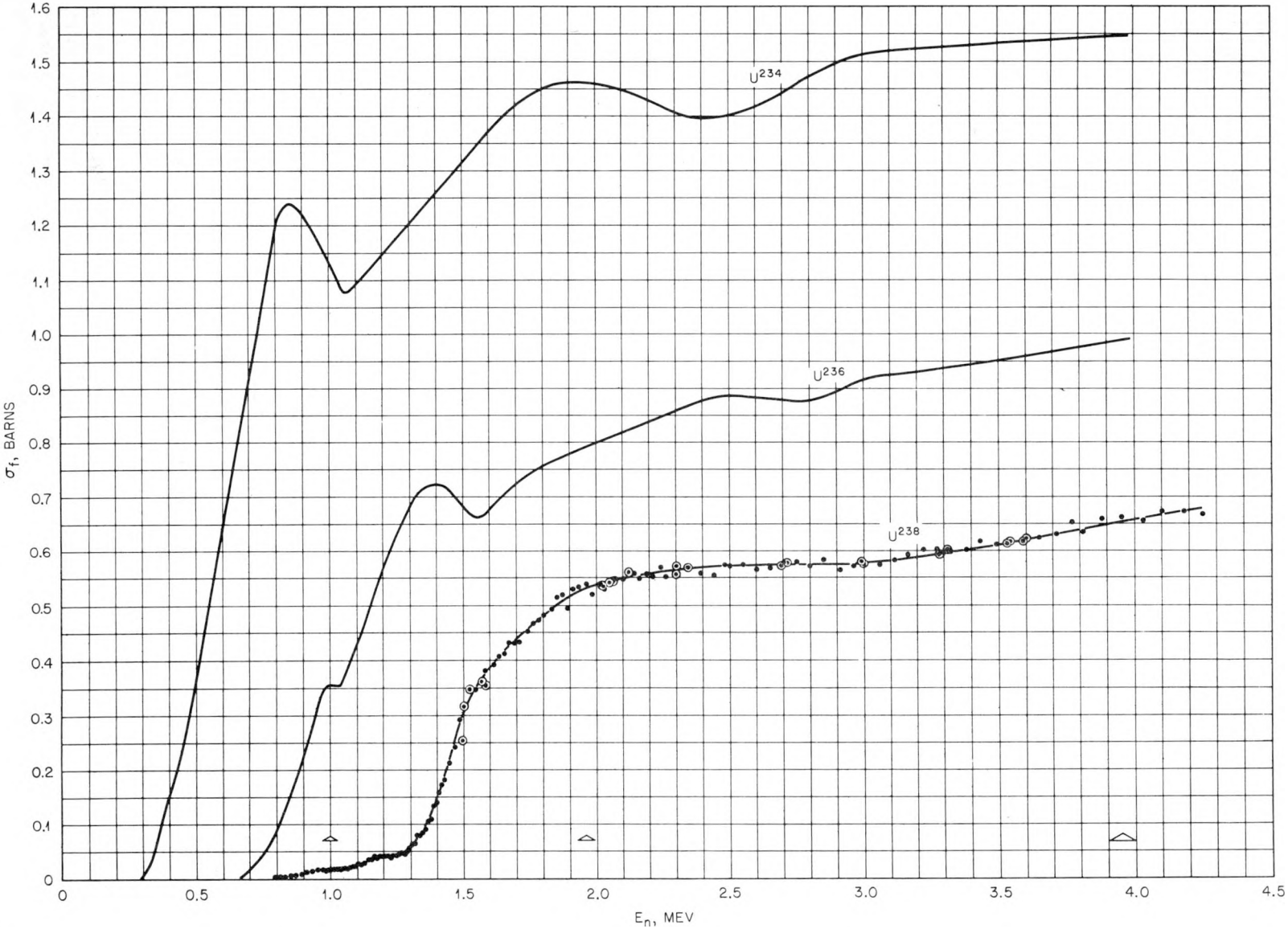

Fig. 1—Fission cross sections of U^{238}, U^{236}, and U^{234}. ⊙, points with better than average statistics. Δ, variation in neutron energy spread. (CONFIDENTIAL)

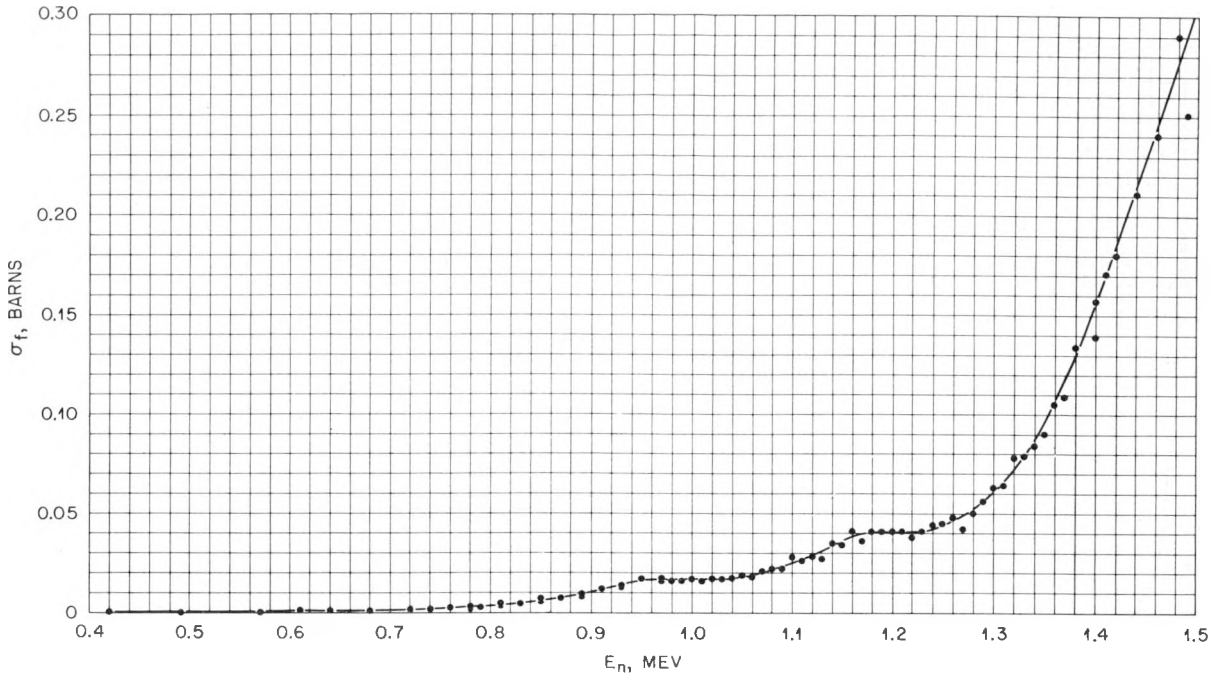

Fig. 2—Fission cross section of U^{238} from 500 to 1500 kev. (CONFIDENTIAL)

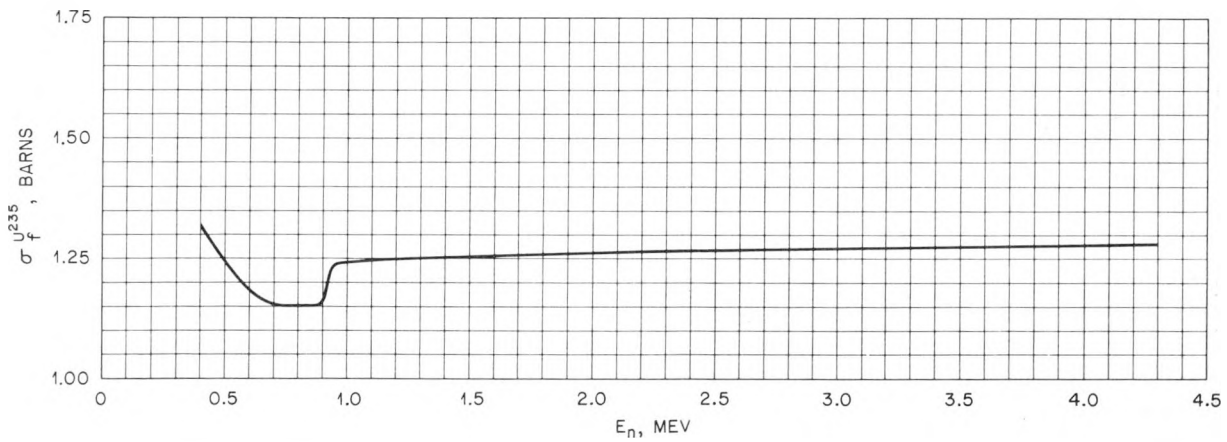

Fig. 3—Fission cross section of U^{235} taken from reference 4 and used to calculate the U^{238} cross section from the comparison data. (UNCLASSIFIED)

4.2 Foil Weights

Equivalent weights, W′, of the foils are listed with their uncertainties in Sec. 6. The standard error of a pair of foils will be $\sqrt{0.5^2 + 0.5^2}$ = 0.7 per cent.

4.3 Statistics

Owing to the slowly varying nature of the curve and the large number of points taken, many to below 1 per cent statistics, the overall statistical uncertainty is estimated to be

0.3 per cent. However, on the rising portion of the curve between 1.3 and 1.5 mev, there is some uncertainty in neutron energy which is estimated to be about ±10 kev.

4.4 Inelastic Scattering

The corrections made for inelastic scattering are believed to be good to a standard error of about 0.5 per cent.

Beam momentum is corrected for in the case of measurements with the 2-foil chamber, as described in reference 7. It very nearly cancels out for the 8-foil chamber, amounting to only 0.3 per cent at 4 mev and 0.15 per cent at 1 mev; therefore an average figure of 0.2 per cent was used. This correction is assumed to be uncertain to 0.1 per cent.

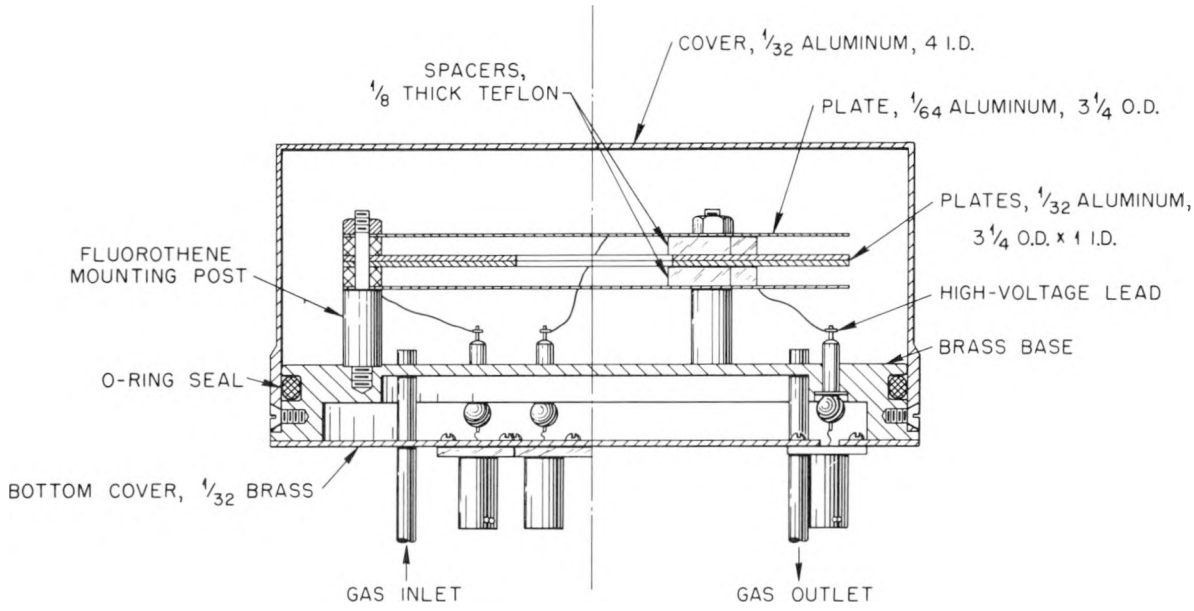

Fig. 4—Sectional view of a 2-foil comparison type fission chamber. Dimensions are in inches. (UNCLASSIFIED)

4.5 Miscellaneous Small Effects

Foil nonuniformity has been discussed and is believed to introduce an uncertainty of not over 0.1 per cent.

Room scattering was found by experiment, as described in reference 7, to cause a 0.3 per cent reduction in the measured cross section. This correction is estimated to be uncertain to 0.2 per cent.

Separation of the foils in the 2-foil chamber by twice the thickness of the backing causes an increase of 0.4 per cent in the measured U^{238} cross section. Neutron absorption by the backing material is negligible, less than 0.1 per cent. The uncertainty arising from these effects is taken as 0.1 per cent.

Relative changes in the gains of the two electronics channels were found to be very slight. Frequent checks were made during all runs. Counting errors from this source are believed to be within 0.1 per cent.

4.6 Systematic Errors

Allowance is made here for unknown sources of error. These are assumed to equal the total of the known sources compounded by taking the square root of the sum of the squares, but omitting the uncertainty in the monitor-foil cross section.

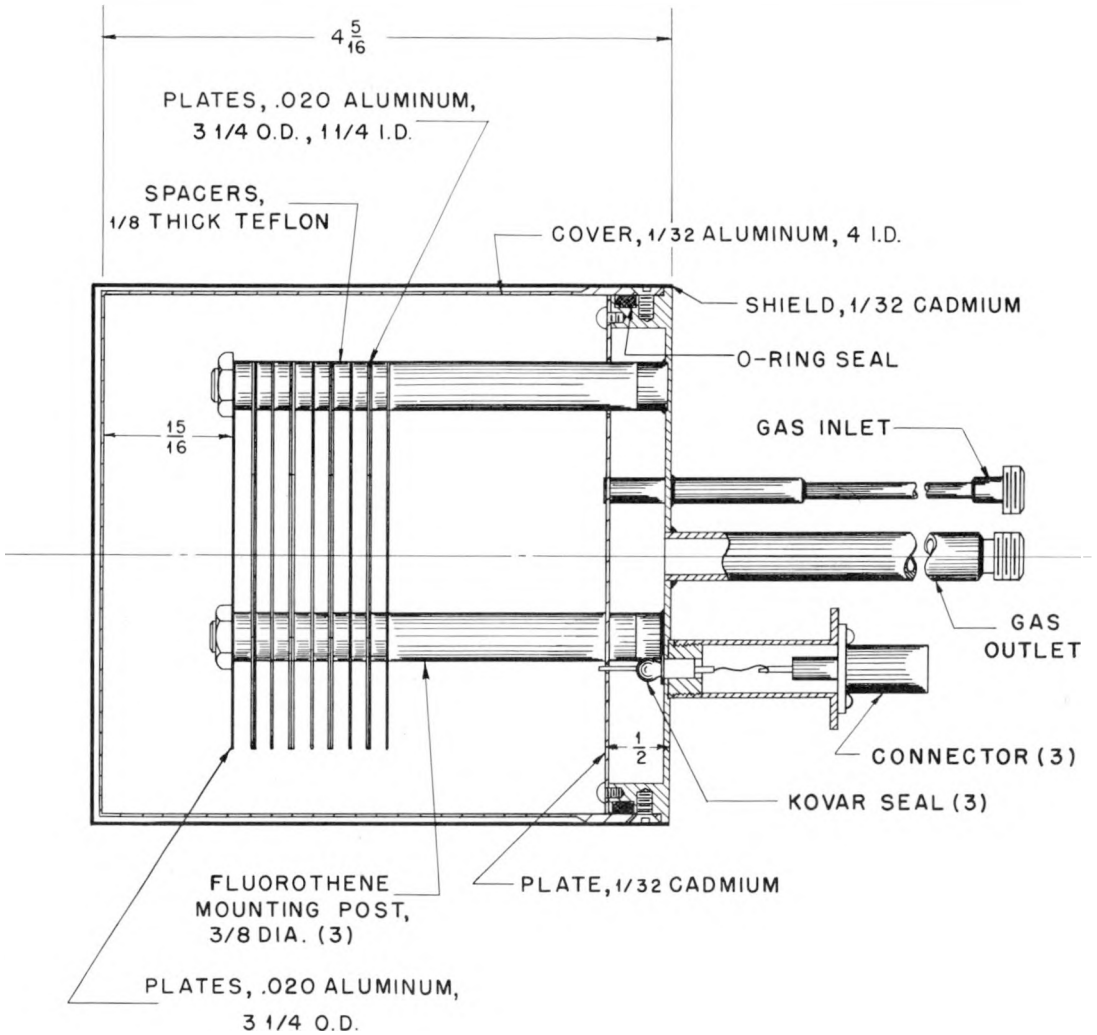

Fig. 5—Sectional view of an 8-foil comparison type fission chamber. Dimensions are in inches. (UNCLASSIFIED)

5. APPENDIX A: INELASTIC-SCATTERING CORRECTION

The results of reference 6 were used to establish a correction for the 2-foil chamber. Since the correction is larger for natural uranium than it is for U^{234} or U^{236}, a somewhat more accurate estimate of it is attempted here. In reference 6 the correction was taken to be constant with neutron energy. For U^{238} it is clear that this effect will be considerably less down on the long tail of the curve below 1 mev than it will be above 2 mev. Some idea of the way this correction will vary can be obtained by considering how large it was found to be for the flat parts of the curves for U^{234}, U^{236}, and natural uranium and by noting the shapes of the fission cross sections of these three materials. With these things in mind we estimated the inelastic-scattering correction, s, to vary with neutron energy as shown in Table 4. The values of s in this table are probably good to 0.4 per cent standard error above 2 mev and to 0.7 per cent or better below 2 mev. (For example, at 2.3 mev, s = 2.7 ± 0.4 per cent.)

Table 4 — Inelastic-scattering Correction (s) for 2-foil Chamber

E_n, mev	s, %
0.80	0.6
0.85	0.7
0.90	0.8
0.95	0.9
1.00	1.0
1.05	1.1
1.10	1.2
1.15	1.3
1.20	1.4
1.25	1.5
1.30	1.6
1.35	1.7
1.40	1.8
1.45	1.9
1.50	2.0
1.55	2.1
1.60	2.2
1.65	2.3
1.70	2.4
1.75	2.5
1.80	2.6
2.30	2.7
2.80	2.8
3.20	2.9
3.70	3.0
4.20	3.1

The scattering correction for the 8-foil counter shown in Fig. 5 was found by comparing the results of several measurements made with it to measurements made with the 2-foil counter. The correction was found to average 4.8 per cent between 2 and 4 mev, or 1.7 times as much as for the 2-foil counter. It is assumed to vary with energy in the same way as it does for the small counter. A rough calculation of the scattering correction for the large counter was made for the case of primary neutrons with 3-mev energy. This checked very well with experiment and indicated that well over half the effect is due to the aluminum plates inside the counter.

6. APPENDIX B: FOIL COMPARISONS

Foils were compared as described in reference 6. The results for the thin foils are listed in Table 5.

Table 5 — Thin-foil Comparisons

Foil	Mass, μg	Δf, %	Δα, %
	U^{235} foils		
25K5	198.4	0.48	0.46
25K6	194.8	0.7	0.18
25K7	198.3	−0.74	−0.65
25K8	198.2	−0.54	−0.65
25K9	199.0	0.07	0.18
25K10	198.5	0.68	0.46
Standard error		0.21	0.19
	Natural-uranium foils		
NK1	196.9	+0.8	+0.9
NK2	198.3	−0.7	−0.6
NK3	195.9	+0.2	+0.4
NK4	198.1	−0.7	−0.7
NK5	197.0	+0.1	+0.1
NK6	195.9	−0.3	−0.1
Standard error		0.22	0.23

Table 6 — Thick-foil Equivalent Weights

Foil	W′, mg	
	8-foil chamber	2-foil chamber
NK7	3.597	3.597
25K15	3.602	
25K14	3.571	3.571
NK8	3.580	
NK11	3.550	
25K11	3.554	
25K13	3.524	
NK12	3.480	

The first group is composed of thin U^{235} foils and the second of natural uranium. Mass is given in micrograms. Δf and Δα are the percentage of deviation from the average specific fission and alpha activity, respectively. Counting statistics were 0.2 per cent for the U^{235} foils and for the fission activity of the natural uranium. Statistics were 0.37 per cent for the alpha activity of natural-uranium foils. The standard errors listed refer to the average for the group in each case since this average was used in determining the W′ values.

The thick foils were weighed in a flux of thermal neutrons by comparing their activity with

that of the thin foils. These measurements were made in the counter in which the thick foils were to be used and with the same bias and gain settings to be used later in the cross-section measurements, since W′ is a function of bias and amplifier gain settings. These are monitored by a pulse generator having a signal that is fed into the high-voltage plate (or plates) of the counter. Since capacities between high-voltage and collector plates will be different for different counters, the W′ determined for one counter will not in general be right for a different counter, unless the bias is adjusted to a particular value to bring this about. However, this was done for the two foils in question.

Over-all statistical accuracy is 0.25 per cent for the equivalent weights. The foils were placed in the chamber in the order that they appear in Table 6, from the front to the back of the chamber. The estimated error from all sources is 0.5 per cent for each foil.

ACKNOWLEDGMENTS

It is a pleasure to acknowledge the help of R. E. Greene and his group for their very fine work in preparing the uranium foils. The method that they used is described in reference 6. Thanks are also due to the members of the Van de Graaff group, J. K. Bair, H. O. Cohn, J. D. Kington, P. H. Stelson, and H. B. Willard, for operating the generator.

REFERENCES

1. A Compilation of the AEC Neutron Cross Section Advisory Group, Report AECU-2040, May 15, 1952.
2. R. R. Carlson, The Ratio of the Fission Cross Section of U^{238} to That of U^{235}, Report ORNL-1458, Feb. 4, 1953.
3. R. L. Henkel, Fission Excitation Curves for U^{233}, U^{235}, U^{236}, U^{238}, Np^{237}, Report LA-1495, Nov. 21, 1952.
4. H. H. Barschall and R. L. Henkel, Summary of Fast Fission Cross Sections, Report LA-1714, August 1954.
5. Benjamin C. Diven, The Fission Cross Section of U^{235} from 0.4 to 1.6 Mev, Report LA-1336, Feb. 3, 1953.
6. R. W. Lamphere and R. E. Greene, The Neutron-induced Fission Cross Sections of U^{234} and U^{236}, Phys. Rev., (100) 1 (October 1955).
7. R. W. Lamphere, The Neutron-induced Fission Cross Section of U^{234}, Phys. Rev., 91: 655 (1953).
8. H. B. Willard, J. K. Bair, and J. D. Kington, The Reactions $T(p,n)He^3$ and $T(p,\gamma)He^4$, Phys. Rev., 90: 865 (1953).
9. B. B. Rossi and H. H. Staub, "Ionization Chambers and Counters," Division V, Volume 2, National Nuclear Energy Series, McGraw-Hill Book Company, Inc., New York, 1949.

ABOUT THE AUTHOR

R. W. Lamphere is a research engineer at the Oak Ridge National Laboratory, where he has been employed since 1947. He received the M.S. degree in electrical engineering from Massachusetts Institute of Technology in 1938.

SOLID-STATE BONDING AND CANNING OF THORIUM WITH ALUMINUM

SAMUEL STORCHHEIM

Sylvania Electric Products, Inc.

August 31, 1955

ABSTRACT

Hot-pressure-welding studies of both wrought and powder-metallurgy thorium and 2S aluminum were conducted. The resultant data showed that bond strengths as high as 7800 psi could be obtained by the proper combination of hot-pressing temperature, pressure, and time. The intermetallic alloy zones formed between the two components showed an increase in width with both increasing temperature and pressure.

The requisite conditions for best bonding were applied to the canning of thorium slugs 6 in. in length by 1 in. in diameter in aluminum cans of 35-mil wall thickness. It was found that the canned thorium was uniformly well bonded to the aluminum. In addition, the bond areas were found to have a high degree of corrosion resistance to 170°C steam.

1. INTRODUCTION

The Savannah River operations of E. I. du Pont de Nemours & Company requested that the Sylvania Electric Products, Inc., Atomic Energy Division, can thorium in 2S aluminum. The requisites were that the aluminum be metallurgically bonded to the thorium; that the metallurgical bond have strength; and that, when ruptured, it have corrosion resistance. The specimens desired were to be approximately 1 in. in diameter and 6 in. in length.

To provide data for use in the canning operation, a vacuum-hot-pressing study was initiated concerning bond strengths developed between thorium and aluminum reacted at various conditions of temperature, pressure, and time. In addition, studies were made of the rate of growth of the intermetallic alloys formed between aluminum and thorium. The basic object of this preliminary investigation was to determine optimum canning conditions by which satisfactorily clad thorium fuel elements could be manufactured. This article contains the data of the preliminary investigation and the canning results that were obtained when application was made of these data.

2. PROCEDURE

2.1 Materials Used

In the fundamental study the materials used were 2S aluminum rod and either reguline thorium metal or hot-pressed powder thorium. The powder-metallurgy thorium used in the experiments was obtained by the hydriding and dehydriding of Ames chip or bar stock that was subsequently comminuted to −80-mesh size.[1] This powder in turn was hot-pressed in vacuo at 650°C and 12 tsi (tons/sq in.) held 15 min. The

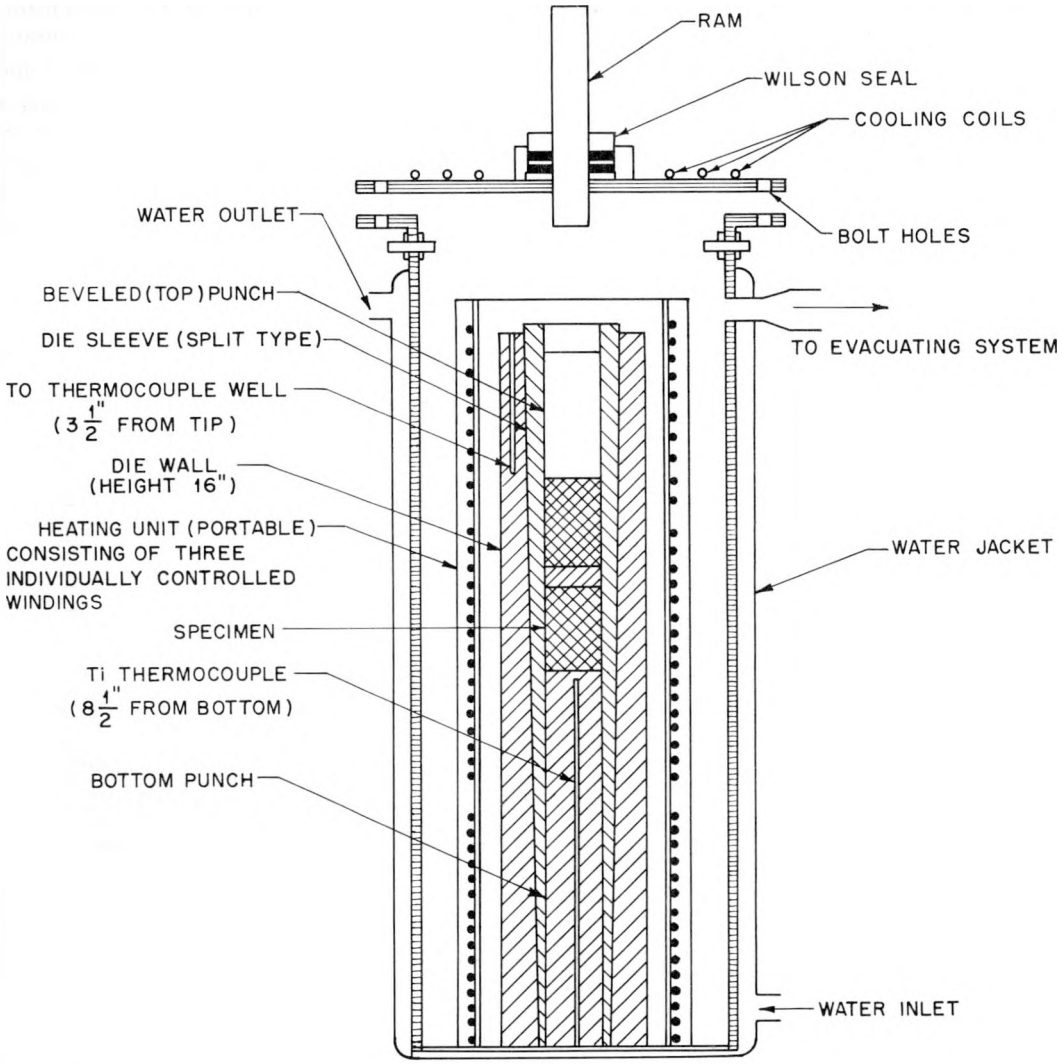

Fig. 1—Hot-pressing apparatus.

resultant density of slugs so fabricated was 11.5 g/cm^3.

2.2 Specimen Dimensions and Cleaning Technique

The specimens used for the fundamental study were arranged in tensile and diffusion couples such that thorium slugs $\frac{1}{4}$ in. thick were sandwiched between aluminum pieces 1 in. long. These couples were in turn slipped into an aluminum sleeve with a 30-mil wall. The object of this sleeve was to line up the coupled pieces and keep contaminants from falling or being entrapped at the aluminum-thorium interfaces. The diameter of each tensile couple used was 1.440 in., this being the only size die available for the preliminary studies at the time.

The contacting interfaces of the aluminum and thorium pieces were abraded clean immediately prior to assembly and insertion into the aluminum sleeve. During the actual canning of fuel elements, which is discussed later, the aluminum was chemically cleaned as follows:

1. Degreased in acetone.
2. Water rinsed.
3. Immersed 5 min in 10 per cent NaOH at 70°C.
4. Water rinsed.

5. Immersed 2 min in 50 per cent HNO_3 at room temperature.
6. Water rinsed.
7. Paper-tissue dried.

The thorium slugs were either hand abraded or dry machined prior to insertion in the chemically cleaned aluminum can.

2.3 Equipment and Hot-pressure-welding Technique

The apparatus used for the hot-pressing of both tensile and diffusion couples, as well as for the canning of full-sized slugs, is shown in Fig. 1. The hot-pressure-welding technique used has been described elsewhere.[2] Briefly, the specimens to be hot-pressed were inserted into an aquadag-lubricated Inconel-X die containing two thermocouple wells. The die in turn was placed in a heating unit consisting of three individually controlled windings. This assembled unit was in turn placed in a stainless-steel water-cooled pot. A cover was bolted onto the pot, and the entire apparatus was evacuated to less than 5 μ Hg pressure. The three windings were energized, and the specimens in the die were brought to temperature.

At this point pressure was applied to a ram in the top cover, the ram being movable through a Wilson seal. At the end of the desired pressing time, pressure was released and current to the furnace was cut off. The maximum pressure within the system caused by outgassing was on the order of a maximum of 400 μ, which at the time of pressing was restored to below 5 μ. The length of heat-up time varied between 45 and 90 min. The time for ejection of hot-pressed specimens was on the order of 3 to 5 min after pressure and furnace current had been turned off.

2.4 Testing Technique

After a hot-pressed specimen was ejected from the die, the outer aluminum sleeve was machined off, and the aluminum ends of the couple were threaded, as shown in Fig. 2. The specimen in this condition was then tensile tested; the strengths reported are ultimate tensile strengths in pounds per square inch. In all these studies fracture always occurred at one of the aluminum-thorium interfaces. The aluminum-thorium interface remaining intact was, in a number of instances, sectioned and studied under the microscope for determination of the rate of intermetallic alloy zone formation. These rate determinations were made by measuring the entire width in centimeters of any zone or zones seen, squaring this value, and dividing it by the time in seconds that the couple was held under pressure. This value was then termed "zone-growth rate" and is reported in square centimeters per second.

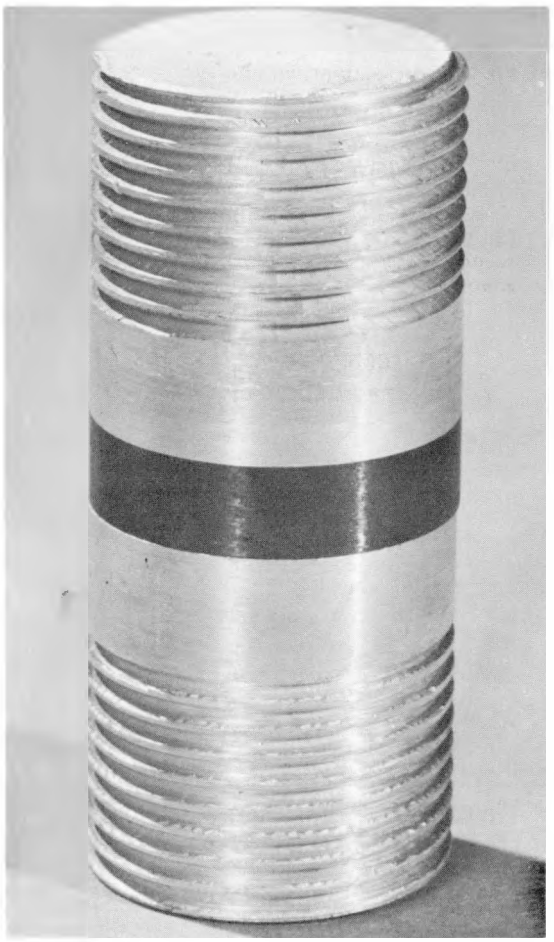

Fig. 2—Typical aluminum-thorium tensile couple ready to be tension tested. (Magnification 2×.)

3. RESULTS AND DISCUSSION

3.1 Tensile Data

(a) Effect of Hot-pressing Temperature. Figure 3 shows the relation between ultimate tensile strength and hot-pressing temperature

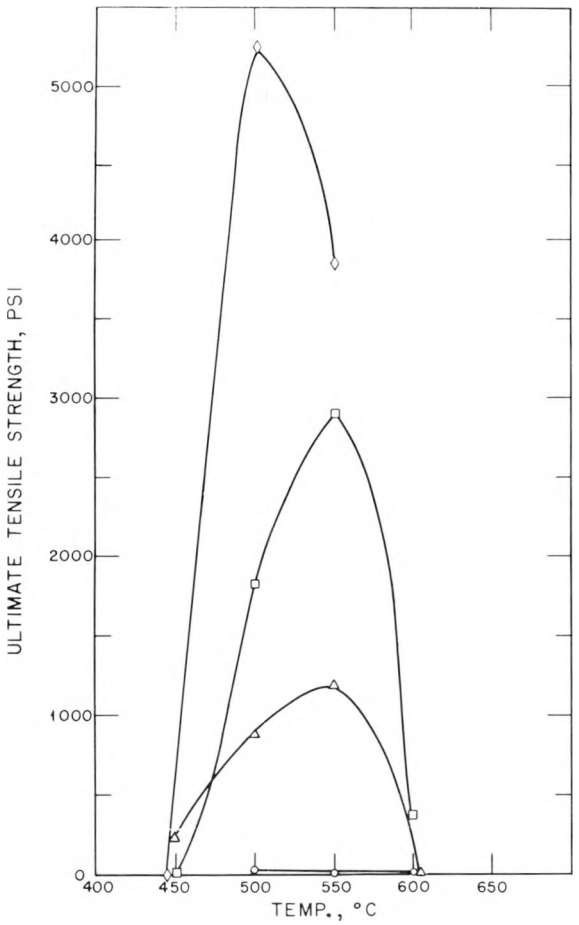

Fig. 3—Tensile strength of reguline thorium–2S aluminum as a function of temperature at various isobars held 2 min in vacuo. ○, 5 tsi. △, 10 tsi. □, 15 tsi. ◇, 20 tsi.

for the isobars 5, 10, 15, and 20 tsi held 2 min in vacuo. These data were obtained from couples made of aluminum and reguline thorium. The indication is that almost no bond occurs at any temperature for specimens pressed at 5 tsi. With increasing pressure for the remaining three isobars, tensile strength increased, peaked, and then decreased. As the pressure was increased, greater peak tensile strengths were obtained, and the approximate temperature where the peak occurred shifted to lower values. The highest tensile strength shown in this figure is approximately 5300 psi, occurring at about 500°C at 20 tsi.

Figure 4 is the same type of graph as Fig. 3, with the exception that the tensile couples were made of aluminum and powder-metallurgy thorium. The specimens were hot-pressed at 15 tsi held 10 min in vacuo. A maximum strength of approximately 6800 psi was obtained. It was observed that the peak of the curve occurred at about 400°C.

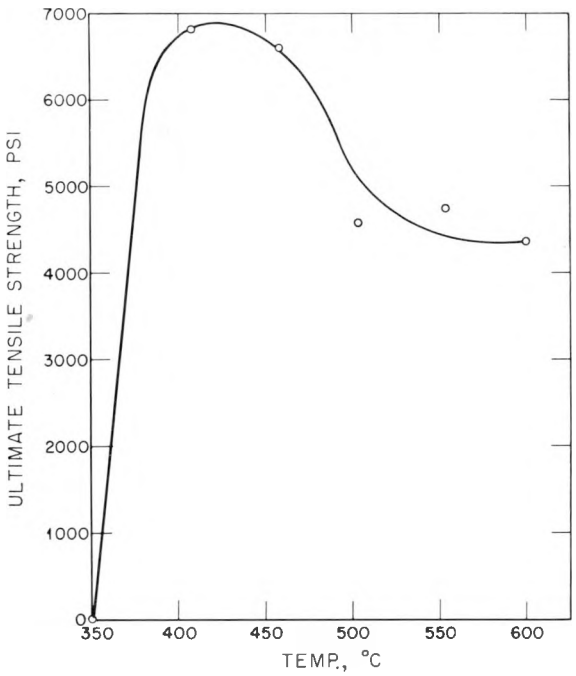

Fig. 4—Tensile strength of hot-pressed powder-metallurgy thorium–2S aluminum as a function of temperature at 15 tsi held 10 min in vacuo.

(b) Effect of Pressure. Figure 5 shows how increasing pressure affects the ultimate tensile strengths of the bonds. Four curves are depicted for the isotherms 450, 500, 550, and 600°C. For this series of experiments pressure was held 2 min, and reguline thorium was bonded to aluminum. Very little bonding was obtained at 450°C, whereas bond strengths increased with great rapidity at both 500 and 550°C. Bond strengths given for the 600°C isotherm were quite low. The maximum strength obtained at the greatest pressure used, namely, 20 tsi, was 5300 psi at 500°C.

Figure 6 is similar to Fig. 5, with the exception that powder-metallurgy thorium was used for the couples and the pressure was held 10 min in vacuo at 550°C. For the particular temperature used, strength showed only nominal increase with increasing pressure. The maximum value that was attained was approximately 5000

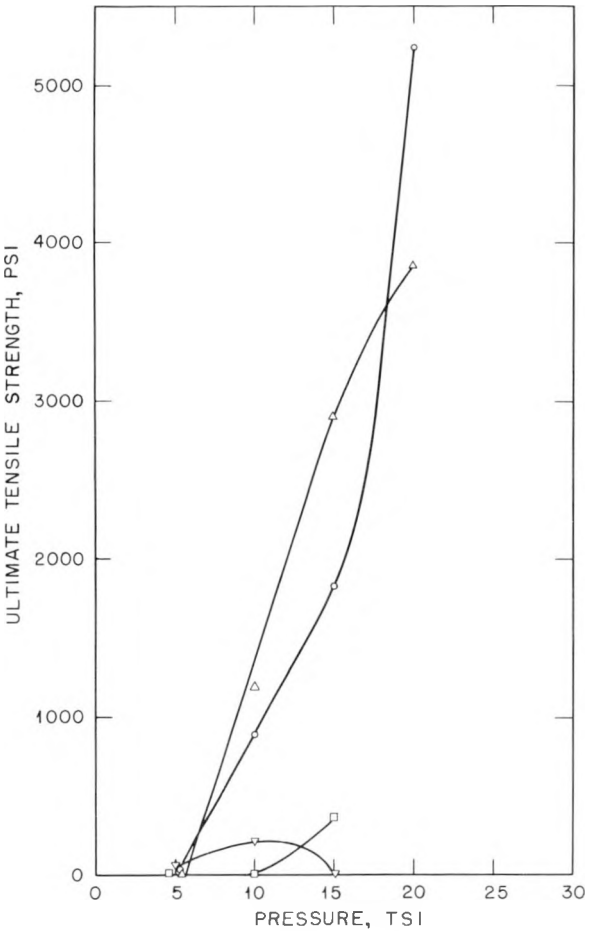

Fig. 5—Tensile strength of reguline thorium–2S aluminum as a function of increasing pressure at various isotherms held 2 min in vacuo. ∇, 450°C. ○, 500°C. △, 550°C. □, 600°C.

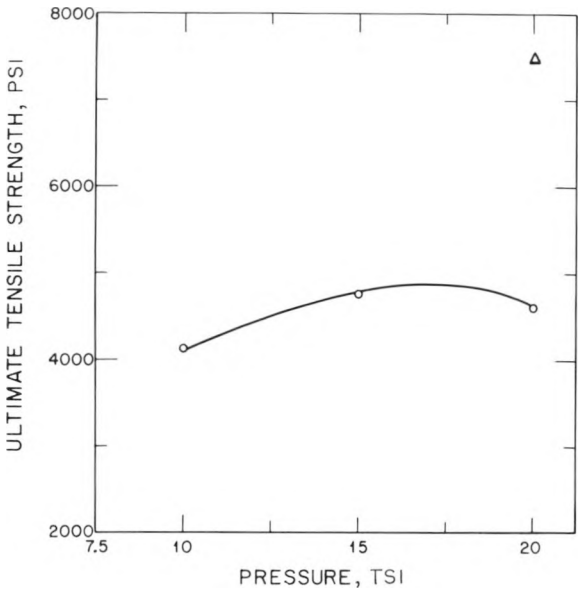

Fig. 6—Tensile strength of thorium–2S aluminum as a function of pressure held 10 min at 550°C in vacuo. ○, powder-metallurgy thorium. △, reguline thorium.

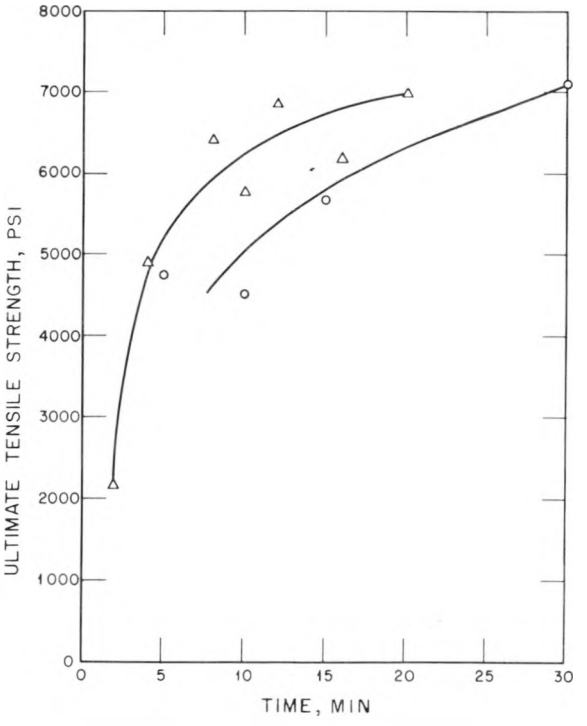

Fig. 7—Tensile strength of both reguline thorium and powder-metallurgy thorium with 2S aluminum as a function of increasing time at 575°C and 15 tsi in vacuo. △, reguline thorium. ○, powder-metallurgy thorium.

psi at about 16 tsi. One bond-strength value, about 7800 psi, representing reguline thorium is also shown in Fig. 6 for comparative purposes.

(c) Time. The effect of time on the ultimate tensile strengths developed is shown in Fig. 7. The two curves represent a comparison of reguline thorium and aluminum vs. powder-metallurgy thorium and aluminum. All specimens were hot-pressed at 575°C at 15-tsi pressure. For the reguline thorium curve strength increases rapidly, knees at approximately 5000 psi, and reaches a maximum value of about 7000 psi. The powder-metallurgy curve shows strength increasing to a maximum of approxi-

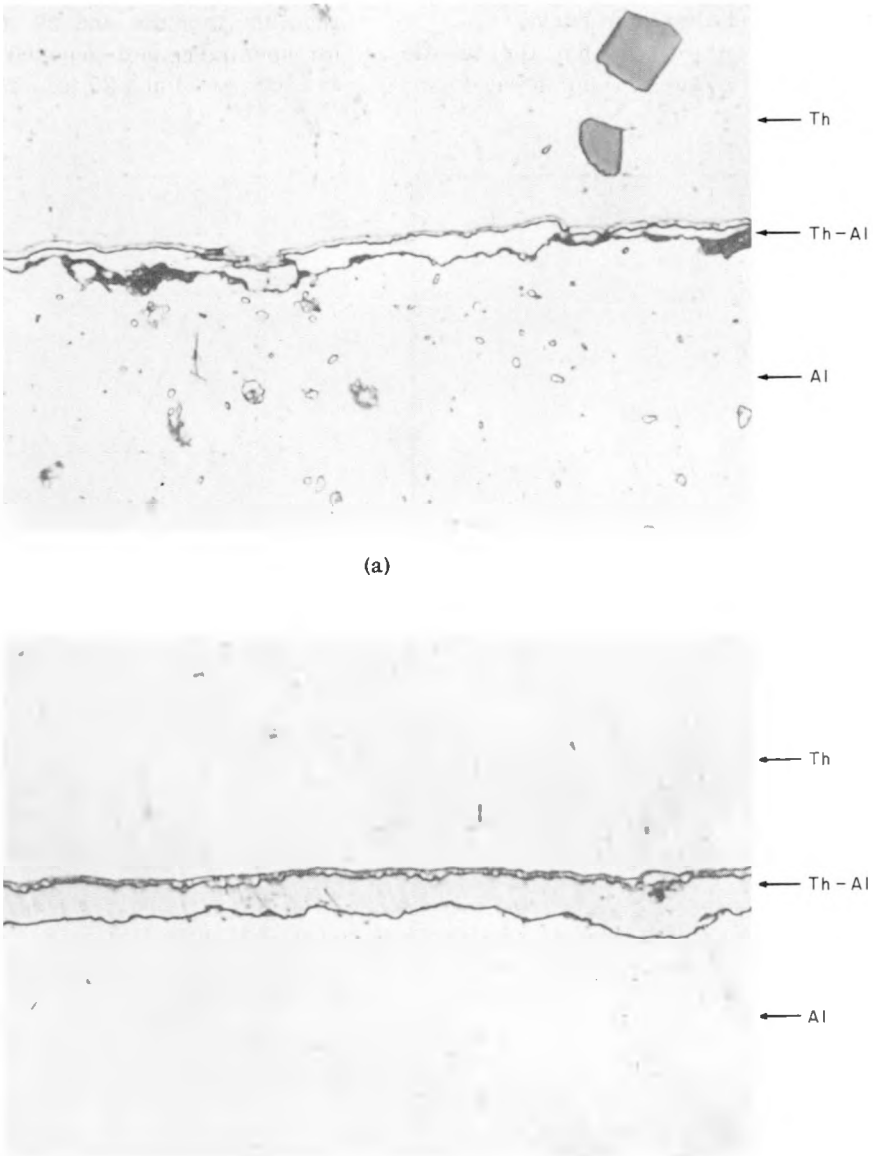

Fig. 8—Reguline thorium–2S aluminum interfaces of two couples reacted at 500°C for 2 min in vacuo. (a) Hot-pressed at 10 tsi; HNO_3 etch. (Magnification 1000×.) (b) Hot-pressed at 20 tsi; HNO_3 etch. (Magnification 1000×.) Note how much thicker and better formed the intermetallic zones are in (b). Two zones are evident in both specimens.

mately 7000 psi with increasing time. However, at the temperature used the rate of increase does not appear to be as rapid as that for the reguline thorium and aluminum curve.

It should be pointed out that the tensile strengths developed by these couples were used basically as an indicating evaluation of what the optimum canning conditions should be. In actuality it was felt that the tensile values obtained were not true tensile strengths but merely parameters to be used for the proper selection of canning conditions. In this study the greatest strength achieved for the conditions outlined was 7800 psi.

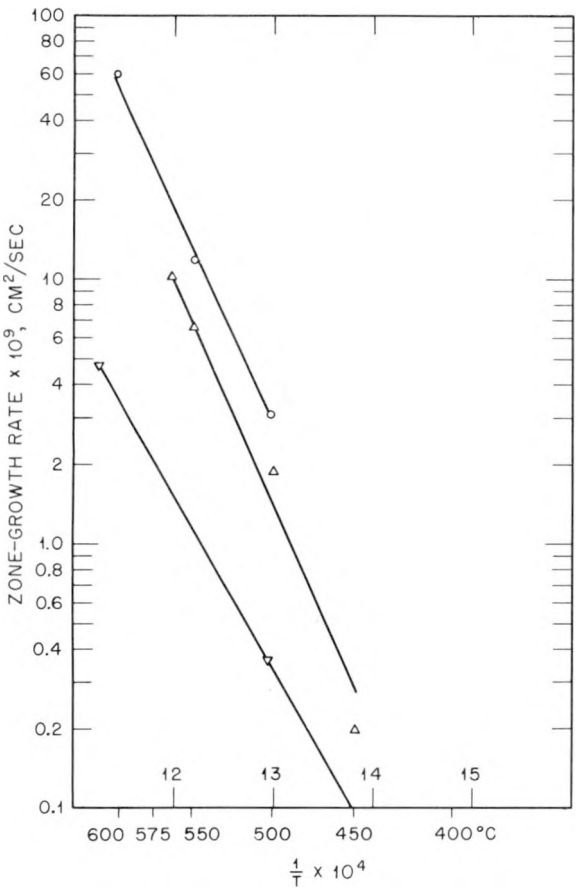

Fig. 9—Intermetallic zone-growth rates of reguline thorium and 2S aluminum as a function of the reciprocal of the absolute temperature. ○, diffused at 20 tsi. Δ, diffused at 12 tsi. ∇, furnace diffused in vacuo (BMI data); based on four points.

3.2 Zone-growth Rates

The two photomicrographs in Fig. 8 show reguline thorium and 2S aluminum interfaces for specimens hot-pressed at 500°C for 2 min in vacuo at 10 and 20 tsi. The indication in both specimens was that one thick and one thin intermetallic alloy layer formed. The thickness of the alloy zones was considerably greater for the specimen pressed at 20 tsi than for the one pressed at 10 tsi. Under polarized light the thin intermetallic zone was shown to be made of

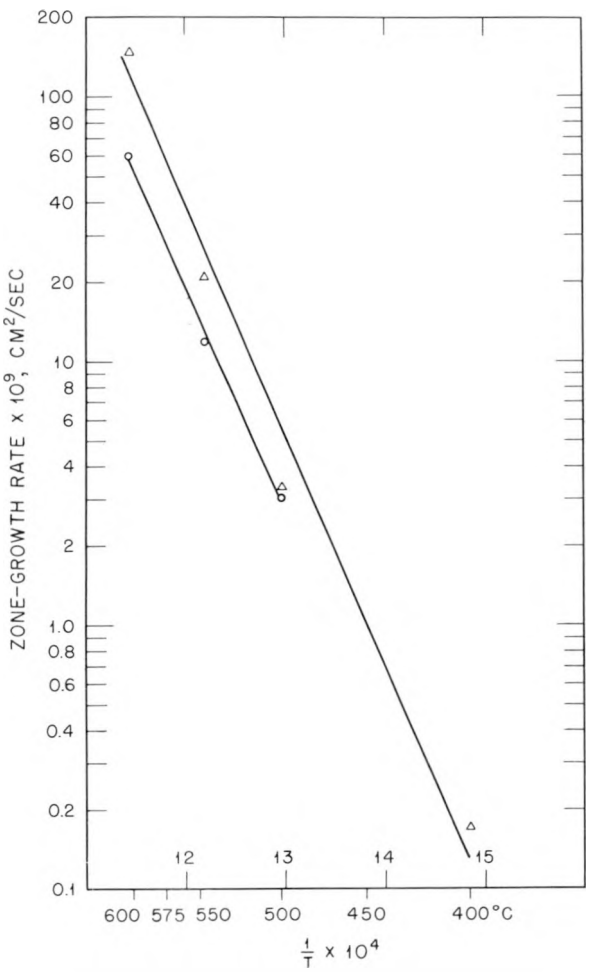

Fig. 10—Intermetallic zone-growth rates of reguline thorium and powder-metallurgy thorium with 2S aluminum vs. the reciprocal of the absolute temperature. Δ, powder-metallurgy thorium hot-pressed at 15 tsi. ○, reguline thorium hot-pressed at 20 tsi.

columnar grains. Hot-pressed powder-metallurgy thorium and aluminum interfaces showed very much the same type of microstructure as did reguline thorium and aluminum.

(a) Effect of Temperature. Figures 9 and 10 show curves of the log of zone-growth rates vs. the reciprocal of the absolute temperature. Figure 9 is for reguline thorium, and Fig. 10

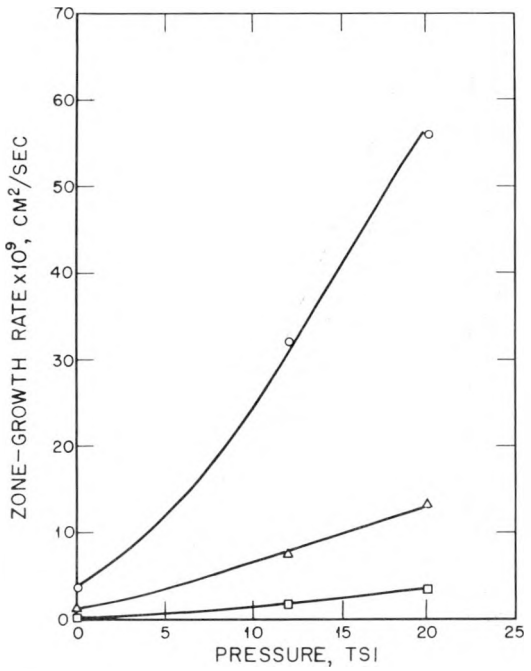

Fig. 11—Intermetallic zone-growth rates of reguline thorium and 2S aluminum as a function of pressure for various isotherms. ○, 600°C. △, 550°C. □, 500°C.

shows a comparison of the growth rates of reguline thorium and powder-metallurgy thorium with aluminum. Figure 9 shows a series of curves for specimens reacted at various isobars, namely, atmospheric pressure and 12 and 20 tsi. The points plotted indicate that the relations are linear for this type of representation and that pressure appears to exert an effect upon growth rates, i.e., increasing pressure increases the rate of alloy-zone formation.

Figure 10 represents powder-metallurgy thorium and aluminum pressed at 15 tsi and reguline thorium and aluminum pressed at 20 tsi. Again the plotted points show a linear relation. From Fig. 9 it was learned that increasing pressure caused increasing growth rates; therefore the conclusion is that powder-metallurgy thorium reacts faster than reguline thorium when diffused to aluminum.

(b) Effect of Pressure. The curves in Figs. 9 and 10 show that zone-growth rates increase with increasing pressure. These two parameters are plotted in Fig. 11, which shows more clearly this effect for reguline thorium and aluminum at the isotherms 500, 550, and 600°C. The indication is that the effect is relatively small but noticeable at the two lower isotherms. At the highest temperature used the increase in zone-growth rate with increasing pressure, an increase of approximately 15 times from atmospheric pressure to 20 tsi, was considerably more pronounced.

Table 1—Thorium-Aluminum Activation Energies As a Function of Pressure Applied During Alloy-zone Formation

Pressure, tsi	Activation energy (Q), cal/gram-atom
Reguline thorium–2S aluminum	
0	25,600*
12	40,200
20	39,200
Powder-metallurgy thorium–2S aluminum	
15	39,200

*BMI data from Report DPWZ-4256.

Table 1 gives the activation energies for reguline thorium and powder-metallurgy thorium with aluminum as a function of pressure. The indication is that the activation energies are almost the same for specimens of powder-metallurgy and reguline thorium, whereas those specimens diffused at atmospheric pressure show an activation energy of approximately 65 per cent of the preceding two types.

3.3 Canning

Optimum canning conditions for reguline thorium and aluminum were selected from the

preceding data. These included temperatures ranging between 500 and 550°C and double-acting pressures from 12 to 25 tsi held 10 min in vacuo in a die lubricated with MoS_2. Figure 12 is a composite macrophotograph with corresponding photomicrographs of a thorium slug hot-pressed in an aluminum can having a 35-mil wall thickness. Formation of intermetallic layers between the thorium and aluminum is seen to be continuous and uniform.

Figure 13 shows how canned specimens made under optimum bonding conditions reacted to steam autoclaving at 170°C for 15 hr. These specimens had 16 holes drilled through the aluminum to the thorium in the sleeve areas and one hole each drilled through both ends. Under these corrosion conditions normally weak or poor bonding is shown up by either blistering or bursting of the aluminum can. As can be seen, the bond strength obtained for the specimen in Fig. 13 is excellent in that no noticeable distortion is apparent about the deliberately defected can areas.

Figure 14 shows a canned specimen given a chisel peel test. In this instance the aluminum ends were cut through to the thorium in criss-cross fashion. The ends of these crosses were then in turn connected along the sleeves by again cutting through the aluminum to the thorium. A chisel was then placed in the aluminum at the cut areas, and attempts were made to strip the aluminum from the canned thorium. Rupture occurred only within the aluminum, and no lifting of the aluminum at the bond interface was obtained, again showing excellent bond strength between the two components.

A number of specimens were thermally shocked by heating them to 500°C and quenching them in water at 20°C. After each shock the specimens were nondestructively checked by the pulse ultrasonic technique. In no case was any unbonding obtained for these specimens even after as many as 10 and, in some instances, 15 shocks.

4. SUMMARY

The following is a summarization of the effect that various hot-pressing conditions have upon the hot-pressed bond strength and alloy formation of both reguline thorium and powder-metallurgy thorium with aluminum.

1. Increasing the hot-pressing temperature causes strength to rise, peak, and then decline. Optimum bonding temperatures appear to vary between 500 and 550°C for reguline thorium and between 400 and 450°C for powder-metallurgy thorium.

2. Increasing the pressure for reguline thorium for both 500 and 550°C isotherms causes a very rapid rise in bond strength. Increasing the pressure for either lower or higher temperatures than those indicated above has little effect upon bond strength. Increasing the pressure for powder-metallurgy thorium at 550°C causes bond strength to increase slowly.

3. Increasing the time at temperature and pressure causes bond strength to increase rapidly, knee, and level off for reguline thorium. For powder-metallurgy thorium, increasing the time at temperature causes strength to rise continually at a decreasing rate.

4. Increasing the temperature causes an increase in the rate of intermetallic alloy formation for both types of thorium.

5. Increasing the pressure causes an increase in the rate of intermetallic alloy formation for reguline thorium.

Peak tensile strength obtained for both reguline and powder-metallurgy thorium was 7800 psi. For the data presented it appeared that reguline thorium bonded more readily to aluminum than did powder-metallurgy thorium for both increasing pressure and increasing time at pressure. It should be pointed out that peak bonding strengths for the powder-metallurgy specimens were obtained at lower temperatures than for the reguline specimens. The rate of intermetallic formation appeared to be greater between the powder-metallurgy specimens and 2S aluminum than for the reguline-thorium pieces. In addition, the activation energy was higher.

5. CONCLUSION

A fundamental investigation concerning the bonding of thorium to aluminum was conducted. As a result of these experiments optimum bonding conditions were attained such that thorium fuel elements 1 in. in diameter and 6 in. in

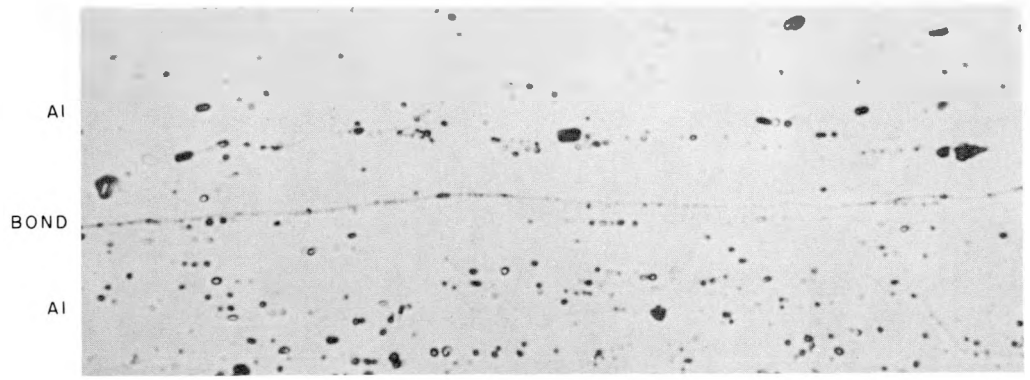

(a)

(b)

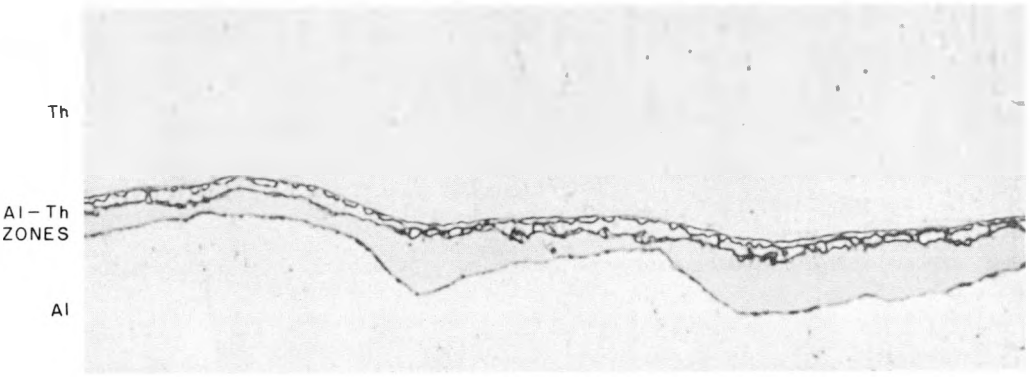

(c)

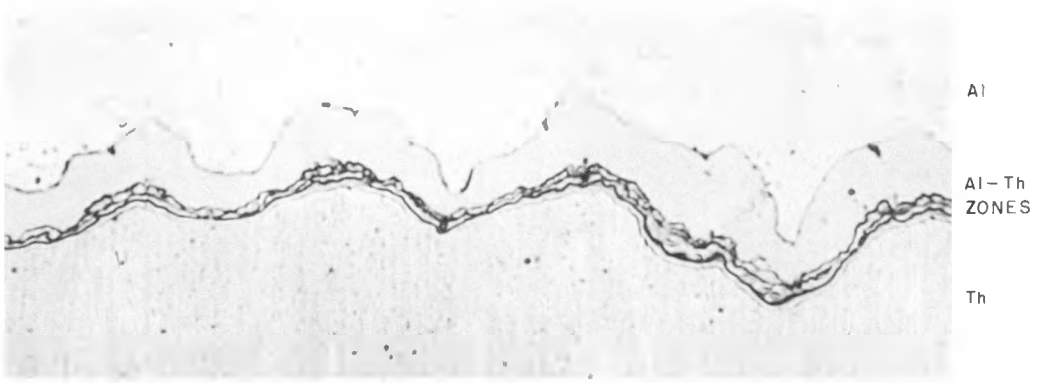

(d)

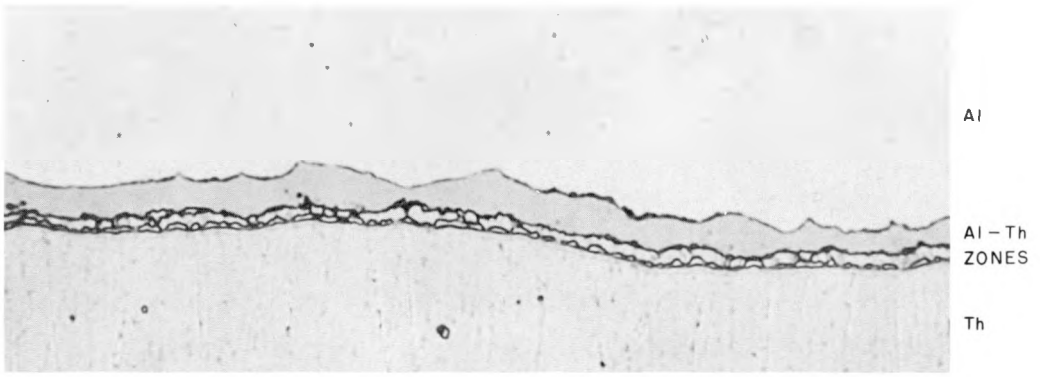

(e)

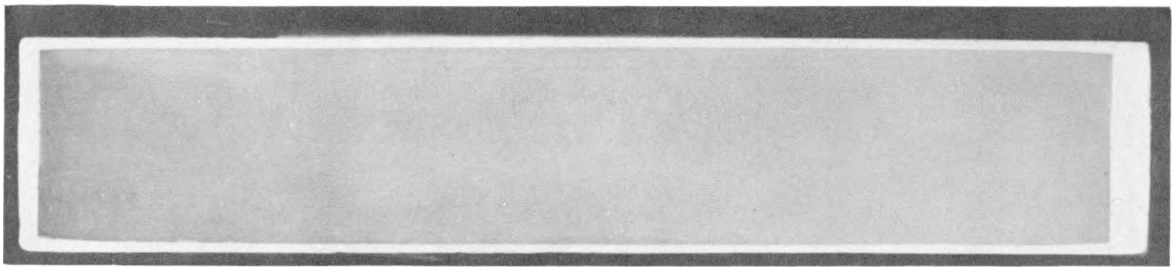

(f)

Fig. 12 — (a) Photomicrograph of cap-to-can bond. (b) Photomicrograph of thorium-to-aluminum top bond. (c) Photomicrograph of thorium-to-aluminum side bond. (d) Photomicrograph of thorium-to-aluminum bottom bond. (e) Photomicrograph of thorium-to-aluminum side bond. (f) Macrophotograph of longitudinal section of aluminum can containing 6-in.-long by 1-in.-diameter reguline-thorium slug, approximately original size. Pressed at 500°C at 12 tsi for 10 min in vacuo; the slug and can were chemically cleaned prior to hot-pressing. Magnification for all photomicrographs is 1000×.

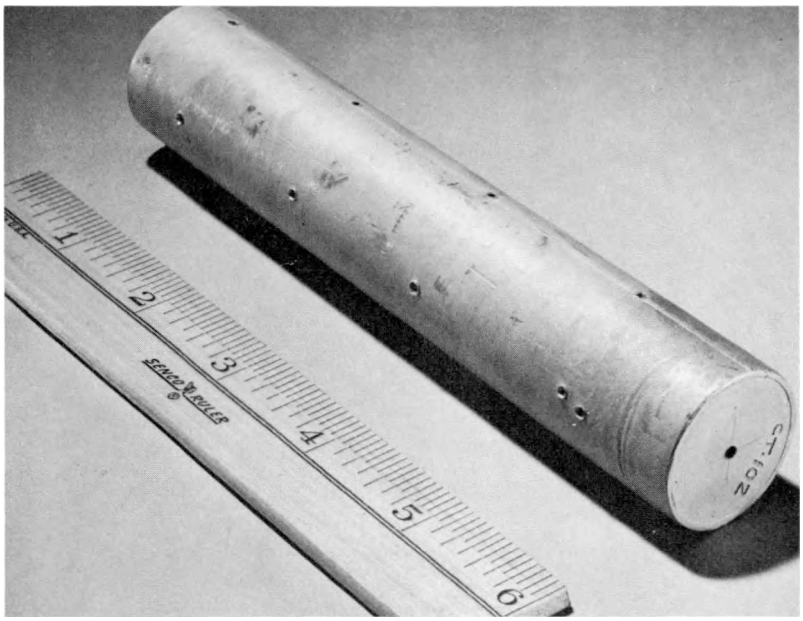

Fig. 13—Canned thorium specimen with aluminum cladding deliberately ruptured. This specimen was steam autoclaved at 170°C for 15 hr. The bond strength between the aluminum and thorium is excellent in that no noticeable distortion of the aluminum is apparent about the holes in the cladding.

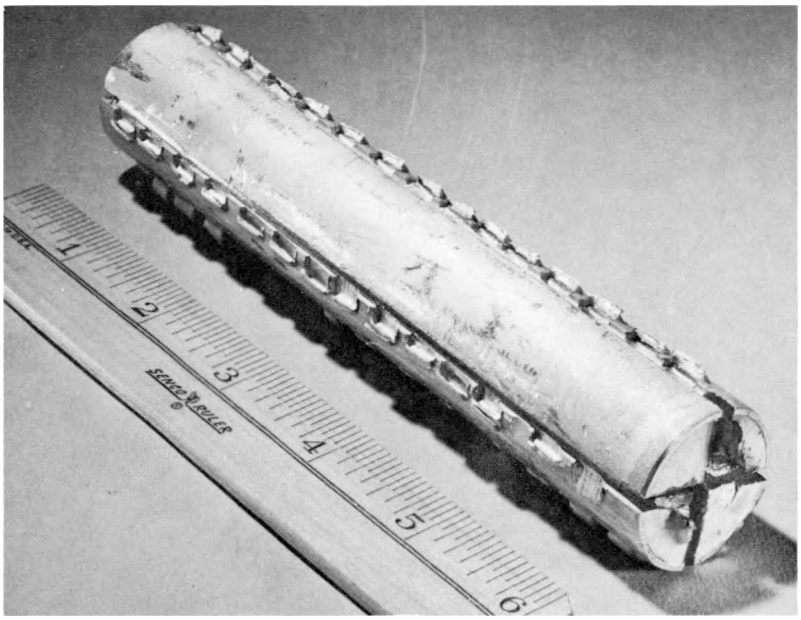

Fig. 14—Canned thorium specimen after chisel peel testing the aluminum cladding. Rupture occurred only within the aluminum, and no lifting of the aluminum at the thorium-aluminum bond interface was obtained. This indicates excellent bond strength between the two components.

length were successfully canned in 2S aluminum cans having a 35-mil wall thickness. The bond strengths attained between these two components were found to be excellent by both destructive and nondestructive tests. In addition, exposed bond interfaces were found to have good corrosion resistance to 170°C steam.

REFERENCES

1. R. B. Wagner and S. Storchheim, Preparation and Consolidation of Thorium and Thorium Hydride Powders, Report SEP-168, Aug. 9, 1954.
2. S. Storchheim, J. L. Zambrow, and H. H. Hausner, Solid State Bonding of Aluminum to Nickel, J. Metals, 6: 269-274 (February 1954).

ABOUT THE AUTHOR

Samuel Storchheim received the B.S. and M.S. degrees in metallurgical engineering from Brooklyn Polytechnic Institute in 1944 and 1949, respectively. Prior to his association with Sylvania, he was employed by the Radio Corp. of America (1944 to 1945), American Electro Metal Corp. (1945 to 1947), and Wilbur B. Driver Co. (1947 to 1950). He joined the Sylvania organization at the Bayside, N.Y., Metallurgical Laboratory as a senior engineer in 1951. He was promoted to Engineer-in-charge in 1953 and to Section Head in the Atomic Energy Division in 1955.

THE FABRICATION OF FUEL ELEMENTS FOR POWER REACTORS

J. F. SCHUMAR

Argonne National Laboratory

September 28, 1955

1. INTRODUCTION

In central-station power reactors with low-cost power as the objective, the characteristics of the reactor must be adjusted to give the highest over-all efficiency per unit investment in plant and fuel. In the case of the fuel the demands are for a long-life fuel element that can be manufactured easily and inexpensively. These demands follow whether the fuel element considered is for use in a thermal reactor with the neutron spectrum in the thermal-energy range or in fast reactors with the neutron spectrum in the high-energy range.

The performance of a nuclear reactor can be no better than the fuel element and core designs permit. A good fuel-element design is a balance between the optimum demands of several major factors: heat transfer, mechanical design and stability, nuclear requirements, materials, and fuel-element fabrication.

The highest power density may be obtained from the fuel element with the maximum ratio of cooling surface to volume. Heat transfer requires bonding between the core and jacket as well as thin or small cross sections and thin clads. Hence fast reactors, which are characterized by small cores and high power densities, require small diameter pins or wire or very thin plates as fuel elements. Thermal reactors require small diameter rods, tubes, or plates as fuel elements.

The nuclear characteristics of the reactor indicate what material may be considered for use in the fuel element. These limit, then, what materials the fuel-element fabricator may select as cladding materials and fuel-element core materials. The fuel fabricator chooses to select fuel core and clad materials that are compatible with each other, and yet he is further restricted in choice by other criteria.

1. The clad material, for example, must be corrosion resistant to the coolant under operating conditions and must be metallurgically bonded to the fuel.

2. The properties of fuel-element materials should meet the operating characteristics of the reactor, such as temperature, radiation, mechanical instability produced by structural loads, vibration, and thermal stresses.

3. The materials selected should be easily fabricable into usable shapes.

In the fabrication of optimum fuel elements for power reactors, the fabricator is governed in his choice of fabrication methods by the metallurgical properties of the uranium core and cladding materials chosen. This will be illustrated in the following discussion of various methods of fabricating fuel elements.

2. METHODS FOR THE MANUFACTURE OF URANIUM AND HIGH URANIUM ALLOY PLATES CLAD WITH ZIRCONIUM AND/OR ZIRCONIUM ALLOYS

Flat-plate type fuel elements for water-cooled power reactors must survive a long lifetime and have a high integrity. At no time during their use should a leak or break in the clad or jacket allow rapid corrosion of the essentially uranium core, resulting in contamination of the cooling water and swelling of the fuel plate. If such a rupture should occur, there should be ample time to schedule a shutdown of the reactor to replace the faulty fuel element. The resulting objectives then are: (1) to produce a plate of pure uranium that is completely clad with zirconium or zirconium alloy and has no known defects and/or (2) to produce a plate of corrosion-resistant uranium alloy clad with zirconium or zirconium alloy. The choice of zirconium vs. a zirconium alloy for the cladding material depends not only on the corrosion rates of the two at the operating temperature of the water but also on their fabrication properties as related to the fabrication properties of the uranium or uranium alloy core. The core alloys considered are pure uranium clad with zirconium and uranium-zirconium-niobium alloys clad with Zircaloy-2. Zirconium and Zircaloy-2, as clad materials, form good alloy systems with the core alloys, diffusion weld to themselves readily, and can be readily welded by shielded arc welding.

The cladding techniques investigated were designed to produce plates of uranium or high uranium alloys clad with zirconium or Zircaloy-2 on all surfaces and with the jacket completely bonded to the core. Further objectives were to produce a flat-plate type fuel element having high bond strength, uniform dimensions, uniform clad thickness, and a flawless clad. Basically, the jacketing of the core alloy is accomplished by enclosing the uranium alloy core in a can of the jacket material to form a composite billet. The composite billet is further enclosed in a steel can to protect the clad material from the atmosphere and is hot rolled into a flat plate.

2.1 Zirconium-clad Uranium Plates

The first experiments at Argonne National Laboratory were initiated to develop techniques for producing plates of pure uranium clad on all surfaces with pure zirconium. To establish a composite billet design, it was necessary to perform some preliminary investigations to understand the effect of contamination on bonding surfaces and to settle on a type of billet geometry to be used. It was brought out that oil, water films, and other surface contaminations prevent metal-to-metal contact and interfere with bonding. Furthermore, the presence of active gases, particularly of air, which forms oxides, hydrides, and nitrides with uranium and zirconium, is undesirable. Unfortunately the presence of surface contamination on metal cannot be completely avoided. For the commercial manufacture of large clad plates, it would be practical to tolerate a certain amount of contamination in the composite billet interfaces and to attenuate the effect by resorting to reduction by rolling or by diffusion of contaminants into the core metal or clad metal.

(a) Effect of Billet Atmosphere on Bonding. A preliminary investigation was undertaken to obtain a practical evaluation of the effect of contaminants on the metal interfaces. The preliminary composite billets were of the type shown in Fig. 1. The billet consisted of a uranium core, $1\frac{3}{4}$ in. by 5 in. by 1 in., enclosed in a zirconium jacket which was assembled about the core without welding, except as noted. The billet was then placed in a steel can to protect the zirconium during heating. The cans were made of C-1020 steel and were fitted with a tube at each end to facilitate evacuation at one end and pressure measurement at the other end (Fig. 2). The design of these billets was based on a proposed reduction of 90 per cent in rolling. All the billet surfaces were carefully cleaned before the parts were assembled into the can. The billets were evacuated to various degrees, heated to rolling temperature, cooled, opened, and examined for contamination of the metal surfaces.

Results from this series of billets are given in Table 1. Billet 1, which was evacuated but not outgassed before sealing, developed considerable scale on the metal surfaces during heating. Outgasses from the steel can were probably responsible for the scale. Billet 3 was evacuated and outgassed during heating. Subsequent heating did not develop noticeable contamination. It is worth noting that the increased interface spac-

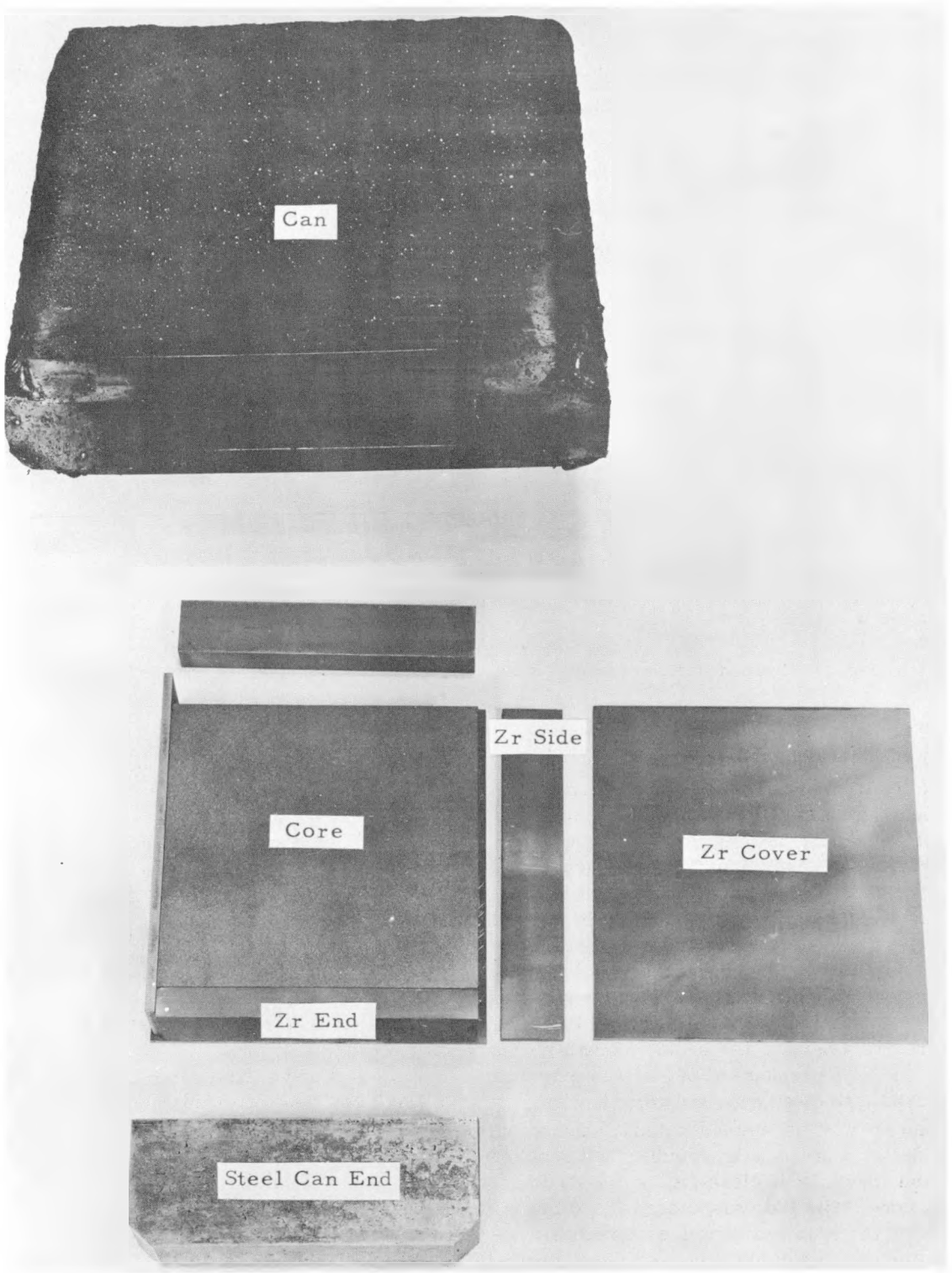

Fig. 1 — Components of a modified picture-frame type billet ready for assembly.

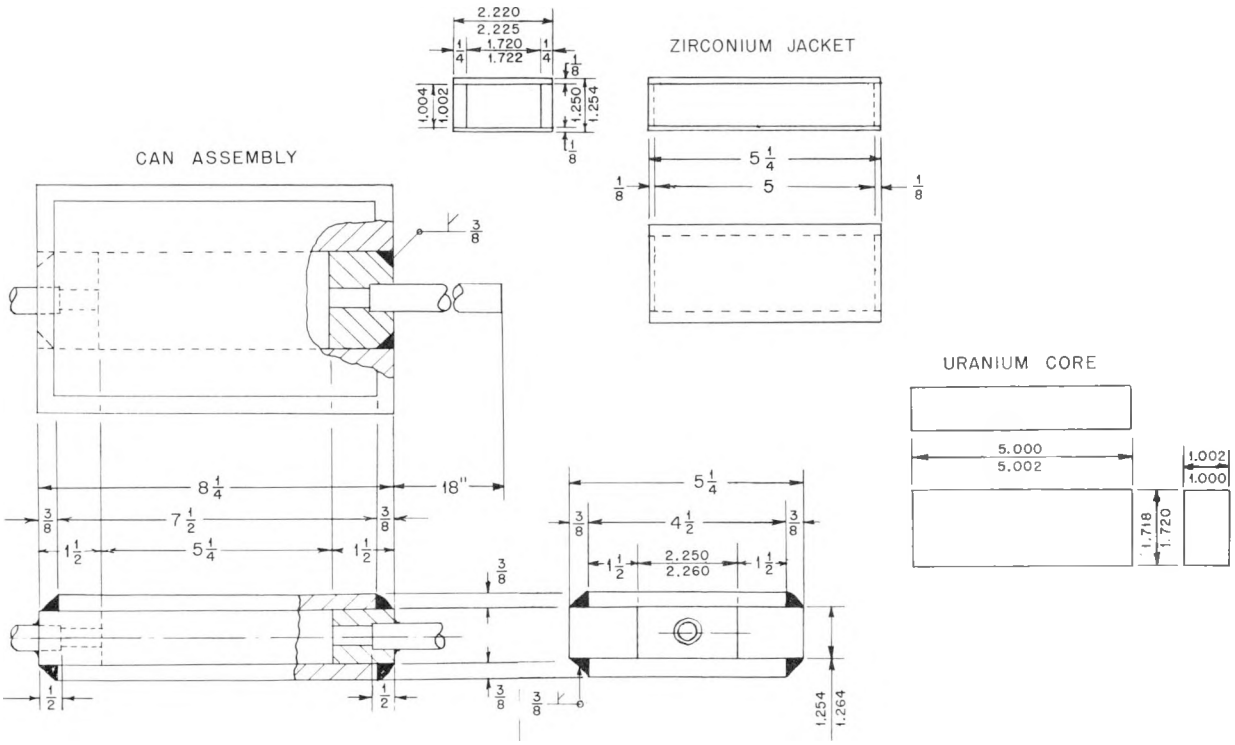

Fig. 2—Modified picture-frame billet assembly. All dimensions are given in inches.

ing, 0.008 in. to 0.030 in. for billets 1 and 3, respectively, improved the evacuation rate without heating; however, 72 hr was required for evacuation during heating for outgassing. Since the uranium was melted and cast in vacuum and the zirconium in inert atmosphere, the steel in the can was the only likely source of the amount of outgassing indicated by the pressure measurements and surface contamination. The steel can material in billet 13 was vacuum annealed for 6 hr at 800°C before assembly. The time required to evacuate the billet, canned in this steel, to 200 μ pressure at 800°C was only 3 hr compared with three days for billet 3.

Billet 2 was assembled without evacuation. This billet was made by welding a zirconium box and inserting a close-fitting polished uranium core. The box was closed by welding a cover on the open end. It was assumed that this arrangement resulted in a sufficient seal to prevent outgasses from the can from reaching the bond interfaces and forming contamination. The estimated 0.004-in.-thick layer of air entrapped in the billet would be the only source of contamination to interfere with bonding. After being heated, the billet was opened and inspected. The zirconium surfaces were clean and bright, but the uranium was uniformly coated with a very thin layer of gray powder, sufficient to be noticeable on the tip of the finger after wiping the core from end to end. It was observed that the amount of contamination developed in the unevacuated sealed billet was not significantly greater than that developed in the evacuated billet 13.

Billets 5 and 6, duplicates of the unevacuated billet 2 and the evacuated billet 13, respectively, were assembled for rolling. These billets were rolled under identical conditions, and the plates were tested. Metallographic and bending tests indicated that bonding between zirconium and uranium had been obtained in both plates. In corrosion testing, the plate from the unevacuated billet 5 survived 286 hr of exposure in water at 250°C. The plate from the evacuated billet 6 failed at the zirconium-zirconium bonds

Table 1 — Effect of Internal Billet Atmosphere on Bonding of Zirconium to Uranium

Billet No.	Can material	Notes on internal billet atmosphere*	Accumulated billet interface spacing on each axis, in.	Zirconium-uranium surface condition after disassembly
1	C-1020 steel	Evacuated 20 min to 500 μ; 24 hr to 25 μ; heated to 845°C, 1 hr	0.008	U: almost covered with fluffy black scale Zr: almost covered with black and white scale
3	C-1020 steel	Evacuated 30 min to 5 μ; 14 hr to 1 μ; max. pressure during heating, 200 μ; total heating time at 845°C, 72 hr	0.030	U: Zr: both were metallic bright
13	C-1020 steel, vacuum annealed	Evacuated 5 min to 50 μ; max. pressure during heating, 200 μ; heating from 400 to 850°C in 3 hr	0.010	U: slightly scaled at center Zr: unaffected
2	C-1020 steel	Not evacuated; zirconium jacket sealed by heliarc welding before assembly into steel can; heated to 800°C, 1 hr	0.008	U: uniformly covered with a very thin gray powderlike deposit Zr: unaffected
5	C-1020 steel	Not evacuated; zirconium jacket sealed by heliarc welding before assembly into steel can; heated to 840°C	0.008	Rolling with 10 to 1 reduction produced bonding of indicated tensile strength of the order > 20,000 psi
6	C-1020 steel, vacuum annealed	Evacuated; billet sealed at 10 μ; heated to 840°C	0.008	Rolled with 10 to 1 reduction; metallographic examination of the plate indicated bonding equal to 5; corrosion tests in 170°C water produced corrosion failures which appeared to originate in the zirconium-zirconium interface at the edges of the plate

*Evacuated billets were connected to a vacuum system at 10^{-5} mm Hg pressure. After the lengths of time noted, the recorded pressures were observed with a thermocouple gauge installed in the end of the billet farthest from the pumping system.

at the plate edges in less than 24 hr at 170°C (see Table 3).

It was concluded that further improvement of the evacuation procedure would require gas-free steel for cans or evacuation of the zirconium jacket after sealing. Further development of a cladding process without billet evacuation seemed to be justified. Such a process offered a promising method of producing serviceable plates with a minimum of development and manufacturing problems.

(b) Investigation of Billet Shapes. In order to facilitate bonding without prior evacuation, the minimum practical interface spacing in the billet is required, regardless of the design selected. This requirement had an influence on billet design. Two billet shapes seemed to offer the most promise: rectangular sections, as in picture-frame and sandwich billets, and cylindrical billets.

Cylindrical billets, shown in Fig. 3, have the advantage of extreme simplicity of assembly.

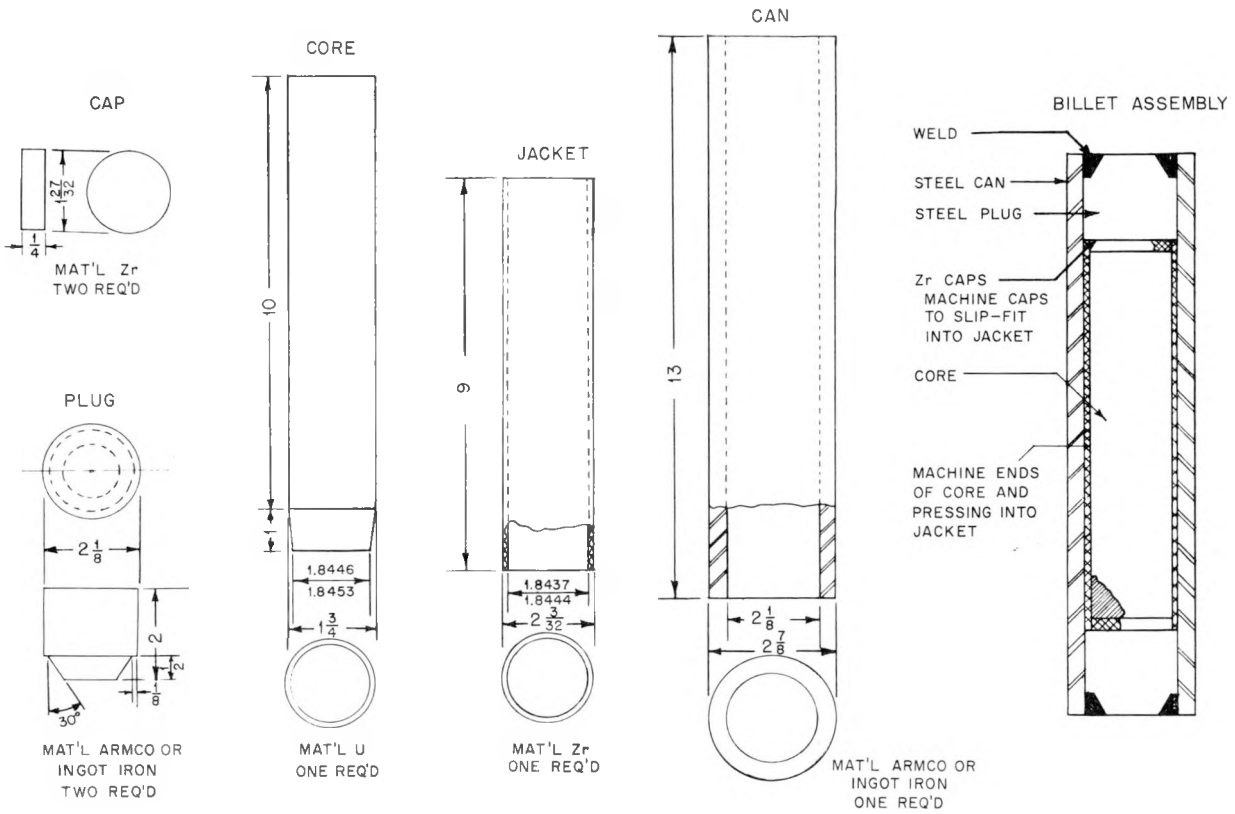

Fig. 3 — Cylindrical billet assembly. All dimensions are given in inches.

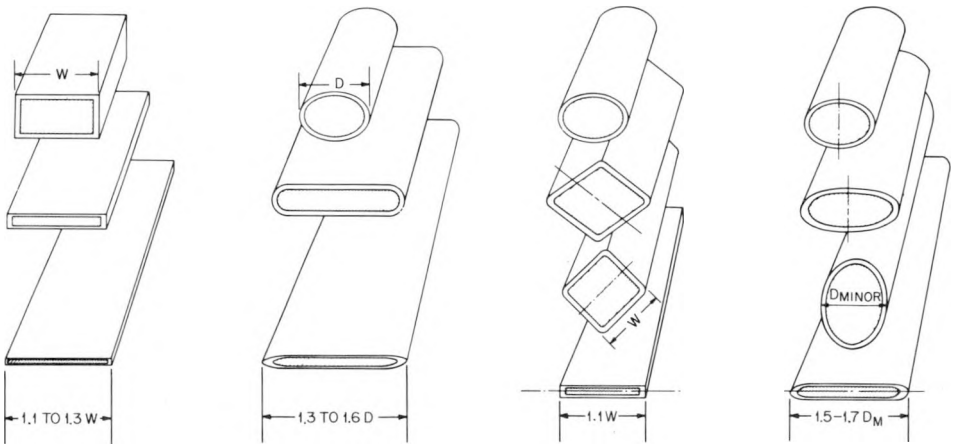

Fig. 4 — Steps in producing zirconium-clad plates from flat billets and from cylindrical billets.

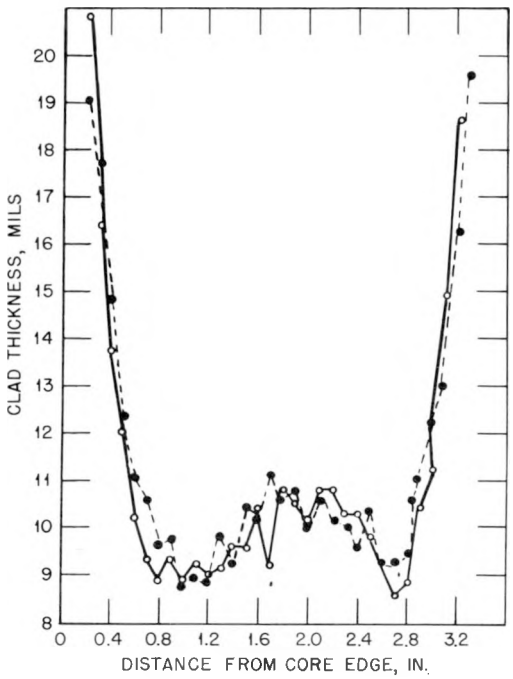

Fig. 5—Cladding thickness of a cylindrical billet rolled directly between flat rolls. Average clad thickness based on: 80 per cent of width, 10 mils; average deviation, 7.3 per cent; and maximum deviation, 22 per cent.

Welded tubes were used for both the steel can and the zirconium jacket, and the cores were made by machining and pressing into the zirconium jacket. Zirconium plugs were fitted into the ends and welded, and the fabricated jacket and core were assembled into a steel can. A fundamental objection to the cylindrical billet seemed to be the poor probability of obtaining a bond near the edges of the plate; however, variations on conventional flat rolling of cylindrical billets seemed to promise some advantages.

A series of exploratory cylindrical billets were assembled for rolling. The first of these billets was rolled directly to a flat plate. In Fig. 4 the progress of the reduction, which is straightforward, is shown schematically. It may be noted that the spread is considerable, amounting to about 50 per cent of the original diameter. Examination of the cladding on one plate rolled directly to a flat plate confirmed the suspicion that bonding would not be obtained near the edges. Distribution of cladding on this plate is shown in Fig. 5.

In order to initiate bonding in those locations on the billet which upon final rolling would become the edge of the finished plate, several billets were rolled in open-square passes, as shown in Figs. 6 and 7, and several in oval-edge oval sequence passes. Both these procedures resulted in plates bonded all the way around the section, as judged on the basis of metallographic examination. In the case of the square passes, however, it was found that the corners were pinched and that the cladding on the flat sides was extremely irregular in thickness (Figs. 6 and 7). Cladding thickness irregularities persist through flat rolling (Fig. 8). In the case of oval-edge oval procedure, it was found that irregularities in cladding thickness existed around the entire perimeter of the core. Considerable difficulty was encountered in attempts to develop oval-edge oval reductions that would not overfill the passes during rolling.

Flat or picture-frame billets require more parts than cylindrical billets, and it was felt that billet fabrication would be proportionately more complicated. The problems resulting from complex design, however, could be resolved in production. Referring to Fig. 4, it will be noted that the spread resulting from rolling cylindrical billets to plate is greater than for rectangular billets. The rectangular sections can be flat rolled quite accurately, and, by variation of the can design and rolling procedure, it is possible to reduce lateral spread in rolling to a very low value.

The two types of can which were used in this investigation are shown in Fig. 9. From a study of the plate widths produced in these designs, it is apparent that the two-piece can of part b of Fig. 9 is superior in restraining spread. Cans were removed from the hot rolled billets either by shearing the edges off and separating the balance of the can or by pickling the can off with dilute nitric acid. Neither of the can designs used presented a problem in decanning. Figure 10 shows a typical decanning operation in which the ends and edges of a hot rolled billet were sheared to remove the weld and the steel cover plates removed to expose the zirconium-clad uranium plate.

(c) Flat-billet Assembly Method. A method of composite billet assembly was devised to

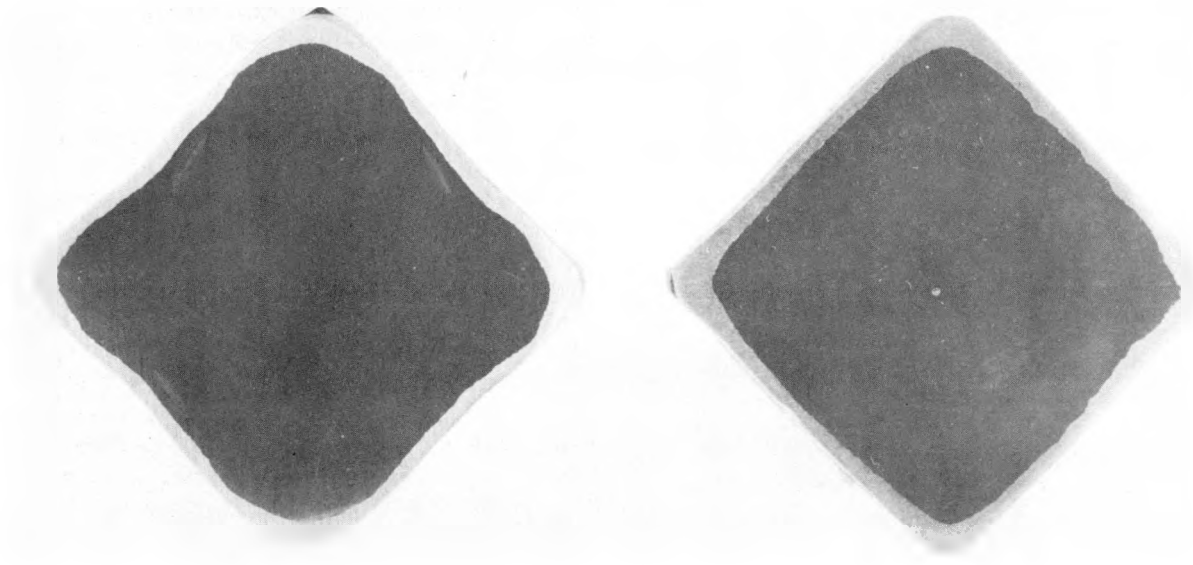

Fig. 6 — Macrosection cylindrical billet 38 after rolling in open-square passes to $1\frac{1}{2}$ by $1\frac{1}{2}$ in. bar. The diamond shape noted in Fig. 7 is less pronounced because the bar was passed repeatedly in the last groove, rotating the bar 90 deg and opening the mill slightly for each pass. (Magnification approximately $1\frac{1}{3}\times$.)

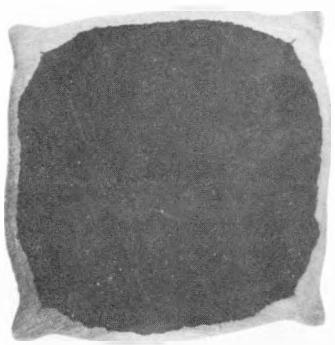

Fig. 7 — Macrosection of cylindrical billet 37 after rolling in open-square passes to 1 by 1 in. bar. The slight diamond shape conforms to the shape of the roll groove. Note folds in each corner and irregular distribution of zirconium. (Magnification approximately $1\frac{1}{2}\times$.)

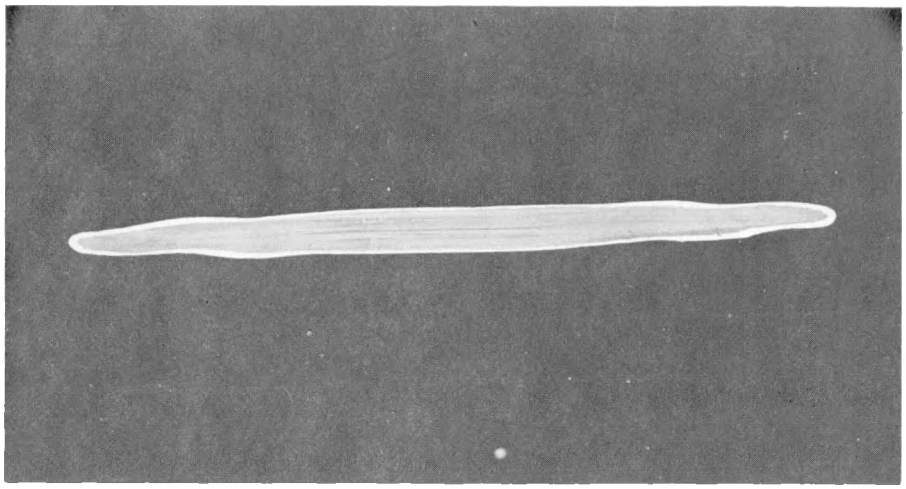

Fig. 8 — Macrosection of a piece of flat rolled plate from billet 37, which was previously rolled to a 1 by 1 in. square in open-square passes (see Fig. 7). Note the occurrence of irregular cladding distribution. (Magnification 3×.)

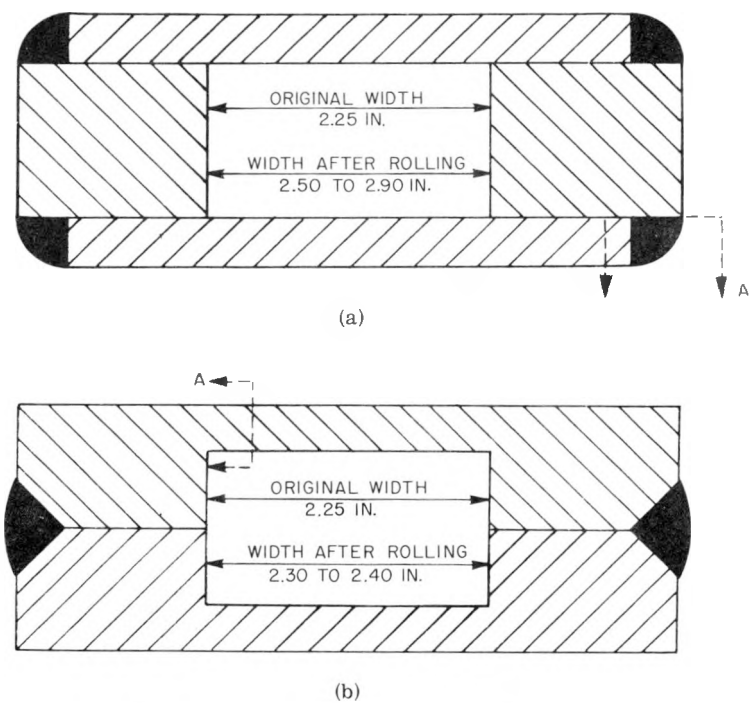

Fig. 9 — Steel can designs for flat or modified picture-frame billets. (a) Cross section of fabricated can. This design depends upon the strength of the section "A" of weld metal at the sides of the billet to restrain lateral spread in rolling. (b) Cross section of two-piece machined can. This design depends upon the strength of the section at "A" to restrain lateral spread in rolling and is superior to the fabricated can in this respect.

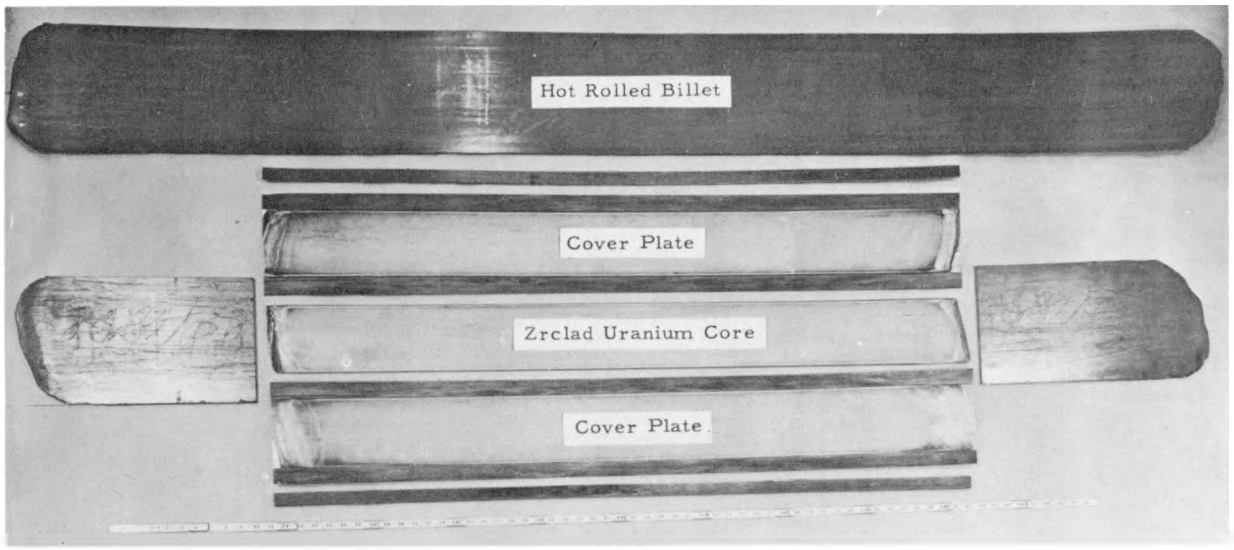

Fig. 10—Decanning of hot rolled billet.

minimize the air gap between the core and cladding. This method is known as the "M.P.F.P.W." (modified picture frame billet, with the billet assembled in a press before the zirconium jacket is welded). The uranium core and zirconium end plugs were machined to tolerances of ±0.005 in., and the zirconium covers and sides were sheared from cold finished zirconium sheet. Billet components are shown in Fig. 11. The zirconium parts were then assembled about the uranium with the ends and sides clamped tightly against the core.

The assembled billet was placed in a hydraulic press with water-cooled copper plates in contact with the billet covers (Fig. 11). Pressure on the billet during assembly was held at 2 tons or more per square inch. As pressure was increased on the assembly, the zirconium cover plates deformed to conform to the surfaces of the core, end plugs, and sides. While under pressure the billet joints were welded with an inert-gas-shielded arc to seal the billet. Cooling of the billet surfaces with chill plates reduced the extent of heat effect in contaminating the interfaces at the edges and also reduced contamination of the weld metal. Contamination of the weld metal is of considerable importance from the standpoint of corrosion.

(d) Billet Processing. Data on rolling variables obtained from rolling flat billets are given in Table 2. All the processing variables affect one another and affect several of the characteristics of the finished plate. Testing results given later in this report established that bonded cladding can be obtained by rolling the billet with a 90 per cent reduction at 635°C. A preliminary 25 per cent reduction at 840°C followed by reduction to a total of 90 per cent at 630°C also develops a bond.

A study of a number of plates indicates that variation of rolling speed, rolling temperature, roll diameter, etc., results in reduction effects similar to effects observed in conventional rolling processes. However, cladding thickness varied significantly.

A series of exploratory billets were rolled to various partial reductions to determine at what stage in processing the cladding thickness variations originated. Cladding distributions for billets rolled to a reduction of 30 and 55 per cent in the gamma temperature range are shown in Fig. 12. The maximum deviations from average thickness are about 14 and 10 per cent, respectively. A billet rolled to 30 per cent reduction in the gamma temperature range plus additional reduction to a total of 75 per cent in the alpha temperature range had a maximum deviation of 23 per cent from average cladding thickness as shown in Fig. 12. These results seem to indicate that wide variations in cladding thickness were initiated during the alpha rolling.

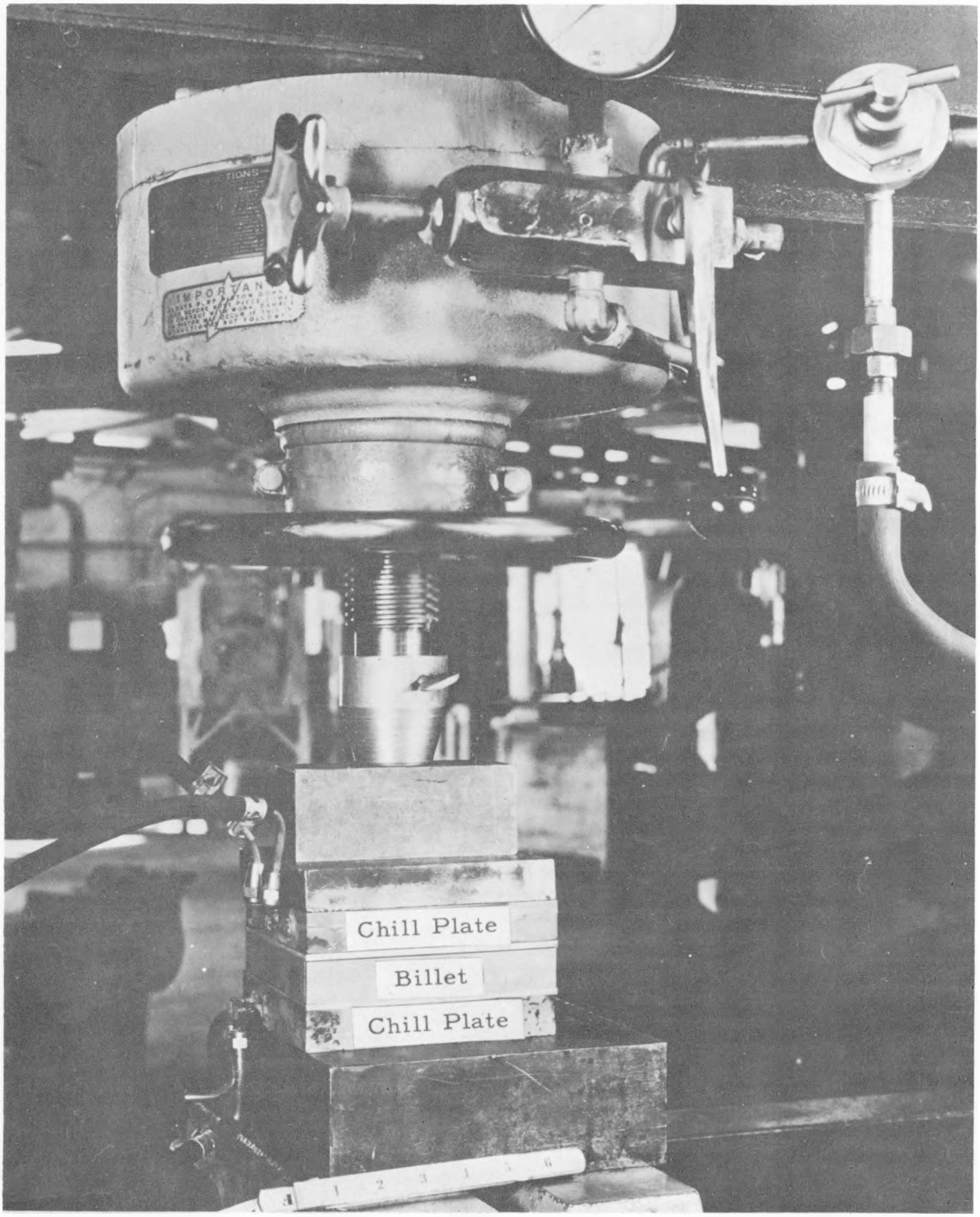

Fig. 11—Components of modified picture-frame type billet assembled in press ready to be welded with inert-gas-shielded arc.

Table 2—Data from Exploratory Rolling of Flat Billets

Billet No.	Billet design*	Preparation		Cladding billet, reduction per pass, %	Total accumulated reduction, %	Rolling temp., °C	Passes per reheat	Bonding evaluation	Cladding surface and dimensions	Significant variable	Remarks	Results
		Clad	Core									
20	M.P.F. P.W.	V.B.†	M.P.‡	1.5 11.0 to 15 10.0 15.0	6 78 84 90	840 635 840 635	1 3 1 3	A§	B¶	0.002-in. interface; jacket assembled on core with pressure of 2 tsi; welded between chill plates	Reduced time for assembly; welds improved	Plate of good quality but intermediate gamma rolling probably coarsened uranium
25	M.P.F. P.W.	V.B.	M.P.	2.5 to 11 15.0	21 95	840 635	1 3	A	B^+	Rolled for 0.005-in.-thick clad	0.150–0.200 in. drafts between 1.0 and 1.5 in. guage stalled mill	Plate was of good quality except for camber
26	M.P.F. box	V.B.	M.P.	2.5 to 11 10.0	21 90	840 635	1 3		B^+	Rolled for 0.025-in.-thick clad	For corrosion tests	Plate satisfactory
27	M.P.F. P.W.	V.B.	M.P.	2.5 to 11 10.0	21 90	840 635	1 3		B^+	Billet altered to provide long (5 in.) zirconium section at end	Long zirconium end to provide end seal; see corrosion testing	Plate satisfactory
28	M.P.F. P.W.	V.B.	M.P.	2.5 to 11 10.0	21 90	840 635	1 3		B^+	Rolled for 0.005-in.-thick clad	See corrosion testing	Plate satisfactory
43	M.P.F. P.W.	V.B.	M.P.	5.0 to 10 10.0	45 90	840 635	2 2		B	Ti-namel can; rolled for 0.010-in. clad for corrosion test	Ti-namel partially bonded to zirconium; see corrosion testing	Plate satisfactory

*M.P.F., modified picture-frame billet; P.W., billet assembled in press before zirconium jacket is welded.
†V.B., vapor blasted.
‡M.P., mechanical polished (equal to 120 grit).
§A, satisfactory; exhibits no microdefects, withstands cold finishing, shearing, and bending. If determined, the bond tensile strength exceeds 20,000 psi.
¶B, doubtful; no apparent defects but can be separated by bending. Tensile strength of bond less than 20,000 psi.

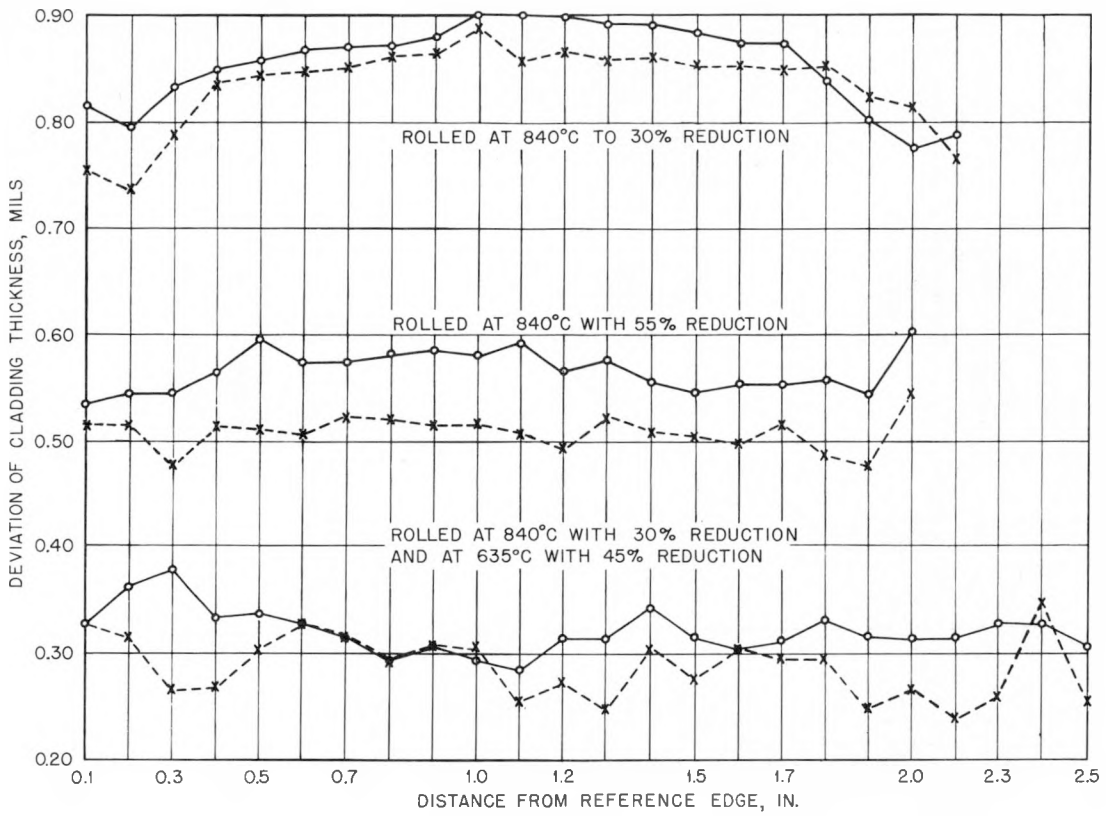

Fig. 12—Cladding distribution on both sides in a transverse section of modified picture-frame billets rolled to partial reduction.

(1) Corrosion Testing. An autoclave corrosion test is an excellent method for locating discontinuities in the cladding on uranium plates. The cladding itself is quite resistant to corrosion by high-temperature water, whereas the uranium corrodes rapidly. Defects in the cladding allow reaction between the uranium core and the hot autoclave water, resulting in rapid and very obvious damage to the plate. These tests were not intended to evaluate the corrosion resistance of the zirconium cladding but to establish the integrity of cladding edge seals and end seals.

The autoclave test consisted in exposure in static water at temperatures up to 250°C and for times up to 286 hr. All joints or closures made by welding the billet and subsequent rolling withstood corrosion exposure of at least 120 hr at 250°C.

Table 3 gives the results of autoclave corrosion tests of plates made by various techniques. In all cases the ends were cut off the as-rolled plates and further sealed by welding. With plate 5b the edges of the as-rolled plate were trimmed and rewelded. Figure 13 is a photograph of plate 5b after corrosion testing. Figure 14 illustrates the type of failure resulting from autoclaving plate 6.

The end seals on all plates that were corrosion tested were effected by shearing the ends off the as-rolled plates and exposing the uranium core, etching the core away from the clad, and sealing by welding with filler metal.

(2) Metallography. Microstructures developed at the interfaces of zirconium-clad uranium are extremely thin and difficult to interpret. Metallographic examination is valuable in establishing the uniformity of cladding and the frequency of inclusions or voids in the bond. Figure 15 shows a layer between zirconium and uranium which is interpreted to be a product of interdiffusion with a phase existing between zir-

Table 3—Autoclave Corrosion Test Results for Zirconium-clad Uranium Plates*

Plate No.	Nominal cladding thickness, in.	Special plate characteristics	Notes on end seals	Autoclave exposure and results†						
				170°C 24 hr	170°C 720 hr	210°C 24 hr	250°C 24 hr	250°C 120 hr	250°C 286 hr	330°C 24 hr
4	0.010	M.P.F. welded before rolling; hot rolled surfaces	Plate sheared to 24 in.; exposed ends were etched and sealed by welding with zirconium–3% nickel filler metal	No effect	Small amount of white corrosion product on weld seals		No change		Weld seal failed at one end of plate	Discontinued
5	0.010	M.P.F. welded before rolling; hot rolled surface	Same as 4	Weld seal failed at one end of plate			Discontinued after 120 hr at 170°C			
5b‡	0.010	M.P.F. welded before rolling; edge trimmed and rewelded after rolling; hot rolled surfaces	Same as 4	Slight red deposit on cladding	Small amount of white corrosion product plus 4 red spots on one end		No change		No change	Cladding ruptured adjoining weld on edge and peeled
6	0.010	M.P.F. billet, evacuated, not welded; depends on bonding for edge seal; hot roll surface	Same as 4	Cladding ruptured, apparently at edges			Discontinued after 120 hr at 170°C			
25	0.005	M.P.F. box type jacket welded before rolling; cold finished	Plate cut 24 in. long; one end sealed by weld technique; other end trimmed and rewelded	No effect		No effect	No effect			
26a	0.025	Same as 25	Same as 25	*No effect*			*Discontinued after 120 hr at 170°C*			
26b	0.025	Same as 25	Plate cut 24 in. long; one end sealed by welding technique; other end zirconium trimmed and tested without further preparation	No effect		No effect	No effect	Small amount of white corrosion product on welds; slight corrosion of zirconium surface		

*Plates were tested in untreated water with resistivity ranging from 350,000 to 83,000 ohm-cm. The only circulation occurred as a result of baffling and heater location in the autoclave.

†Since the purpose of these tests was to detect leakages in cladding, edge seals, and end seals, the remarks do not refer to corrosion of the zirconium unless specifically stated.

‡Welded.

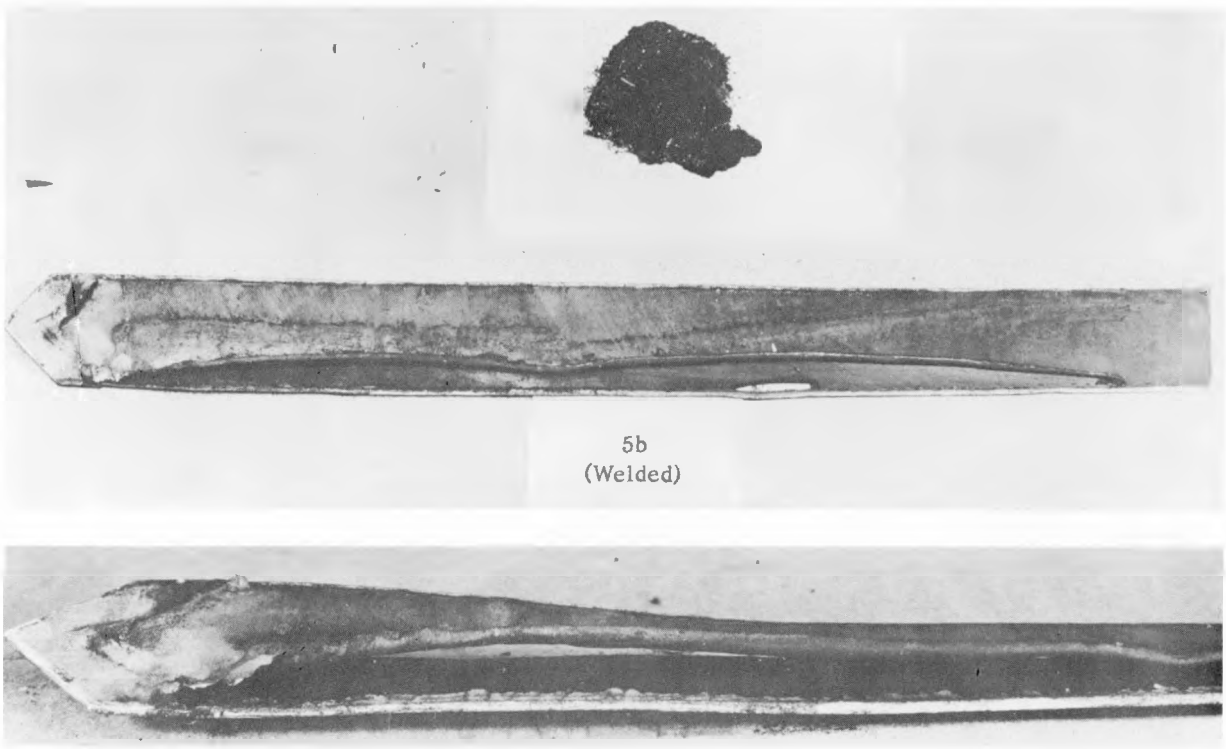

Fig. 13—Views of a plate which survived autoclave exposure for 720 hr at 170°C, plus 286 hr at 250°C, and failed within an additional 24 hr at 330°C. This plate was manufactured by the modified picture-frame technique. After rolling, the plate edges were trimmed and rewelded with inert-gas-shielded arc in air. Considering the quality of the zirconium and the methods of welding, these results might be considered encouraging.

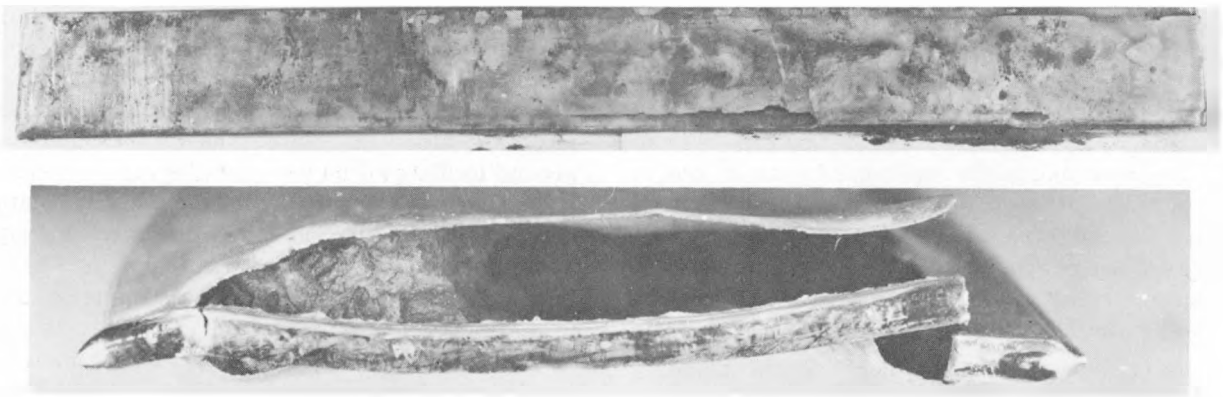

Fig. 14—Views of plate 6, which failed during an exposure for 24 hr at 170°C. This plate was manufactured by the modified picture-frame technique; the zirconium jacket was not welded before rolling, but the billet was evacuated and the can was made from vacuum annealed C-1020 steel. Failure was not typical of the end seal type failure. The conclusion was that zirconium-to-zirconium bonds were inadequate.

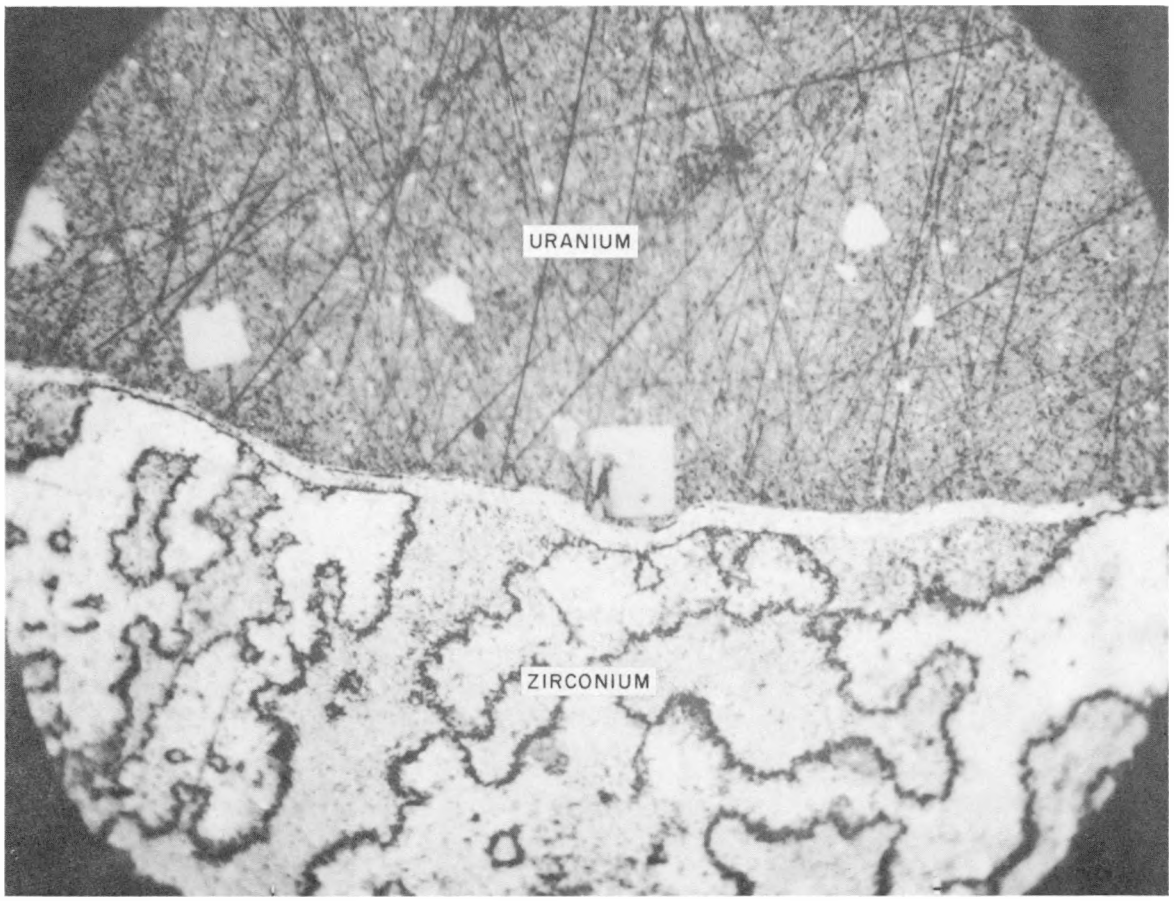

Fig. 15—Microphoto at interface in plate 79. A light etch was obtained with 5 per cent HF-$AgNO_3$. (Magnification 1000×.)

conium and the original interface on one side and between uranium and the original interface on the other. The tiny black stringers are taken to be inclusions in the interface. Discontinuities at the bond interface could be clearly defined from metallographic specimens, as shown in Fig. 16. Judgment of bonding in this investigation depended upon the occurrence of the diffusion layer and lack of voids or inclusions in the interface indicating good contact between the dissimilar metals.

Early in the development of the cladding method, considerable reliance was put on metallographic interpretation. However, experience indicated that slight variations in metallographic procedure were significant, and in some cases plates that proved satisfactory in mechanical tests were underestimated metallographically.

Metallographic measurements of cladding thickness were made on a large number of sections from a variety of plates. Plates were prepared by cutting sections at six regularly spaced intervals along the plate. These sections were ground to 600 grit on wet metallographic grinding paper and heat tinted. The measurements were made with a monocular microscope having an eyepiece calibrated to read 0.0002 in. These measurements were studied to determine the occurrence of localized and general variations in cladding thickness. Figure 17 shows a macrosection of a 5-in.-wide plate. The sections were taken at 7-in. intervals along the length of the plate and illustrate typical width and cladding thickness uniformity.

(3) Autoradiography. A majority of the clad plates produced in this investigation were sub-

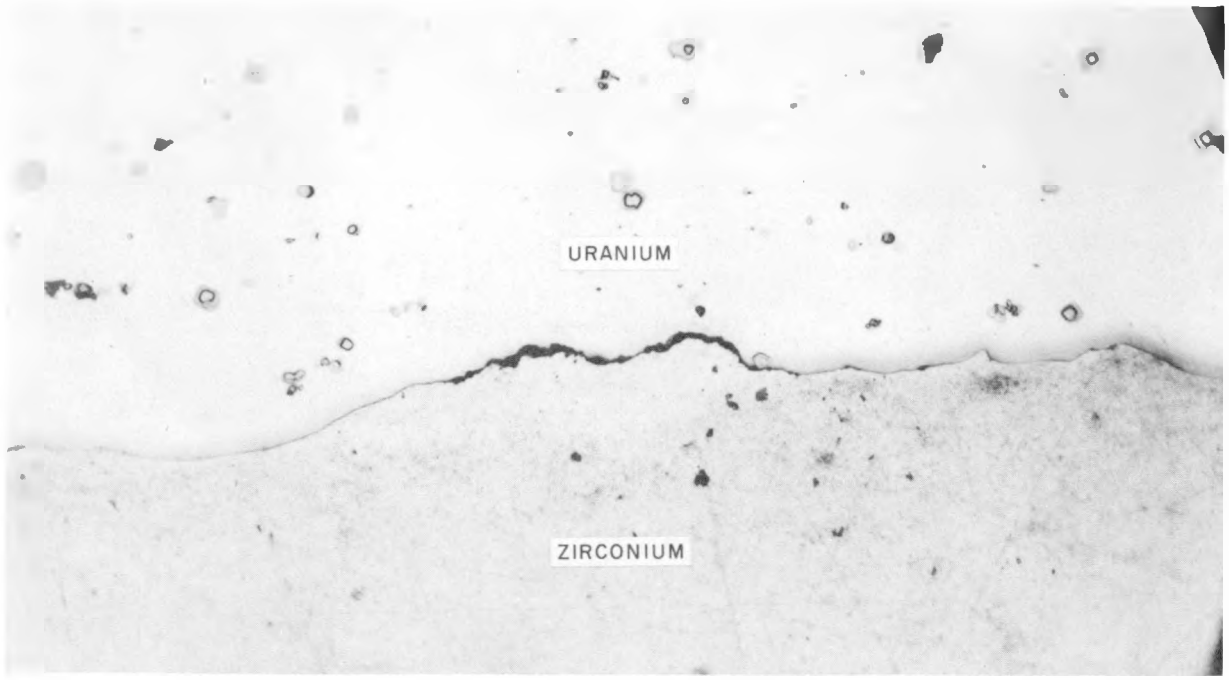

(a)

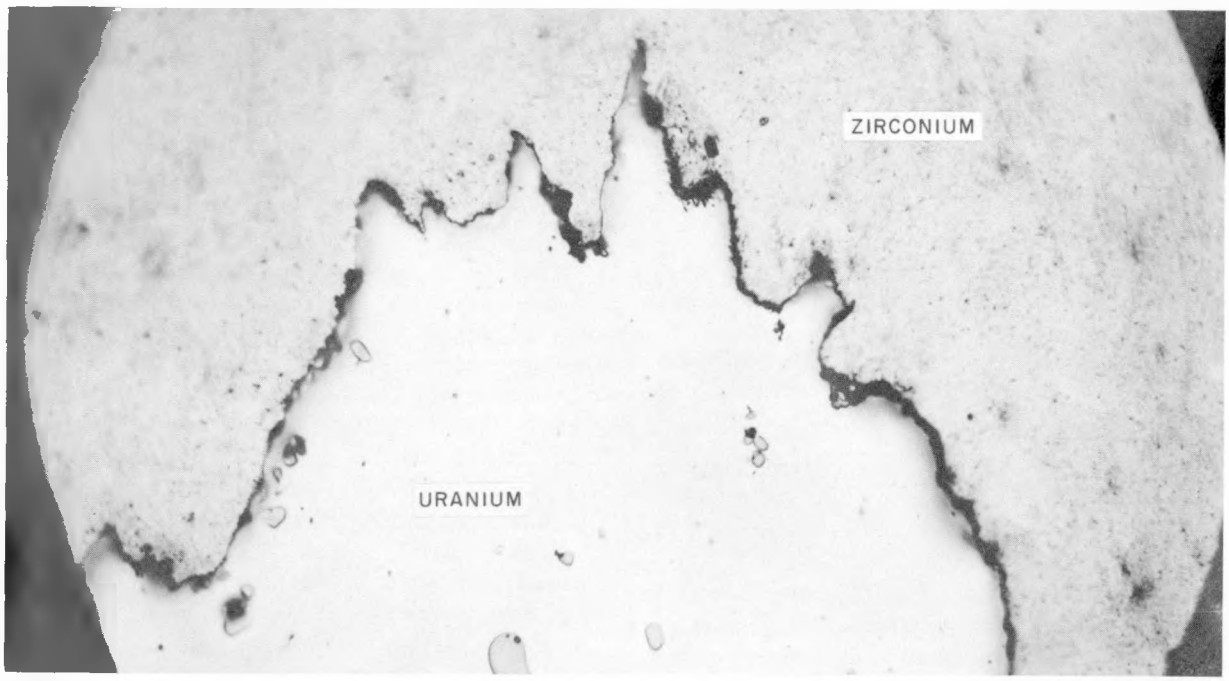

(b)

Fig. 16 — Micrographs showing voids at the bond interface on zirconium-clad plates. (a) Void near the center of a zirconium-clad plate. (b) Voids at the edge of a zirconium-clad plate. Microspecimens were electrolytically polished. (Magnification 500×.)

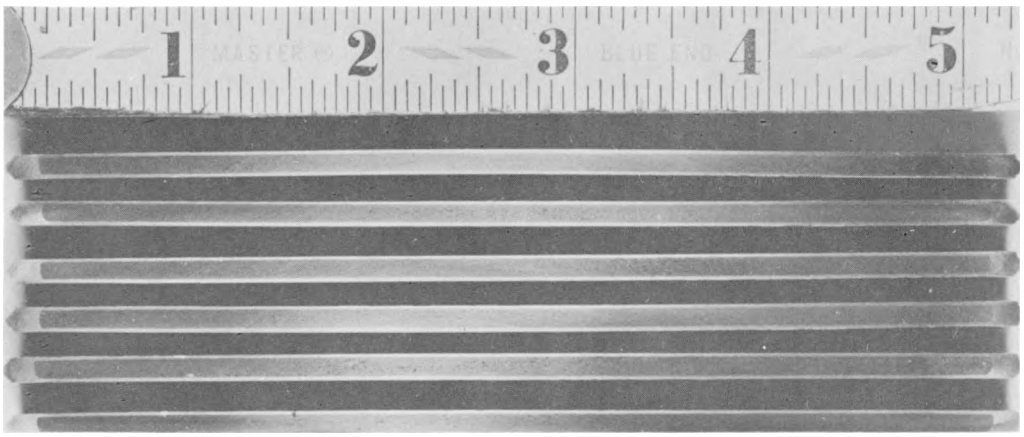

Fig. 17—Macrosections in hot rolled clad plate. Sections were taken at 7-in. intervals along the length of one plate. Notice the uniformity of width.

jected to an autoradiograph examination. Radiation emanating from the normal uranium core resulted in exposures on X-ray film resembling normal X-ray exposures. These autoradiographs proved an effective means of locating the core material relative to the edges and ends of rolled plates and also of revealing defects in the cladding, core separation or segregation, and variations in the cladding thickness.

Clad plates were placed with one side in contact with Kodak type K Industrial X-ray film. Portions of the film extending beyond the plate edges and ends were exposed with a flashlight to furnish an accurate outline of the entire plate. An exposure time of 16 to 20 hr gave a gradient contrast to the film through 5 to 20 mils of zirconium cladding.

Figure 18 shows representative autoradiograph sections which illustrate typical conditions noted in various clad plates.

(c) Conclusions. 1. It was established that the production of zirconium-clad uranium plates using the modified picture-frame technique was feasible.

2. Dimensional tolerances of the following order are possible in finished plates:

Width tolerance: ±0.030 in. in widths of 2 to 5 in.

Thickness tolerances: ±0.005 in. in thickness range of 0.050 to 0.250 in.

Cladding thickness: ±20 per cent on 0.010-in. cladding.

Bonding: estimated 99 per cent of surface area.

3. Corrosion-resistant alloys of uranium for the plate core would diminish the swelling of the fuel plate if the jacket were not perfect.

2.2 Zircaloy-2-clad Uranium (5 Wt. % Zirconium—1.5 Wt. % Niobium Alloy)

Corrosion research proved that an alloy of uranium with 5 wt. % zirconium and 1.5 wt. % niobium was more corrosion resistant to high-temperature water than pure uranium. A commercial alloy of zirconium with 1.5 wt. % tin, 0.1 wt. % iron, 0.1 wt. % chromium, and 0.05 wt. % nickel became available as cladding material for high-temperature water reactors. The hot working properties of the uranium-zirconium-niobium alloy over the temperature range from 775 to 900°C closely resemble those of Zircaloy-2 which make it particularly amenable to roll cladding. From the results of the roll cladding of unalloyed uranium with zirconium into flat-plate type fuel elements, it became apparent that end seals produced during the rolling were possible.

The objectives of this development were to produce flat-plate type fuel elements, $\frac{1}{4}$ in. thick by 3 to 4 in. wide by 50 in. long, consisting of the uranium-zirconium-niobium alloy completely clad and bonded on all surfaces with Zircaloy-2 and with rolled-in end seals.

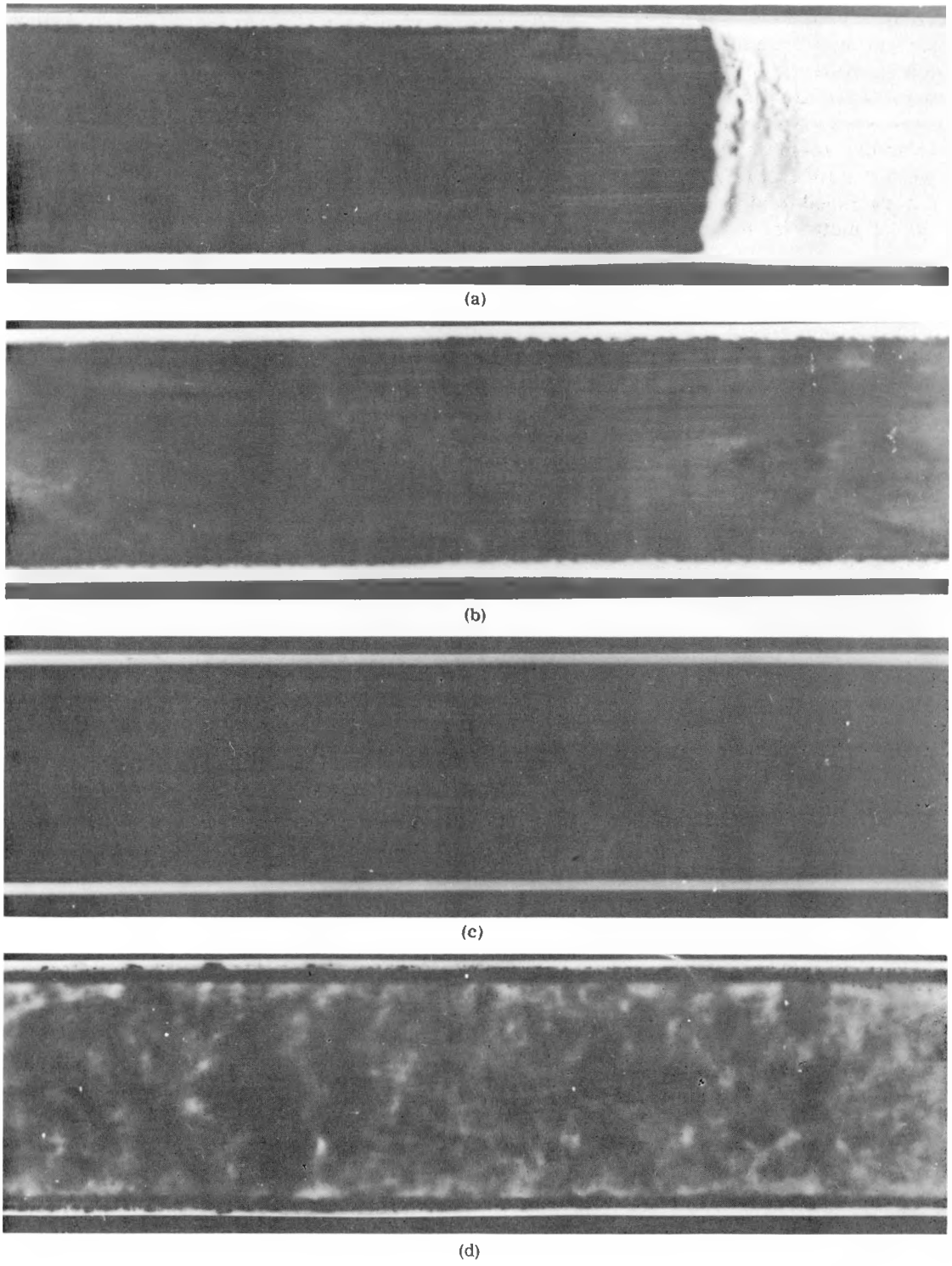

Fig. 18 — Autoradiographs showing typical defects in clad plates. (a) Irregular core end. (b) Irregular deformation of core. (c) Periodic variation or ripple effect in plate. (d) Segregation of core material and edge bond defects.

The plate fabrication steps were performed with conventional equipment and methods, such as welding, rolling, and shearing; machining operations were minimized; and dimensional tolerances were not exacting.

The cladding components, as shown in Fig. 19, were welded into a billet. The alloy core was cast and machined to size by removing 0.020 to 0.030 in. of metal from each face. The ends of the core were preshaped to eliminate surface irregularities at the ends of rolled plate, which occurred during rolling whenever there was an abrupt transition from the core to the end plug. Tests of preshaped cores with both concave and convex ends and various radii and with tapered ends and 60 to 120 deg included angles revealed that derogatory end effects were avoided with end tapers of 60 to 100 deg. Acceptable length of core tapers in finished rolled plates resulted from preshaped ends of 90 to 100 deg. Surface contamination was removed by vapor blasting the core with 320-mesh Al_2O_3 grit before billet assembly.

Zircaloy-2 cover plates were rolled and sheared to size. Side strips and shaped end plugs were machined from rolled plate and bar stock. All Zircaloy-2 components were cleaned before assembly by vapor blasting, followed by pickling in boiling concentrated nitric acid containing 0.5 to 1.0 per cent hydrofluoric acid, which produced a bright surface with no apparent fluoride deposits on the metal.

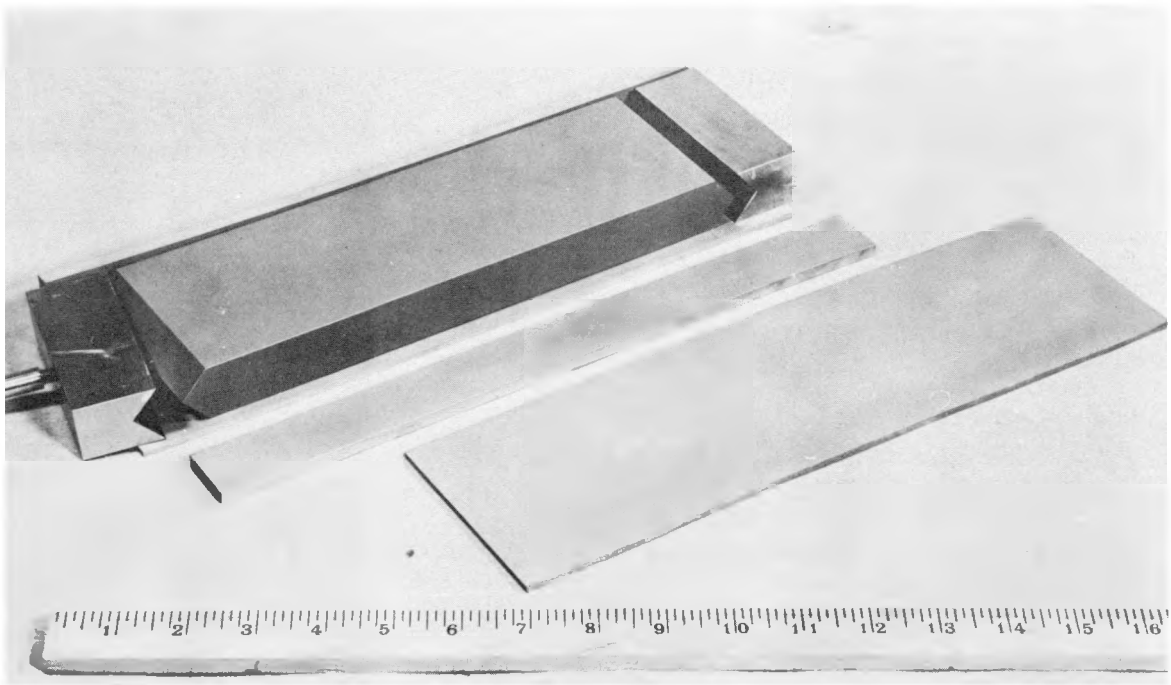

Fig. 19—Cladding billet assembly. Zircaloy-2 cover plates, side plates, and end plugs ready to be assembled around the machined uranium alloy core.

Owing to the positive differential expansion of 0.20 in. per inch between room temperature and 850°C for the alloy core with respect to the cladding, an expansion allowance was made for the core in the billet assembly. Billet welds without this differential expansion allowance were found to crack when heated to the roll cladding temperature, with subsequent contamination of the core and imperfect bonding.

The assembled billet was positioned between water-cooled copper platens on both horizontal and vertical hydraulic rams. A minimum pressure of 4 tons/sq in. was applied to ensure proper contact of the Zircaloy-2 components.

Fig. 20 — Welded cladding billet in steel sheath. The welded billet is sealed in a steel sheath to prevent surface contamination of the billet while rolling.

The gap between core and clad was purged with an inert gas during welding. Argon or helium was introduced through a tube screwed into one end of the billet. Gas flow around the core displaced the entrained air, which would have otherwise contaminated the interface during welding. Welding was done with an inert-gas-shielded arc at 350 amp using a $\frac{1}{8}$-in.-diameter tungsten electrode to obtain good weld penetration. The purging connection was removed, and the inert gas was evacuated after welding. The billet was sealed in vacuum with a zirconium-tipped Zircaloy-2 screwed plug. The welded billet was then jacketed in a steel sheath which protected the billet from excessive surface contamination during heating and rolling. Sheath jackets of 1020 plain carbon steel, as shown in Fig. 20, furnished satisfactory protection.

Incipient bonds between core and clad and clad and clad were observed with 50 per cent reduction at rolling temperatures as low as 775°C. Since increased reductions on rolling permitted the use of more compact cladding billets with a corresponding decrease in the cost of billet preparation, the optimum reduction on rolling was established at 80 per cent. For thinner or longer fuel plates reductions of 90 per cent or greater would be feasible. Although clad plates could be rolled at temperatures as high as 900°C, plates rolled at 850°C were more

uniform and less sensitive to temperature variations. Reductions of 12 to 20 per cent per pass were taken while rolling. Figure 21 shows the uniformity of clad and core of a plate roll bonded at 850°C.

The dimensional tolerances were maintained at ±0.002 in. on thickness, ±0.010 in. on width, and ±0.250 in. on length. Plates were designed with approximately 1 in. of excess Zircaloy-2 at each end, which was removed in trimming the plate to the desired length. Figure 22 shows the rolled end seal and tapered alloy core.

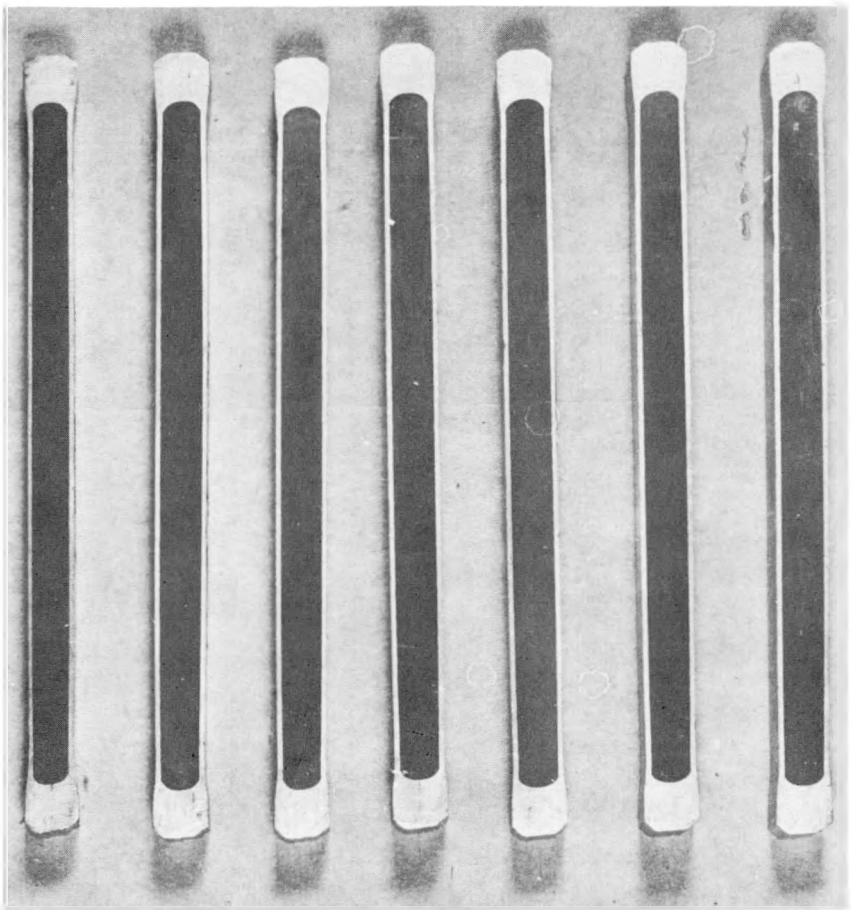

Fig. 21 — Clad fuel plate sections. Transverse sections cut at seven equally spaced intervals from the length of a roll clad fuel element. Same size.

Measurements of clad-to-core bond strength taken along the faces, sides, and tapered ends of clad plates gave an average value of 38,000 psi in tension. Cladding variables, such as reduction, rolling temperature, or heating time, do not show any appreciable effect on bond strength once a bond has been established. The presence of contamination, such as inclusions or oxides, at the interface reduced the bond strength as much as 85 per cent. The bond strength dropped to an average of 17,400 psi on clad plates that were heat-treated for 15 min at 850°C and water quenched. Samples from the same plates quenched and aged 45 min at 425°C had an average bond tensile strength of 22,800 psi.

Although the hardness of the core alloy decreases and its ductility increases as a result of gamma quenching from 850°C, loss of ductility at the clad-to-core interface makes gam-

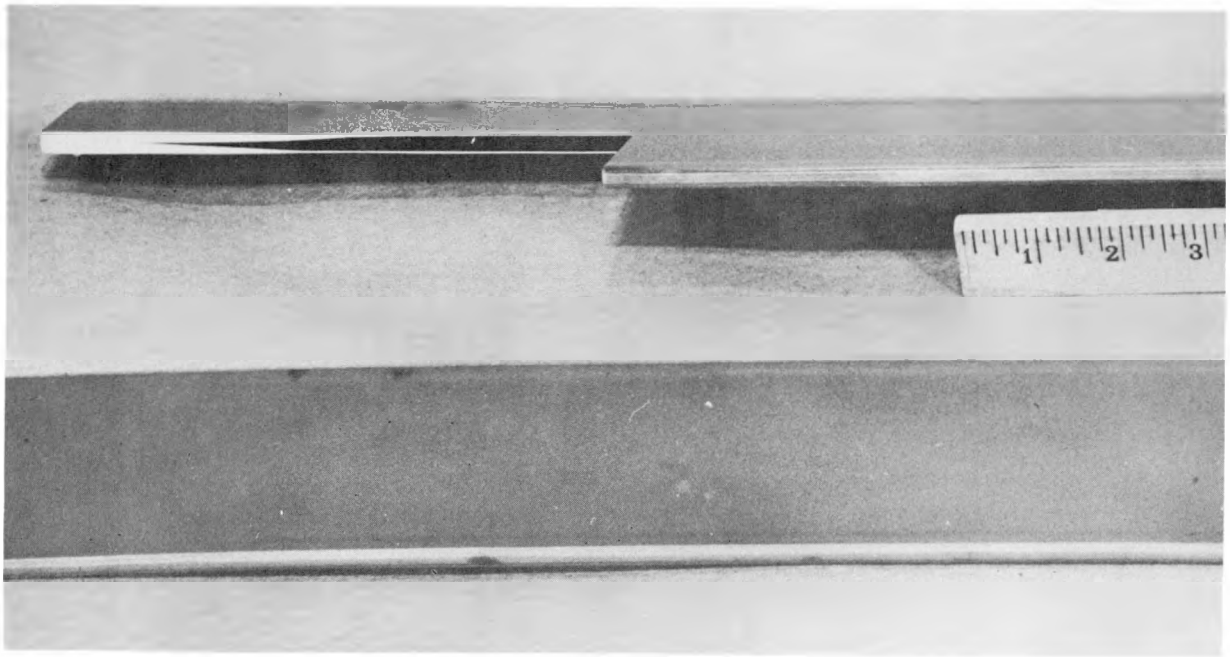

Fig. 22—Section at end of clad fuel plate. Longitudinal section of clad plate at one end showing rolled end closure with tapered core end.

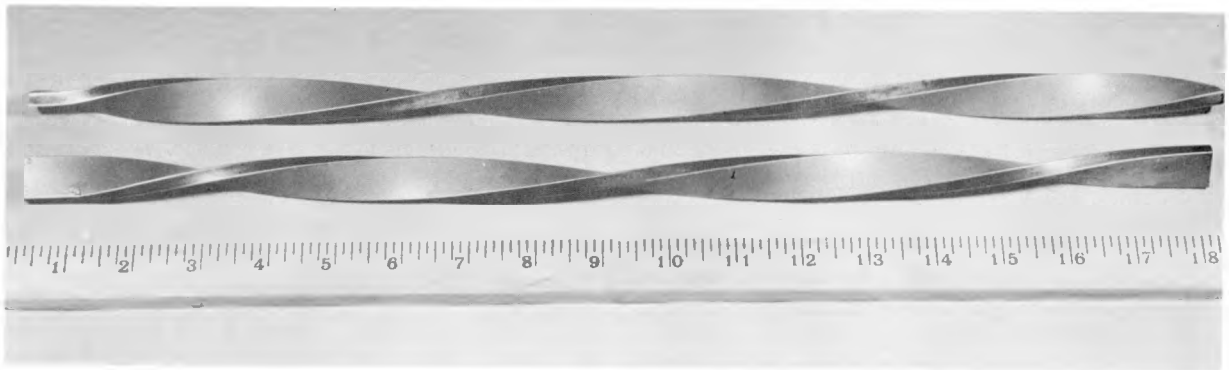

Fig. 23—Twisted plate test specimens. Twisted specimens cut from a non-heat-treated ¼-in.-thick clad plate showing ductility of Zircaloy-2 cladding, alloy core, and clad-to-core interface. Specimens twisted at room temperature 360 deg per foot.

ma quenched clad plates difficult to form. Strips 1 in. wide cut longitudinally from a rolled non-heat-treated plate were readily formed cold by twisting. These strips, shown in Fig. 23, were twisted 360 deg in a 12-in. length with no evidence of separation or cracking at the clad-to-core interface. The total reduction on rolling had little effect on the amount of diffusion, but rolling temperatures and time at temperature after the final pass resulted in considerable diffusion latitude. Figure 24 shows the bond line between the clad and core.

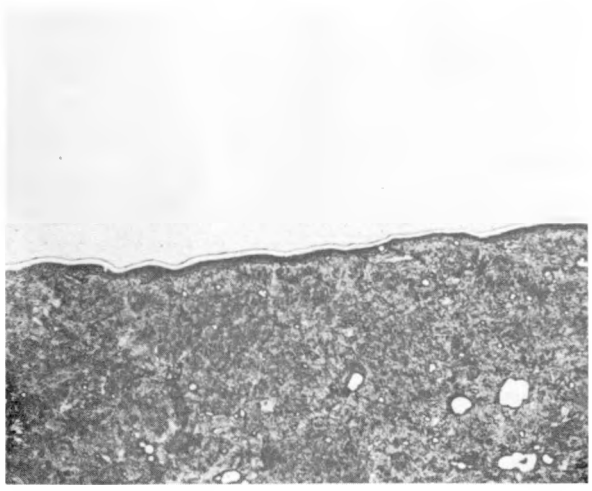

Fig. 24 — Bond line between Zircaloy-2 cladding and uranium alloy core. (Magnification 250×.)

A reliable bond between Zircaloy-2 and Zircaloy-2 along the edges and at the ends of rolled plates proved more difficult to reproduce. Metallographic examination, as shown in Fig. 25, of many bond interfaces from some of the first groups of plates rolled, disclosed small inclusions at the mating surfaces. These inclusions were found to be both intergranular and transgranular in nature. Only contamination of the mating surfaces could be the cause of these defects. Steps taken to minimize or eliminate these defects included careful cleaning of hot rolled strip by the substitution of vapor blasting for sand blasting, use of Al_2O_3 grit for vapor blasting, thorough pickling of vapor-blasted sheet to remove surface asperities, welded assembly of billets using a purging gas, allowance for core expansion in the assembled billet, and

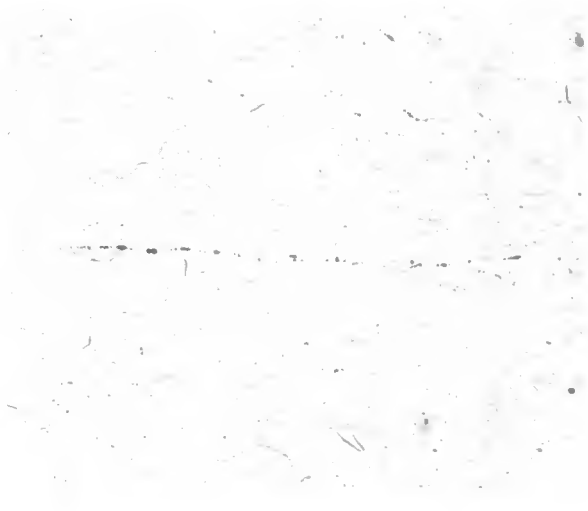

Fig. 25 — Bond at Zircaloy-2-to-Zircaloy-2 interface showing discontinuous inclusions. (Magnification 250×.)

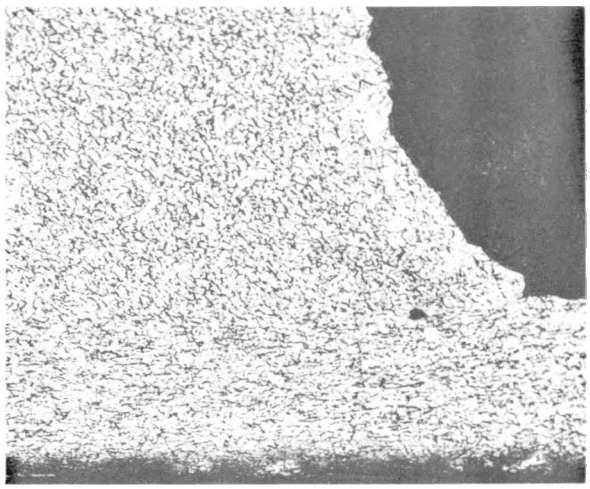

Fig. 26 — Bond at Zircaloy-2-to-Zircaloy-2 interface showing absence of bond line inclusions. (Magnification 50×.)

good weld penetration during billet assembly by a water-cooled press welding jig. Figure 26 illustrates the absence of bond-line inclusions.

A method was developed for nondestructive bond testing of roll clad plates. An ultrasonic through-transmission test using a scanner with an electrosensitive paper recorder indicated both lack of bond and degree of bonding. Un-

bonded areas as small as $\frac{1}{32}$ in. in diameter along the faces, sides, or ends of plates with prepared defects could be detected, and the quality of the bond could be related to bond tensile strength. Mechanical bond tensile tests of scanned areas confirmed this correlation within ±5000 psi. No unbonded areas were detected in the ternary alloy clad plates.

After exhaustive physical, mechanical, nondestructive, and corrosion tests, indications are strong that the ternary alloy plates, fabricated by the techniques outlined in this paper, are suitable for use in a central-station power reactor.

3. ROLL BONDING STAINLESS STEEL AND NICKEL TO URANIUM

Plate type fuel elements for use in power reactors operating with the neutron spectrum in the high-energy range have a high surface to volume ratio, thus resulting in plates of thin cross section. The fuel plates must be capable of operation at elevated temperatures, must have adequate corrosion resistance to the coolant, must be resistant to failure through bond degeneration and diffusion, and must be fabricable at low cost without the loss of dimensional accuracy. Stainless steel and nickel are not corroded by hot liquid sodium or sodium potassium alloy and were selected as the clad material. However, both nickel and iron form low melting eutectics with uranium (700 to 750°C).

Silver was selected as the bonding medium because it is essentially insoluble in uranium, stainless steel, and nickel; it is easily bonded to itself, possesses excellent thermal and physical properties, and has a high melting point (960°C); its resonance is of no concern in fast reactors.

Exploratory work indicated that thin plates of uranium completely clad with stainless steel or nickel could be made by hot rolling silver-plated components. All clad plates were made by shearing as-rolled stock to size, plating with silver, welding the components into a modified picture-frame composite billet, and hot rolling to effect the bond between clad and core. The welded assemblies were rolled without further enclosing in a steel box to protect the stainless steel or nickel from the atmosphere.

All work was done with a view toward producing plates $\frac{1}{16}$ in. thick by 3 to 4 in. wide by over 25 in. long with approximately 0.010-in.-thick cladding.

3.1 Procedure

The fabrication method utilizes electroplating, inert-gas-shielded arc welding, and hot rolling. Figure 27 is a schematic illustration of the composite billet assembly before welding and hot rolling. The composite billet component dimensions were selected based on 50 per cent reduction during rolling.

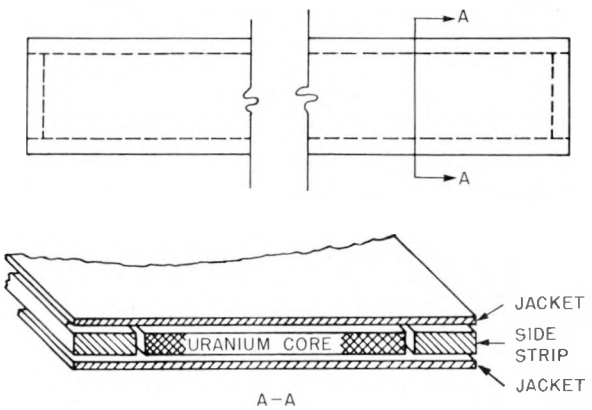

Fig. 27—Schematic drawing of plate assembly.

3.2 Electroplating

The component parts, consisting of top and bottom jacket plates, edge strips, end strips, and uranium core, were sheared to size from rolled material and electroplated with 0.001 to 0.002 in. of silver from a conventional silver cyanide bath. Stainless steel, nickel, and uranium require special pretreatment prior to plating. Cleaning and plating cycles are outlined in Sec. 3.6.

3.3 Billet Assembly

The electroplated parts were assembled as indicated in Fig. 27 and held securely between copper blocks in a hydraulic press at a pressure of approximately 15 tons. The four edges were left exposed at the sides of the copper blocks and were heliarc welded all around to close the composite billet assembly. The pres-

ence of silver on the stainless-steel or nickel cladding pieces did not interfere with weldability owing to the lack of solubility of silver in stainless steel and nickel. The silver on the external surfaces was dissolved away with nitric acid after roll bonding.

3.4 Roll Bonding

Bonding was accomplished by hot rolling at a temperature of 640°C to a total reduction in thickness of 50 per cent. Better dimensional uniformity was obtained in the core when lower reductions were used. Rolling temperature was also important in providing dimensional uniformity in the core, and a temperature of 640°C is preferable since it provides greater assurance that the rolling will not be done at or above the alpha-beta transformation temperature of the uranium. Since the object of this rolling was bonding of the components in the composite billet, it was reheated after each pass. Reductions of the order of 10 per cent per pass were used. The billet was rotated 180 deg after each pass. Final sizing was obtained by cold rolling approximately 10 per cent. Typical rolling schedules for (1) stainless-steel-clad and (2) nickel-clad uranium plates are listed below.

1. Cladding with Stainless Steel (50 per cent reduction in thickness)

Composite billet	0.112 in. thick by $3\frac{1}{2}$ in. wide by 16 in. long
Rolling temperature	640°C
Mill	16 in. by 24 in. (two high)
Roll speed	100 ft/min
Preheat time	40 min in air furnace
Reheat time per pass	10 min

Rotate 180 deg after each pass

Pass	Reduction, in.	Rolled thickness, in.
1	0.009	0.103
2	0.005	0.098
3	0.013	0.085
4	0.010	0.075
5	0.013	0.061–0.065

Cold roll: 10 per cent to size and roller level

Finish dimensions: 0.056 to 0.060 in. thick by $3\frac{5}{8}$ in. wide by $28\frac{1}{2}$ in. long

2. Cladding with Nickel (50 per cent reduction in thickness)

Composite billet	0.125 in. thick by $2\frac{1}{2}$ in. wide by $5\frac{1}{2}$ in. long
Rolling temperature	640°C
Preheat time	50 min
Reheat time per pass	10 min

Rotate 180 deg after each pass

Pass	Reduction, in.	Rolled thickness, in.
1	0.005	2 passes, 0.120
2	0.015	1 pass, 0.105
3	0.020	1 pass, 0.085
4	0.024	3 passes, 0.061

Finish dimensions: 0.061 in. thick by $2\frac{1}{2}$ in. wide by $10\frac{7}{8}$ in. long

3.5 Discussion and Results

A good quality bond between the clad and core was produced by this process as indicated by Fig. 28, which shows a photomicrograph of the stainless steel–silver–uranium interface after rolling at 640°C. There is no evidence of dif-

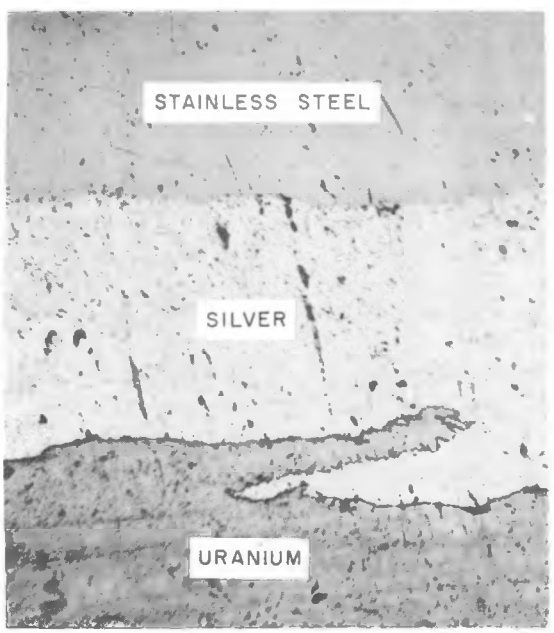

Fig. 28—Stainless steel–silver–uranium interface. (Magnification 500×.)

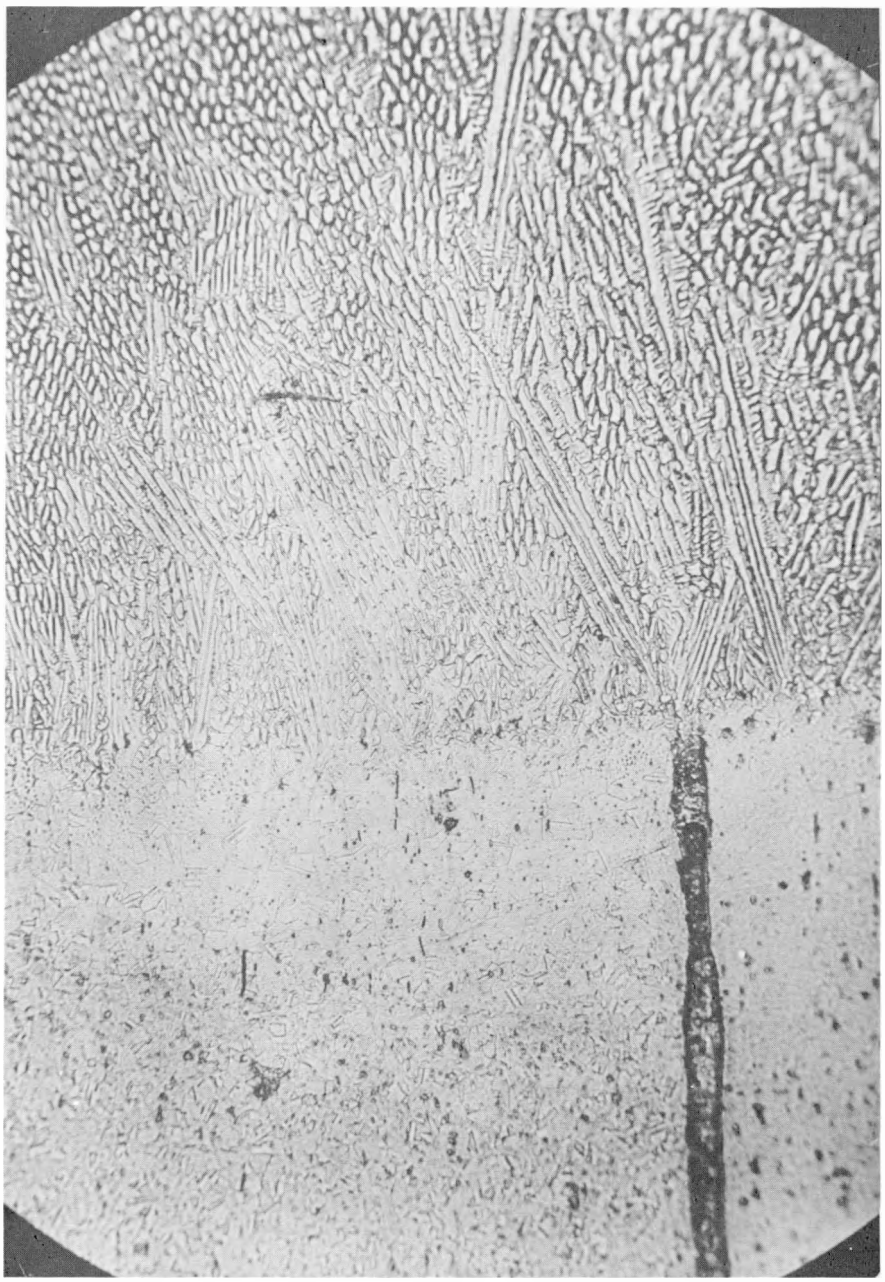

Fig. 29—Cross section of weld. (Magnification 500×.)

Table 4—Results of Tensile Tests on Stainless-steel-clad Uranium

Sample No.	Load, lb	Stress, psi
A4	703	13,784
B3	750	15,000
C3	692	14,416
D4	630	12,115

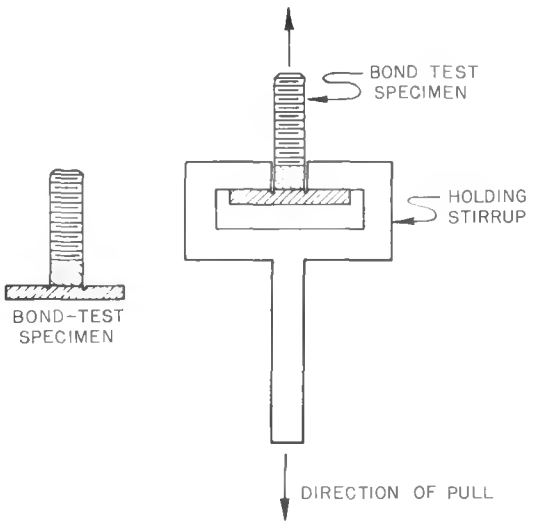

Fig. 30—Schematic drawing of arrangement used for obtaining tensile strengths of clad bond.

fusion occurring. Figure 29 is a photomicrograph of a cross section of the stainless-steel weld. The weld is sound, and good bonding of silver to stainless steel is evident.

Tensile strength measurements were made to determine how well the cladding was bonded to the core. Bond strengths as high as 15,000 psi were obtained. All fractures occurred through the silver. Table 4 gives the results of tensile tests on stainless-steel-clad uranium. Tensile specimens were prepared by percussive welding of small diameter rods to the stainless-steel clad and pulling in tension as shown in Fig. 30.

Dimensional accuracy of the cladding thickness was determined by the eddy-current technique and was found to be uniform. Variation of clad thickness was not more than ±0.001 in.

3.6 Appendix: Electroplating Silver on Uranium, Stainless Steel, and Nickel

Solutions used

1. Organic solvent degreaser
2. Alkaline electrocleaner
   - Work, cathodic
   - Temperature, 85–90°C
   - Voltage, 6 volts
3. Nickel strike bath

$NiCl_2$	32 oz/gal
HCl	1 pt/gal
Voltage	4–6 volts
Anodes	Nickel or stainless steel
Temperature	25°C
Plating time	2–4 min

4. Silver plating bath

AgCN	4 oz/gal
KCN	7.5 oz/gal
K_2CO_3	6.0 oz/gal
Temperature	25°C
Current density	5–10 amp/sq ft
Deposition rate	~0.8–1.6 mils/hr

5. 70% solution of HNO_3 at 50°C
6. Phosphoric acid anodizing bath

H_3PO_4 (conc.)	50 vol. %
HCl (conc.)	20 cm^3/liter
Temperature	40°C
Current density	0.5 amp/sq in.

7. Silver strike bath

AgCN	0.6 oz/gal
NaCN	9.0 oz/gal
Temperature	25°C
Voltage	6 volts
Plating time	30–60 sec

8. 10 vol. % concentrated starting acid
   H_2SO_4 25°C

Steps in electroplating silver on uranium

1. Degrease in solution 1
2. Rinse in water
3. Pickle in solution 5 for 5–10 min
4. Rinse in water
5. Anodize in solution 6 for 10 min
6. Rinse in water
7. Pickle in solution 5 for 5 min
8. Rinse in water
9. Electroplate with silver solution 4
10. Rinse in water
11. Dry with acetone

Steps in electroplating silver on stainless steel

1. Degrease in solution 1
2. Clean in solution 2
3. Water rinse
4. Strike with nickel in solution 3
5. Rinse in water
6. Dip in solution 8 for 5 sec
7. Rinse in water

8. Strike with silver from solution 7
9. Plate with silver from solution 4

Steps in electroplating silver on nickel
1. Degrease in solution 1
2. Clean in solution 2
3. Water rinse
4. Dip in solution 9 for 10 sec
5. Water rinse
6. Silver strike in solution 7
7. Plate with silver in solution 4

4. CENTRIFUGAL CASTING OF URANIUM FUEL COMPONENTS

Large numbers of small-dimension enriched-uranium fuel components with thin sections are required in liquid-metal reactors; the fuel components are bonded to the jacketing material with a liquid metal. To produce such parts by individual casting or by other techniques of fabrication involves operations that are complex and time consuming. Hence, multiple mold centrifugal casting was selected as a method to be investigated.

The objectives of the program were: (1) to design and build a machine to produce fuel components by multiple mold centrifugal casting, (2) to study the characteristics and properties of the fuel produced by this method, (3) to reduce the number and complexity of operations required in fabricating fuel components, and (4) to provide a method of manufacture for fuel component shapes which were not easily fabricated by other techniques.

4.1 Design of Machines

The casting machine consists essentially of a vacuum melting furnace superimposed over a spinning rotor assembly which contains a distributor and a number of radially arranged chill molds. The metal charge is induction melted in the furnace and is bottom poured into the rotating central runner, which distributes the molten metal to the molds arranged symmetrically around it.

The following requirements were set for the design of the machine:

1. The machine should be designed for convenience of operation and for complete recovery of the metal melted.

2. A vacuum pumping system should be provided which is capable of evacuating the furnace and rotor housing to 10^{-5} mm Hg while melting, casting, and cooling.

3. Provision should be made for preheating and outgassing the distribution runner and molds before pouring the melt.

4. The metal should fill the molds and solidify under centrifugal force to promote high density and soundness.

5. Provision should be made for speed variation and control to allow a study of the centrifugal effect.

6. The molds should be of high conductive material.

7. The rotor should be designed for safety at the highest operating speed of the machine.

4.2 Upper Furnace Section

The induction melting section of the centrifugal casting machine is shown in Fig. 31, which clearly illustrates the arrangement of the melting ceramics. A zirconia shield lined with a $\frac{1}{32}$-in.-thick tantalum metal heater was placed around the ceramics as shown, and the entire assembly was contained within a quartz or Vycor tube, which served as a vacuum-containing envelope. The upper and lower ends of this tube were vacuum sealed against silicone rubber gaskets mounted within water-cooled flanges. A water-cooled copper induction heating coil, located around the outside of the quartz tube as shown, furnished the power for melting. All melting ceramics were of high-purity magnesia (MgO); these included the crucible, crucible pedestal, stopper rod, and crucible cover. A truncated tantalum metal funnel was inserted between the tapered bottom of the crucible and the crucible pedestal to facilitate pouring. This funnel served as a heater at a location where excessive cooling could result in an unsatisfactory pour. The pouring of each melt was accomplished by raising the water-cooled rod shown extending from the upper end of the furnace through a Wilson type vacuum seal. This rod was attached to the MgO stopper rod by means of a tantalum wire linkage.

4.3 Lower Centrifuge Section

The lower centrifuge section of the casting machine is schematically illustrated in Fig. 32.

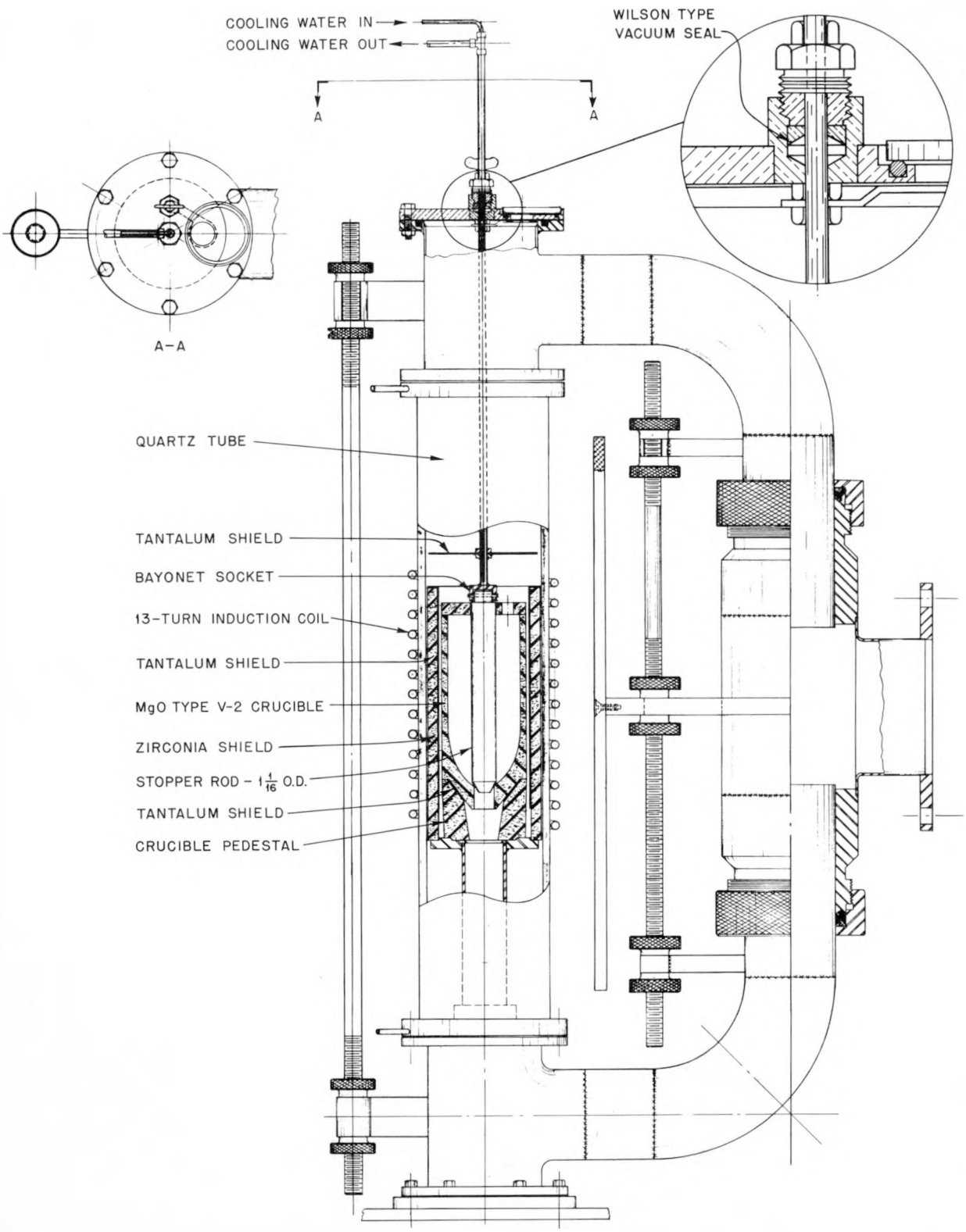

Fig. 31—Schematic drawing, showing upper half of centrifugal casting machine.

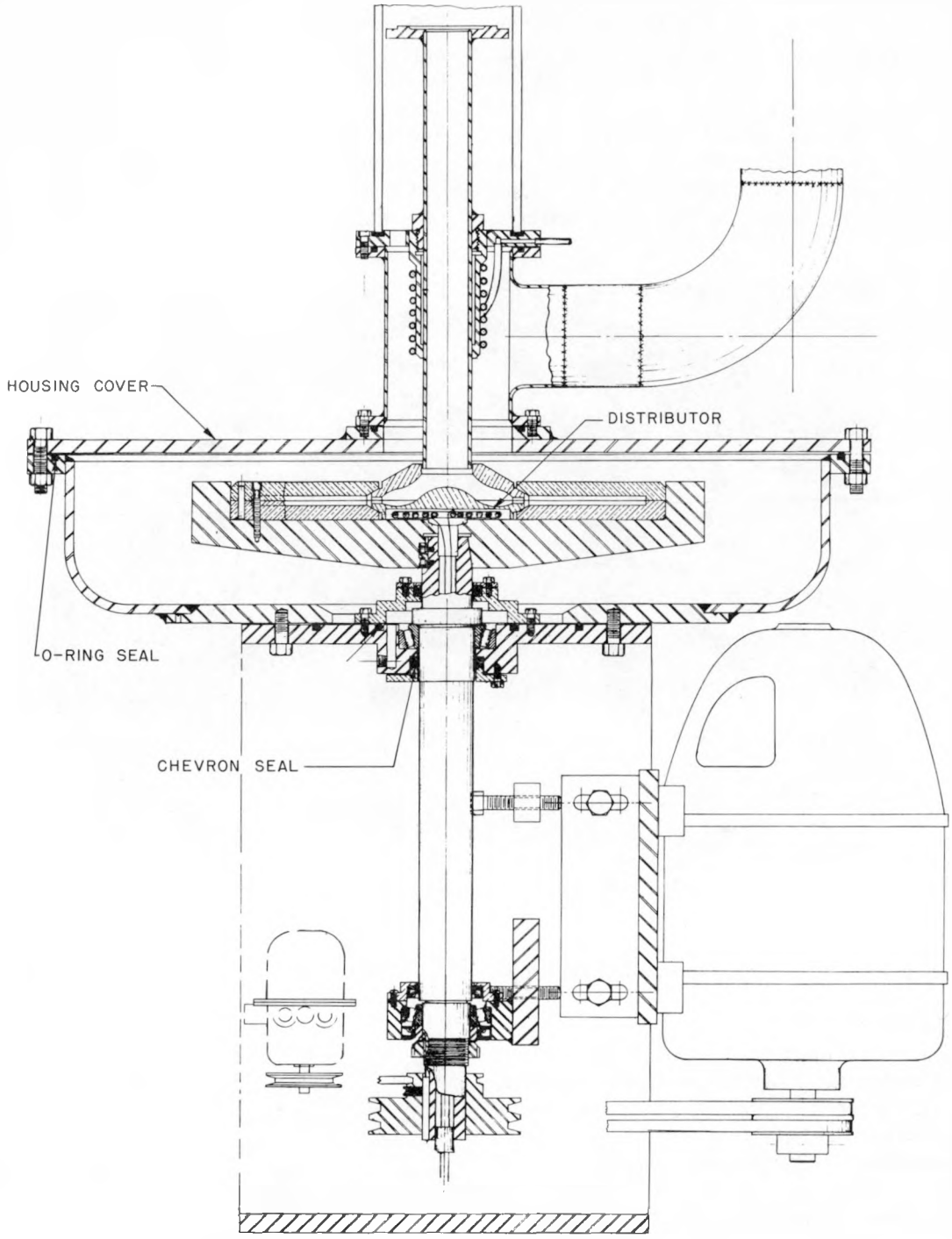

Fig. 32—Schematic drawing, showing lower half of centrifugal casting machine.

This section contained the forged steel rotor to which the distributor and molds were attached. A resistance heating coil was used beneath the distributor to preheat the latter in order not to chill the liquid stream too severely during the pouring operation. The electrical leads to this heater passed down through the hollow spindle shaft and through an ordinary black rubber stopper, which served as the vacuum seal at the lower end of the shaft. An "O" ring seal was used between the housing cover and the rotor housing, and a chevron seal was used on the rotating shaft.

The arrangement of the distributor and the molds within the rotor is shown clearly in Fig. 33. The raised cone-shaped center of the distributor split the falling stream of molten metal and imparted to it a gradual change in its direction; it was found to be quite indispensable to the proper filling of the fuel slug molds.

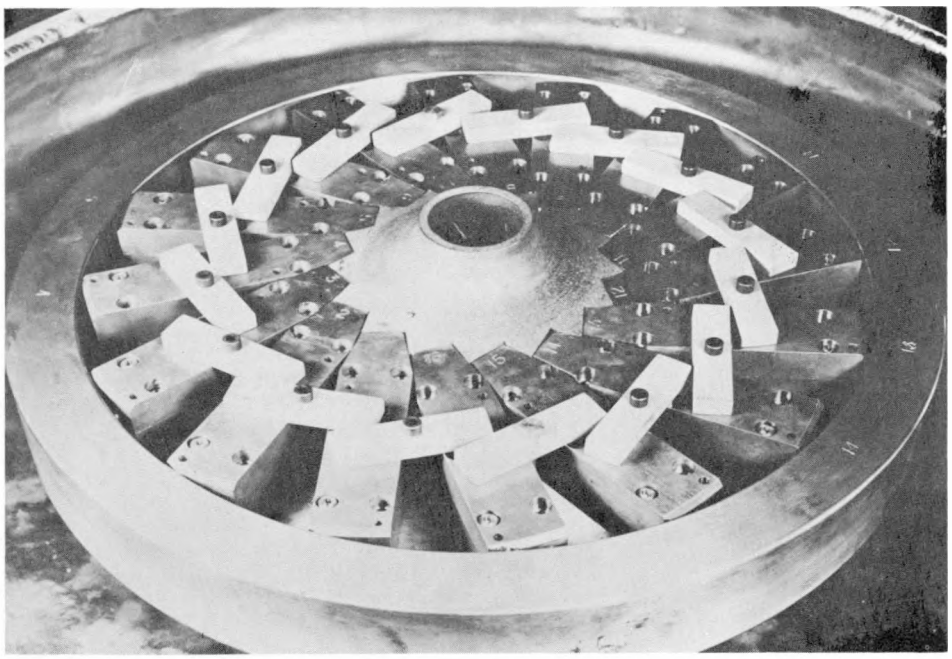

Fig. 33—Distributor and molds in place ready for use.

4.4 Assembly Apparatus

Two views of the assembled casting machine are shown in Figs. 34 and 35. Figure 34 also shows the auxiliary equipment used in conjunction with the casting machine, namely, the vacuum pumping system and the power source for induction heating. The vacuum system was a portable unit, consisting of a 6-in. oil diffusion pump, a 4-in. oil diffusion pump as a booster, and two mechanical roughing pumps. The power source was a motor-generator set delivering a maximum power output of 15 kw at 10,000 cycles.

The electrical leads to the distributor heater (see Fig. 32) were disconnected before the rotor containing the distributor and the molds were set in motion.

4.5 Charging, Melting, and Casting

A melting charge weighed approximately 2 to 3 kg of metal and consisted of virgin metal as well as remelt scrap. The remelt scrap was made up of sprues cropped off a previous set of cast slugs and of metal remaining in the distributor after casting. After the charge was seated in the crucible, the machine was closed and evacuated to 10^{-4} mm Hg before the induction unit was turned on. The metal was heated slowly to 1000°C to avoid thermal cracking of the ceramics and then was heated to 1425 to

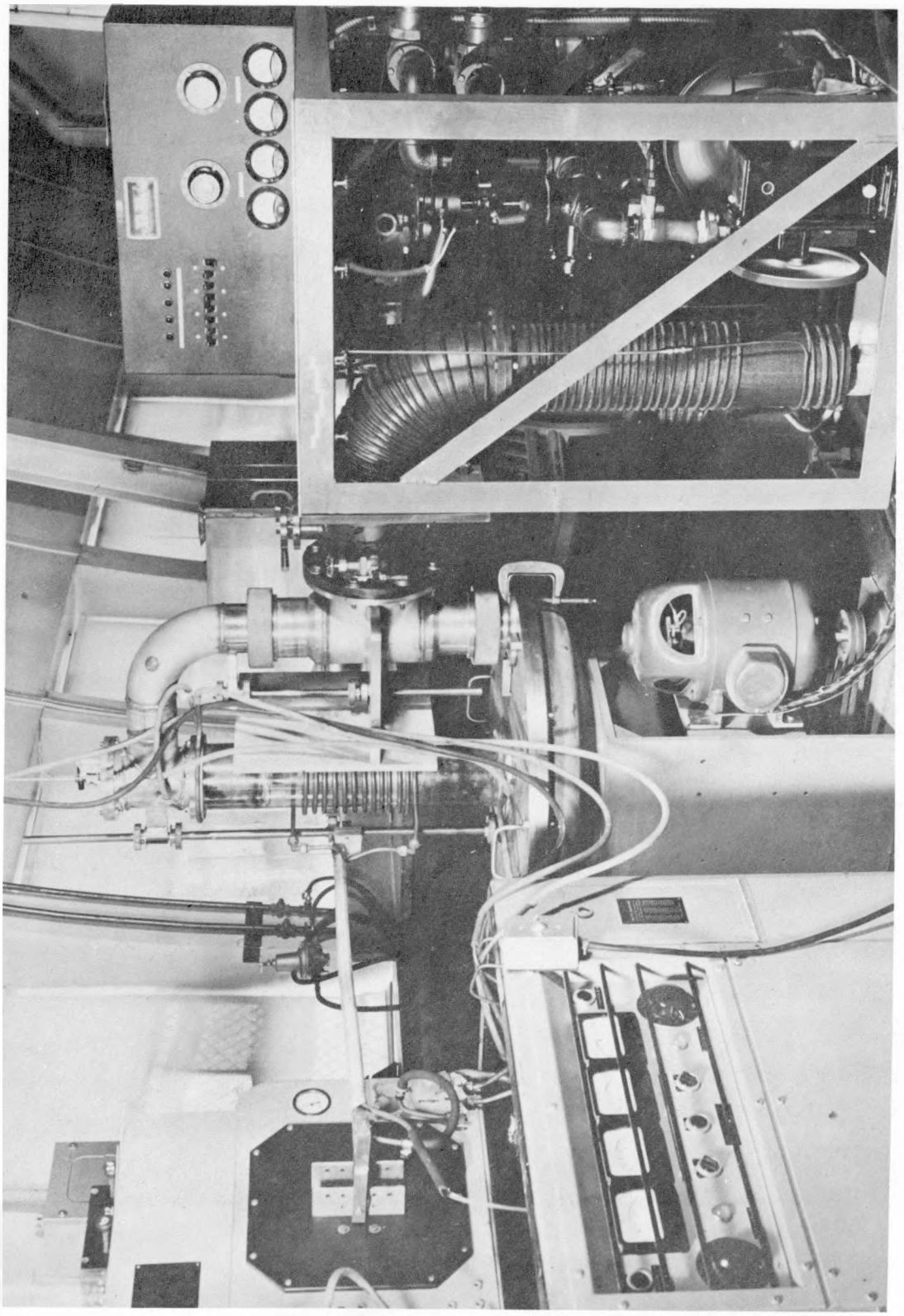

Fig. 34—Centrifugal cast machine, showing drive unit and vacuum system.

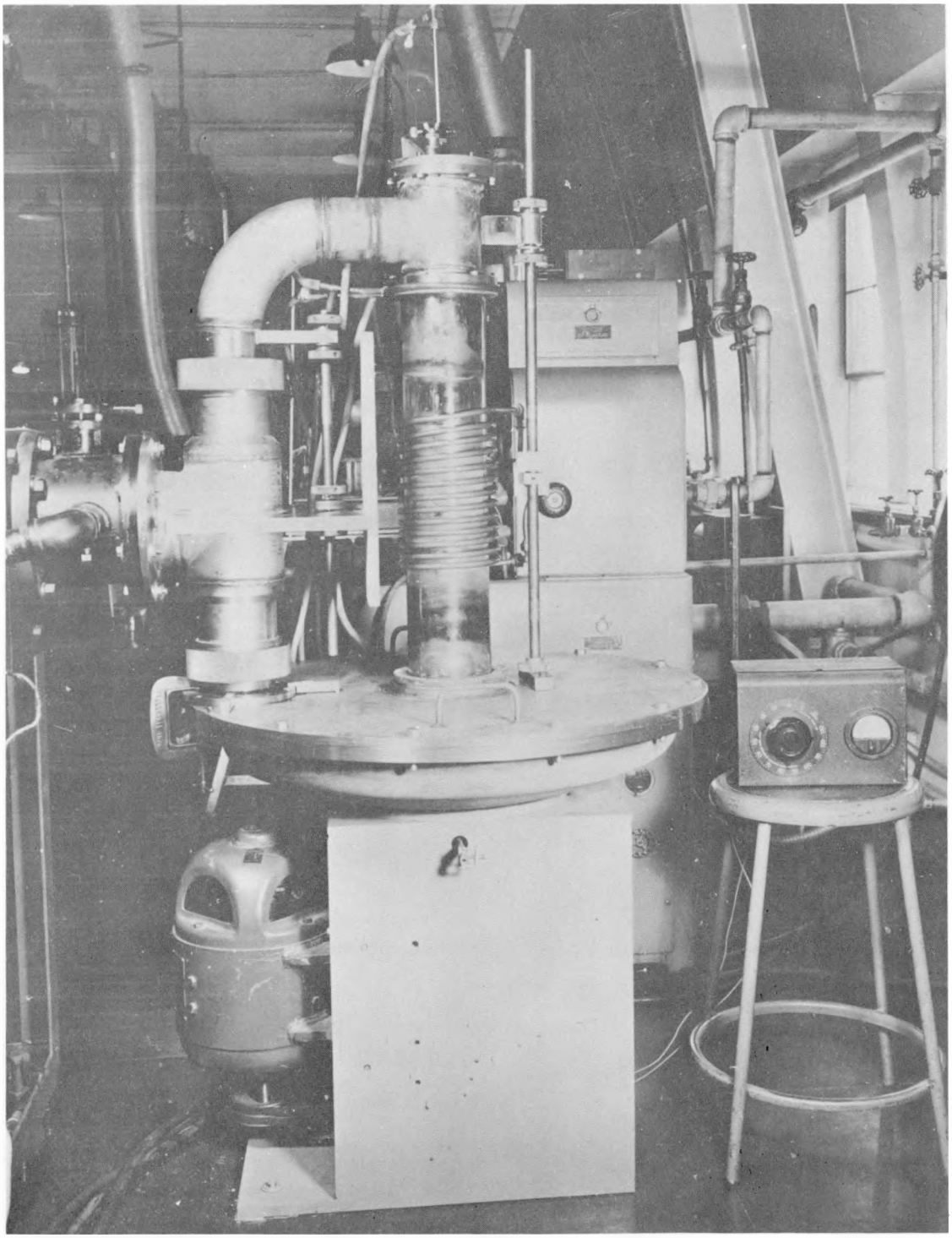

Fig. 35—Assembled casting machine.

1450°C at a rapid rate. Temperature readings were taken with an optical pyrometer by sighting into the crucible through the quartz window shown in view A-A of Fig. 31.

The melt was poured at 1450°C after holding at this temperature for 10 to 15 min to ensure homogenization of the scrap with the virgin

justing the mold diameters to allow for metal shrinkage, accurate diameters were possible; the yield of finished fuel components was 73.4 per cent and usable metal remelt scrap was 24.3 per cent (a total recovery of 97.7 per cent).

The centrifugal casting method has proved satisfactory for producing small-diameter fuel

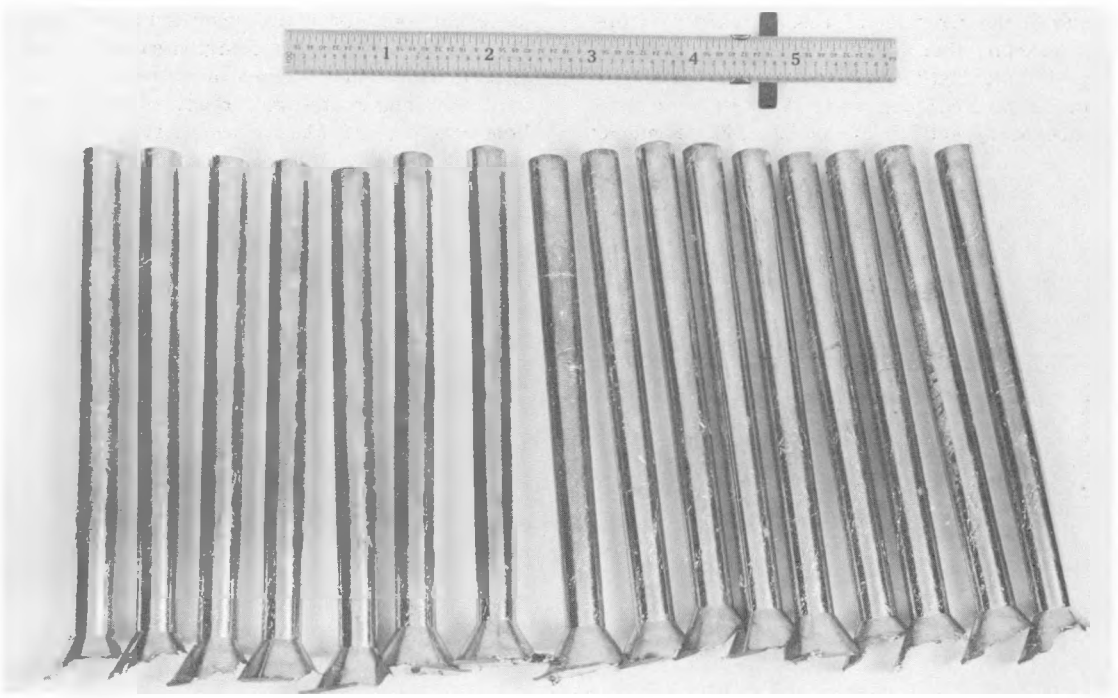

Fig. 36—Sixteen uranium castings before the sprue was cropped.

metals, the pour being made by lifting the stopper rod when the rotor was accelerating through the 350 to 400 rpm range. The rotor speed was increased to 600 rpm and was held there for 3 min; vacuum at the time of pouring was 4×10^{-5} mm Hg. The castings were cooled at a rate not faster than 1000°C/hr, were allowed to remain under vacuum for a minimum of 4 hr, and then were removed.

4.6 Results

Castings ranging from $^{3}/_{16}$ to $^{3}/_{8}$ in. in diameter and 8 to 10 in. in length have been obtained by this technique; no additional processing of the castings before use was necessary, other than cropping the sprue end to the desired length. Figure 36 illustrates castings produced. By adcomponents. Its principal advantages over conventional fabrication techniques are:

1. It uses fewer operational steps; thus it has fewer residues.
2. Fuel components are cast closer to sizes; thus minimum amounts of machining are required.
3. It has a high percentage of recovery of usable U^{235}.
4. The casting process is readily applicable to remote control operations.

ACKNOWLEDGMENTS

The author wishes to acknowledge that the experimental work of Sec. 2 was performed by

Messrs. Macherey, Bean, and Lindgren, of Sec. 3 by Messrs. Noland and Walker, and of Sec. 4 by Mr. Shuck.

ABOUT THE AUTHOR

James F. Schumar is Associate Director of the Metallurgy Division of Argonne National Laboratory and assists in the direction of research and development on materials that are used in nuclear reactors. He attended Case Institute of Technology, Cleveland, Ohio, receiving the B.S. degree in 1939. Prior to joining the laboratory staff in March 1946, Mr. Schumar was associated with the Wolverine Tube Division of the Calumet & Hecla Consolidated Copper Co., as senior metallurgist from 1939 to 1946. During this time at Wolverine he was responsible for jacketing the uranium fuel rods that were used in the Argonne heavy-water reactor, which was a result of early development work on the fabrication of uranium, thorium, and beryllium. Uranium fuel rods for the Laboratory's Experimental Breeder Reactor were developed and jacketed under his direction, and in this connection there was established and operated a U^{235} fabrication shop. In addition, he has contributed to the design and development of fuel rods and other reactor components for the submarine thermal reactors, the Argonne–Du Pont reactor, and other proposed reactors.

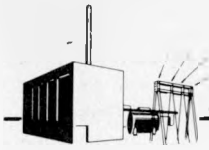

REACTOR FUTURES

A Design Study of Two Helium-cooled Reactors

R. H. ARMSTRONG, A. LOVOFF, and
L. J. TEMPLIN
Argonne National Laboratory

October 6, 1955

ABSTRACT

This study contains a conceptual design for two reactors, one of 500-Mw and the other of 189-Mw heat output. The reactors are cooled with helium so that they can be matched to an external closed-cycle gas-turbine system. The helium operates at a pressure of 1000 psi and a reactor outlet temperature of 1400°F.

Because of the high temperatures, graphite moderator and thorium fuel are considered. The 500-Mw reactor operates with 17.5 tons of thorium containing 3.61 wt. % U^{233}; the 189-Mw reactor operates with 6.2 tons of thorium containing 3.47 wt. % U^{233}. Both reactors have initial conversion ratios of approximately 0.92 and require an indeterminate extra enrichment for long-term operation.

The primary design limit chosen is that of a maximum heat flux of 291,000 Btu/hr/sq ft. Materials temperature limitations are roughly compatible with this value.

1. INTRODUCTION

This article describes two reactors that may be constructed in line with present technology and that offer the advantage of a coolant without corrosive and radioactive characteristics. The lack of radioactivity permits the coolant to be expanded directly through a turbine with a corresponding high net cycle efficiency. Since the many advantages of the closed cycle are well documented,[1-12] they will not be discussed in this article.

Although the idea of a helium-cooled power system is not new, recent developments favor its reinvestigation now. These are:

1. The continuing difficulty of eliminating corrosion with aqueous and liquid-metal coolants.
2. The satisfactory performance of graphite as a high-temperature material.
3. The growing attention to problems of coolant contamination of heat exchangers and turbine machinery.
4. The favorable prognosis for thorium metal and/or ceramic fuel elements as high-temperature radiation-stable materials.
5. The interest of other countries in gas-cooled reactors.

The advantages of helium over other gases in its ability to extract heat from surfaces and its complete chemical inertness are the main general arguments for its use. Predicted on these

arguments is the feasibility of a very high temperature gas-turbine system. On the other hand the difficulties of containing helium and of pumping it efficiently must not be overlooked.

In this study an attempt has been made to select a design which might be feasible for construction, utilizing present knowledge and practices. Thus such advanced materials as ceramic or cermet fuel elements have not been considered. The reason for this is that such a "conservative" concept is more readily evaluated, and it may more easily be determined whether the system shows enough promise to merit more detailed study.

The reactors sketched out must not be considered as optimized systems but must be considered more nearly as concepts. In fact the degree of design optimization for the two reactors is probably different. Further effort on optimized design would be wasted until such time as a system evaluation, including the turbine cycle, is performed.

For study purposes the same design points are used as those outlined in the American Turbine Company's report[4] on a closed-cycle gas-turbine nuclear power plant by S. T. Robinson. The reactors described in this report, however, are based on 500 and 189 Mw of heat instead of the 148.5 Mw used by the American Turbine Company. The state points and heat balance are the same as those described,[4] with the volumetric and mass flow rates increased proportionately.

Since the turbine cycle is ably described in the afore-mentioned report, this analysis will cover the reactor phase only.

Table 1 — Physical Characteristics

	Reactor	
	500 Mw	189 Mw
Diameter of active core, ft	11	8
Active length of fuel elements, ft	11	8
No. of 19-rod fuel-element assemblies (flat zone)	300	144
No. of 7-rod fuel-element assemblies (buckled zone)	80	56
Total number of fuel rods in reactor	6260	3128
Diameter of fuel rods, in.	0.345	0.345
Fuel-rod cladding (310 stainless steel), in.	O.D., 375; wall, 0.010	O.D., 375; wall, 0.010
Thermal bond between fuel rod and cladding (sodium), in.	0.005	0.005
Coolant channel diameter (flat zone), in.	2.875	2.722
Coolant channel diameter (buckled zone), in.	1.781	1.685
Moderator and reflector material	Graphite	Graphite
Lattice spacing, in.	6	6
Reflector thickness (radial and axial), in.	24	24
Pressure vessel, O.D.	17 ft $6\frac{3}{4}$ in.	14 ft $3\frac{3}{8}$ in.
Pressure vessel, wall thickness, in.	4.25	3.50

2. REACTOR DESIGN

The reactors consist of an array of graphite blocks of square cross section, arranged to form a rough circle. The central part contains one coaxial hole per block, which forms the coolant passage and into which the fuel elements are inserted. The fuel elements are rod arrays. This reactor core is surrounded on the sides and ends by graphite reflectors and is enclosed by thermal shields, thermal insulation, and the pressure vessel, in that order. Figures 1 to 4 illustrate the system, and Tables 1 to 4 contain the basic design data.

Table 2 — Heat-transfer Characteristics

	Reactor	
	500 Mw	189 Mw
Reactor gas inlet temp., °F	886	886
Reactor gas outlet temp., °F	1400	1400
Reactor gas flow rate, lb/hr	2656×10^3	1002×10^3
Reactor gas velocity in core (av.), ft/sec	334	300
Maximum heat flux, Btu/hr/sq ft	291,000	291,000
Reactor pressure, psi	1000	1000
Electrical power output at estimated 32.5% efficiency, Mw	162.5	61.4
Plant heat rate at estimated 32.5% efficiency, Btu/kw	10,500	10,500
Electrical output at estimated 32.5% efficiency and 80% plant factor, kw-hr/year	11.4×10^8	4.3×10^8

Table 3 — Nuclear Characteristics

Item	500-Mw reactor			189-Mw reactor		
	Flat zone	Buckled zone	Total	Flat zone	Buckled zone	Total
k	1.0325	1.2403		1.0514	1.2587	
η_f	1.410	1.378		1.430	1.399	
ϵ	1.0	1.0		1.0	1.0	
p	0.732	0.900		0.733	0.900	
M^2 axial, cm^2		486.68			485.64	
M^2 radial, cm^2		477.43			483.41	
B^2 axial, cm^2	0.000057	0.000057		0.000094	0.000094	
B^2 radial, cm^2		0.000448			0.000440	
ICR	0.952	0.522	0.915	0.970	0.540	0.920
Core radius, ft	4.87	0.63	5.50	3.37	0.63	4.00
Core volume, %	88.5	11.5		70.9	29.1	
Enrichment $\frac{N_{U^{233}}}{N_{U^{233}} + N_{Th}}$	0.0361	0.0361	0.0361	0.0347	0.0347	0.0347
Critical mass, kg of U^{233}	475.0	46.6	521.6	172.8	24.7	197.0
Thorium, tons	15.4	1.5	16.9	5.25	0.75	6.0
Average flux, radial	1.00	0.978	0.995	1.00	0.973	0.992
Average flux, axial	0.753	0.753	0.753	0.783	0.783	0.783
Absolute average fluxes $\times 10^{-13}$, neutron/cm^2/sec	4.00	3.95		4.50	4.30	

Table 4 — Definition of Symbols and General Data

Symbol	Definition	Value 500 Mw	Value 189 Mw
A	Flow area (total), sq ft	9.532	4.00
A_{FZ}	Flow area per unit pass (flat zone), sq ft	0.0288	0.0241
A_{BZ}	Flow area per unit pass (buckled zone), sq ft	0.0113	0.00946
C_p	Specific heat of He at constant pressure, Btu/lb/°F	1.250	1.250
C_v	Specific heat of He at constant volume, Btu/lb/°F	0.750	0.750
De_{FZ}	Equivalent diameter (flat zone), 4× flow area/ wetted perimeter, ft	0.0396	0.0336
De_{BZ}	Equivalent diameter (buckled zone), 4× flow area/ wetted perimeter, ft	0.0359	0.0307
f	Friction factor, $0.046/Re^2$, dimensionless	0.0045	0.0045
G	Mass velocity of He (total), W/A, lb/hr/sq ft	278,637.77	250,692.74
G_S	Mass velocity of He (total), W_s/A, lb/sec/sq ft	77.40	69.64
g	Gravitational acceleration, ft/sec/sec	32.2	32.2
h_{FZ}	Coefficient of heat transfer (flat zone), Btu/hr/sq ft/°F	908.46	862.22
h_{BZ}	Coefficient of heat transfer (buckled zone), Btu/hr/sq ft/°F	926.13	894.24
K	Entry loss	0.05	0.05
k_c	Ratio of specific heats of He, C_p/C_v	1.66	1.66
K_c	Thermal conductivity of He, Btu/hr/sq ft/°F/ft	0.179	0.179
L	Channel length, ft	11.0	8.0
P_1	Reactor inlet pressure, psia	1015.0	1015.0
P_2	Reactor outlet pressure, psia	997.0	997.0
ΔP	Reactor pressure drop, $P_1 - P_2$, psi	18.0	18.0
Q	Volumetric flow (total), cu ft/sec	3181.22	1200.42
Q_M	Volumetric flow (total), cu ft/min	190,873.20	72,025.20
Q_{FZ}	Volumetric flow per unit pass (flat zone), cu ft/sec	9.60	7.23
Q_{BZ}	Volumetric flow per unit pass (buckled zone), cu ft/sec	3.77	2.84
q_{FZ}	Average heat flux (flat zone), Btu/hr/sq ft	219,162.0	227,894.0
q_{BZ}	Average heat flux (buckled zone), Btu/hr/sq ft	214,341.0	221,741.0
Re	Reynolds number, DeG_S/μ_S (average)	119,195.0	119,195.0
R_G	Gas constant, ft/°R	386.3	386.3
r_{FZ}	Hydraulic radius (flat zone), flow area/ wetted perimeter, ft	0.0099	0.00841
S	Heat-transfer surface (total), sq ft	7801.0	2835.0
S_U	Heat-transfer surface (unit rod), sq ft	1.246	0.906
T_1	Reactor-coolant inlet temperature, °R	1346.0	1346.0
T_2	Reactor-coolant outlet temperature, °R	1860.0	1860.0
ΔT	Reactor-coolant temperature rise, °F	514.0	514.0
$\Delta t_{f\,FZ}$	Film drop (flat zone), q_{FZ}/h_{FZ}, (average), °F	241.3	264.3
$\Delta t_{f\,BZ}$	Film drop (buckled zone), q_{BZ}/h_{BZ}, (average), °F	231.4	248.0
$V_{av.}$	Velocity of He (average in core), ft/sec	334.0	300.0
V_{ent}	Velocity of He (entry plenum), ft/sec	32.23	19.92
V_{ex}	Velocity of He (exit plenum), ft/sec	45.18	27.92
$\overline{V}_{av.}$	Specific volume of He (average), cu ft/lb	4.312	4.312
W	Weight of flow of He (total), lb/hr	2,655,836.0	1,002,169.0
W_s	Weight of flow of He (total), lb/sec	737.73	278.38
W_{FZ}	Weight of flow of He per unit (flat zone), lb/hr	8014.00	6037.00
W_{BZ}	Weight of flow of He per unit (buckled zone), lb/hr	3146.50	2372.36
$\rho_{av.}$	Density of He (average), lb/cu ft	0.232	0.232
$\mu_{av.}$	Absolute viscosity of He (average), lb/hr/ft	0.093	0.093
$\mu_{av.\,sec}$	Absolute viscosity of He (average), lb/sec/ft	0.0000257	0.0000257

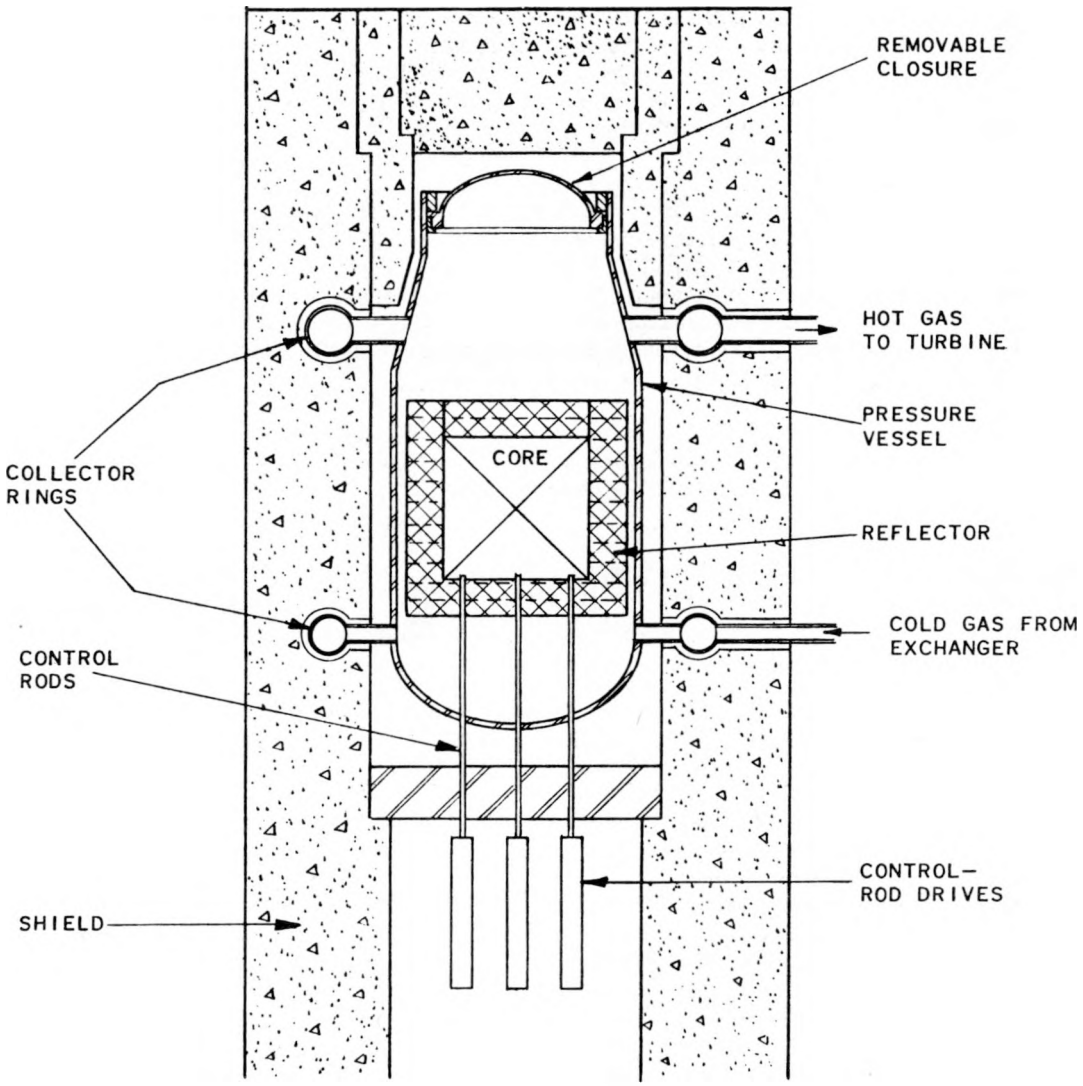

Fig. 1 — Cross section of reactor.

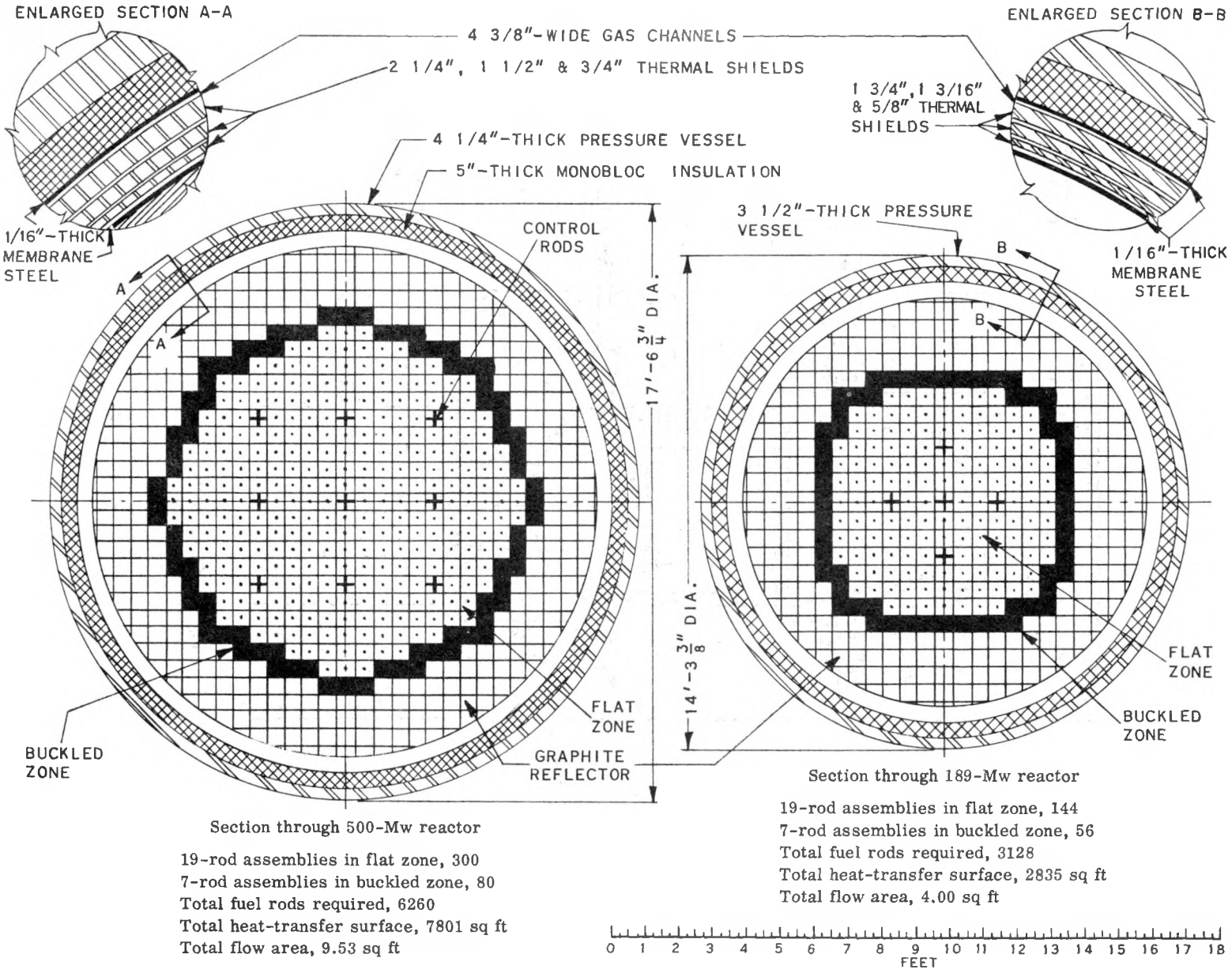

Section through 500-Mw reactor

19-rod assemblies in flat zone, 300
7-rod assemblies in buckled zone, 80
Total fuel rods required, 6260
Total heat-transfer surface, 7801 sq ft
Total flow area, 9.53 sq ft

Section through 189-Mw reactor

19-rod assemblies in flat zone, 144
7-rod assemblies in buckled zone, 56
Total fuel rods required, 3128
Total heat-transfer surface, 2835 sq ft
Total flow area, 4.00 sq ft

Fig. 2—Sections through the 500-Mw and the 189-Mw reactors.

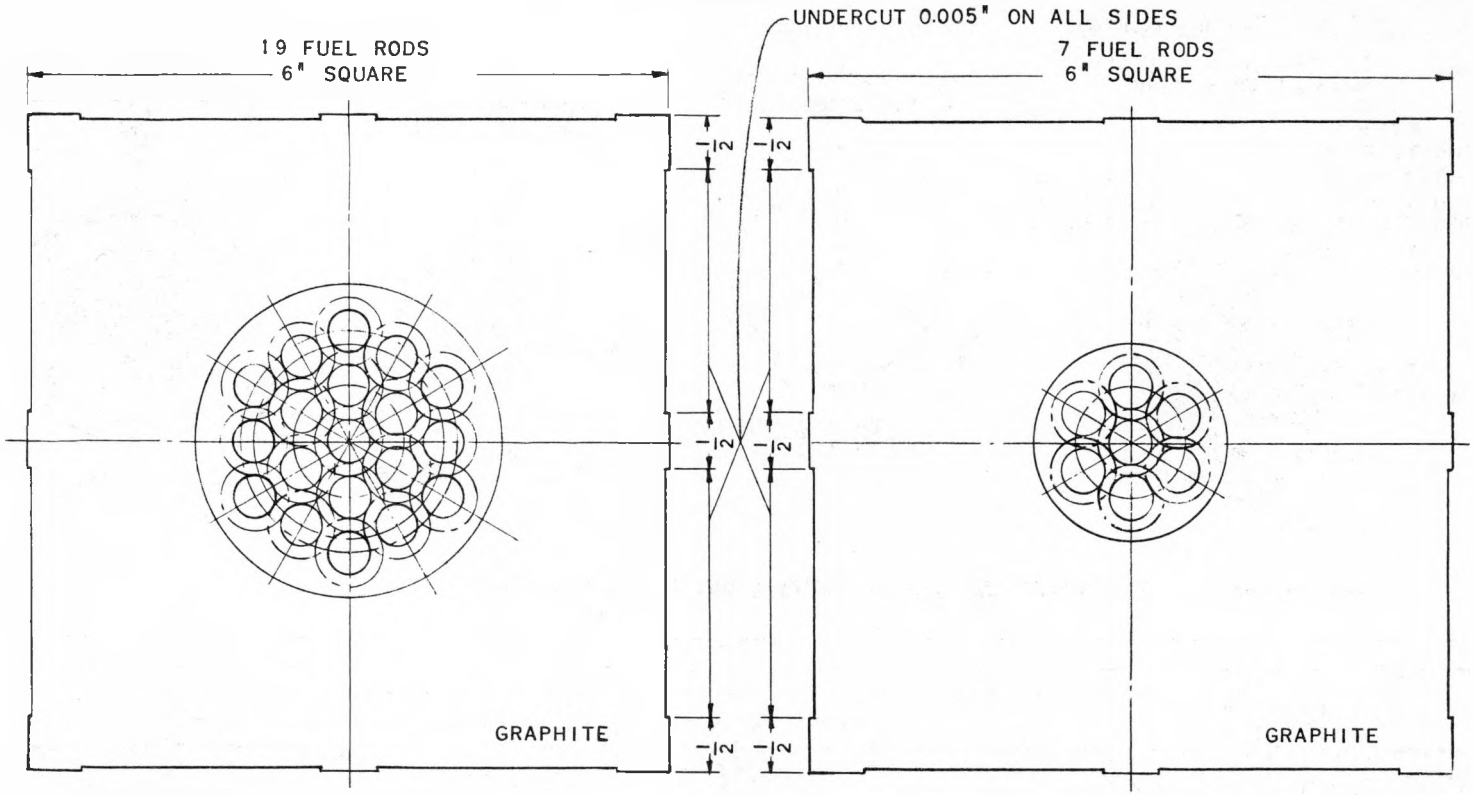

Flat zone fuel lattice

Power, Mw	500	189
Hole dia., in.	2.875	2.722
Hole area, sq in.	6.492	5.818
Metal area, sq in.	2.350	2.350
Flow area, sq in.	4.142	3.468
Flow area, sq ft	0.0288	0.0241
Equiv. dia., in.	0.475	0.403
Equiv. dia., ft	0.0396	0.0336
(Equiv. dia.)^2, ft	0.524	0.507

Buckled zone fuel lattice

Power, Mw	500	189
Hole dia., in.	1.781	1.685
Hole area, sq in.	2.492	2.229
Metal area, sq in.	0.866	0.866
Flow area, sq in.	1.626	1.363
Flow area, sq ft	0.0113	0.00946
Equiv. dia., in.	0.430	0.368
Equiv. dia., ft	0.0359	0.0307
(Equiv. dia.)^2, ft	0.514	0.498

Fig. 3—Typical fuel lattice.

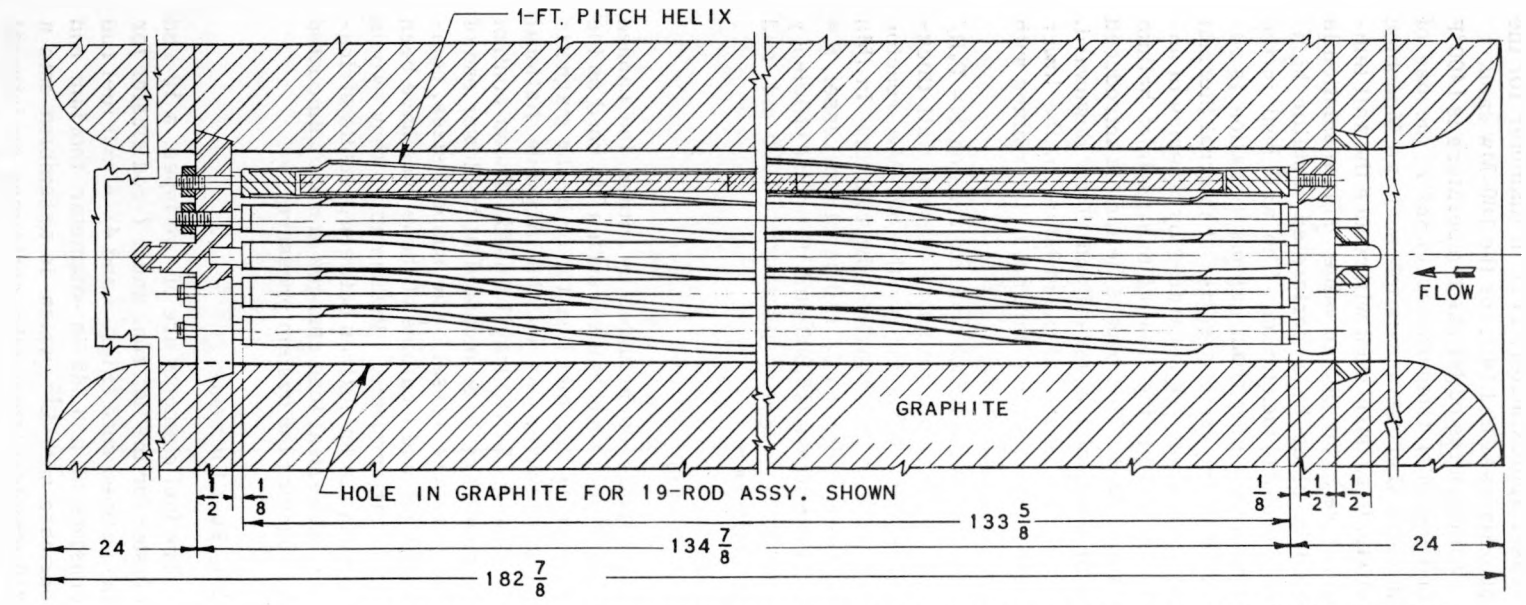

CROSS SECTION THROUGH REACTOR SHOWING 19-ROD FUEL ASSEMBLY IN 500-MW REACTOR

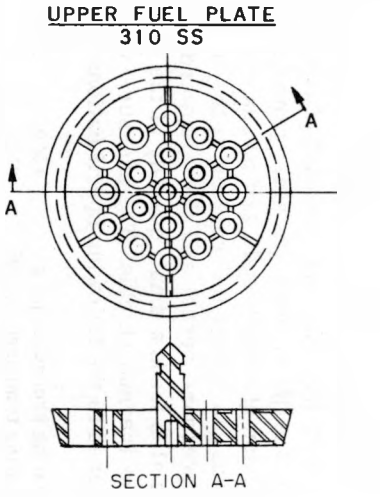

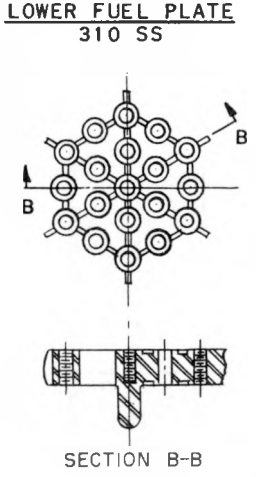

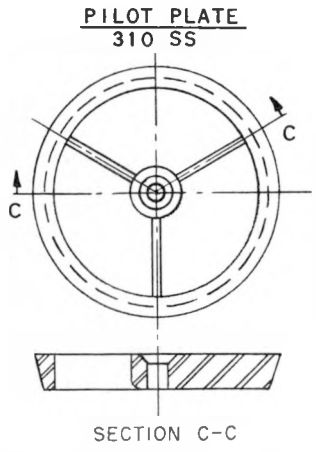

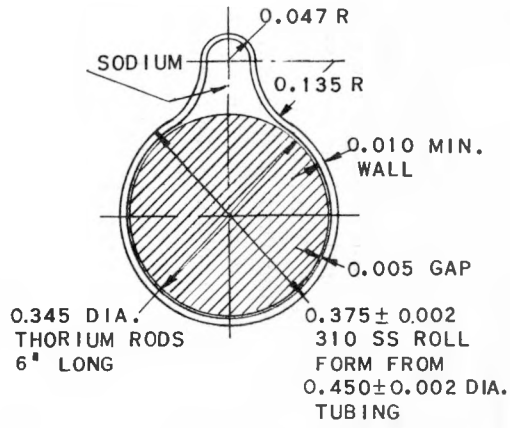

AREA = 0.1237 sq in.
PERIMETER = 1.3595 in.

SECTION THROUGH FUEL ROD

Fig. 4 — Section through reference reactor.

2.1 Core and Reflector

The core consists of 6-in.-square graphite lattice units, 134 $\frac{7}{8}$ in. long for the 500-Mw reactor and 98 $\frac{7}{8}$ in. long for the 189-Mw reactor. These lattice units contain a hole on the longitudinal axis for the insertion of the fuel assembly and for coolant flow. The coolant passages are shown in Fig. 3 and vary in diameter between reactor sizes and between the flat and buckled zones so as to optimize the flow rates and film-temperature drops. The radial area adjacent to the core contains uncored graphite reflector blocks (Figs. 1 and 2). The fuel assemblies extend to 24 in. from the ends of the graphite stringers to provide an axial reflector of that thickness at each end (Figs. 1 and 4).

Inserted between the core and the lower end reflector, as shown in Fig. 4, are pilot plates made of 310 stainless steel which act as guides when the fuel assemblies are inserted. The upper reflector plug acts as a clamp to immobilize the fuel assembly after it has been placed in the core. Thus the removal of a fuel assembly would require, in this system, the removal of the upper reflector plug; a better design would include a latch or locking device to secure the fuel assembly without requiring the removal of the upper reflector.

The entire core and reflector are supported by a structural lower support plate made of 310 stainless steel. This support plate is similar in function to a tube sheet except that the openings are square. Interconnected to the lower support plate are vertical structural members also made of 310 stainless steel.

2.2 Pressure Vessel and Thermal Shields

The pressure vessel is cylindrical with ellipsoidal heads. The upper closure is removable to permit insertion and removal of fuel assemblies; the lower head contains openings for the insertion of control rods and mechanisms. The helium gas enters the reactor at the bottom of the pressure vessel and flows upward. A bypass also feeds a small quantity of the inlet gas to the thermal shields. The pressure vessel is designed to the following specifications:

Operating pressure, psig	1000
Operating temperature, °F	650
Proposed material	Carilloy T_1 or equiv.
Allowable working stress, psi	26,000

The requirements of the systems make for a vessel approximately 17 ft in diameter for the 500-Mw case and 14 ft for the 189-Mw case.

Although the outlet gas temperature is 1400°F and the inlet temperature is 886°F, the use of internal thermal insulation such as Monobloc or stainless-steel wool will reduce the wall temperature to the design value. This insulation is held in place by a perforated metallic high-temperature membrane. The wall heat in the pressure vessel from gamma radiation is reduced by the use of a series of internal thermal shields, which are separated by a series of annuli to permit the flow of bypass inlet helium as a coolant. This bypass helium is introduced at the top of the vessel and flows downward, where, by means of bleed holes in the lower ends of the thermal shields, it intermixes with the main inlet flow.

Based on the ASME code expression $T = P_2R/(SE - 0.6P_2)$, the pressure vessel wall thicknesses are 4.250 in. for the 500-Mw reactor and 3.500 in. for the 189-Mw reactor. In this expression R = inside radius of the vessel, S = working stress (26,000 psi), E = joint efficiency = 0.95, P_2 = system pressure = 1000 psi, and T = thickness.

2.3 Control

Control rods actuated by either the canned motor type of mechanism such as is used on the Submarine Thermal Reactor or by the magnetic actuator developed by the Argonne National Laboratory (ANL) may be used. These control elements are to be mounted at the lower end of the pressure vessel. The shapes, sizes, compositions, and locations of these rods have been left indeterminate. Presumably, they would move in the interstices between graphite stringers. Electrical load changes are accommodated by changing the system pressure.

2.4 Fuel Elements

The fuel elements are of two types: a 19-rod cluster for the flat zone and a 7-rod cluster for the buckled zone (Figs. 3 and 4). A unit fuel rod consists of a 0.345-in.-diameter thorium rod enriched with U^{233} which is assembled into a 310 stainless-steel tube containing an integral spacing fin. A 0.005-in. radial clearance between the thorium and stainless steel is filled

with a thermal bond of sodium. The tube ends are closed with suitable end pieces and welded in place. The reference tube in 0.375 in. O.D. with a 0.010-in.-thick wall. The reference fin height is 0.125 in. but is subject to modification since the height is governed by the spacing required for adequate coolant flow.

A similar fuel rod might be conceived using thorium enriched with U^{235} or uranium oxide enriched with U^{235}. Also, NaK or lead may be substituted for sodium as the thermal bonding material. Such modifications would require an adjustment in enrichment and diameter.

The unit fuel rods are assembled into bundles, as shown in Fig. 4, which illustrates a 19-rod assembly. The total number of fuel rods and assemblies are shown in Table 1.

The upper end fitting on the fuel assembly contains a projection that engages a grabbing device for fuel-assembly removal. A series of pilot plates are embedded at the lower end of the core in the end reflector to secure the fuel assembly. When the fuel assembly is inserted into the core, the locating pin at the lower end of the fuel assembly engages the opening in the pilot plate, thus centering the assembly in the graphite lattice.

3. HEAT GENERATION

3.1 Power

The heat power generation in all zones of both reactors is based on a maximum heat flux of 291,052 Btu/hr/sq ft. This is based on a finned rod, assuming the fins are 100 per cent effective as heat-transfer area. The average radial and axial fluxes will vary as shown in Table 3. The coefficient of heat transfer between the gas and the surface of the fuel element is computed in the standard manner[18] and varies from an average of 878 Btu/hr/sq ft/°F for the 189-Mw reactor to 917 Btu/hr/sq ft/°F for the 500-Mw reactor. The film drop Δt_f averages about 236°F for the 500-Mw reactor and 256°F for the 189-Mw reactor. The gas velocity through the core will average about 334 ft/sec for the 500-Mw reactor and 300 ft/sec for the 189-Mw reactor. The specific velocities, V; volumetric flow, Q; mass flow, W; and mass velocity, G; etc., are given in Table 4.

Based on the maximum heat flux and the average radial and axial fluxes indicated in Table 3, the heat power outputs in the flat and buckled zones are as follows:

	500-Mw	189-Mw
Flat zone, kw	456,170	165,589
Buckled zone, kw	43,830	23,084
Total output, kw	500,000	188,673

3.2 Maximum Fuel Temperature

In a calculation of the maximum fuel temperature, the fuel is assumed to have a cylindrical cladding without fins. Consequently the heat flux used in this calculation is 13 per cent higher than that listed in the preceding paragraph. No fin allowance is made; therefore the calculations are on the conservative side. With a 100 per cent fin credit, the temperature drop from the metal to the bulk gas phase would be 13 per cent lower than that presented by the curves in Fig. 5.

Figure 5 represents the calculations for the 500-Mw reactor having fuel clusters 11 ft long. The average heat flux is 252,400 Btu/hr/sq ft. The maximum to average heat flux ratio is the same as the maximum to average neutron ratio, 1 to 0.749. This yields a maximum heat flux of 337,000 Btu/hr/sq ft. The hot-channel factors applied are conventional at ANL and are largely due to the uncertainties in measurements of gas temperatures.

The temperature drop between the center of the thorium metal and the bulk gas at the point where the thorium metal is the hottest (8 ft along the rod at a point where the heat production is 33,100 Btu/hr per foot of rod) is 400°F without hot-channel factors and 560°F with hot-channel factors. This temperature drop is broken down as follows:

1. The gas-film temperature drop[18] less a hot-channel factor is 296°F and with a hot-channel factor of 1.46 is 431°F.
2. Using a thermal conductivity for 310 stainless steel of 130 Btu/hr/sq ft/°F/in., the temperature drop through the 0.010-in.-thick cladding without a hot-channel factor is 22°F and with a hot-channel factor of 1.21 is 26°F.
3. The temperature drop through the sodium thermal bond is assumed to be negligible.

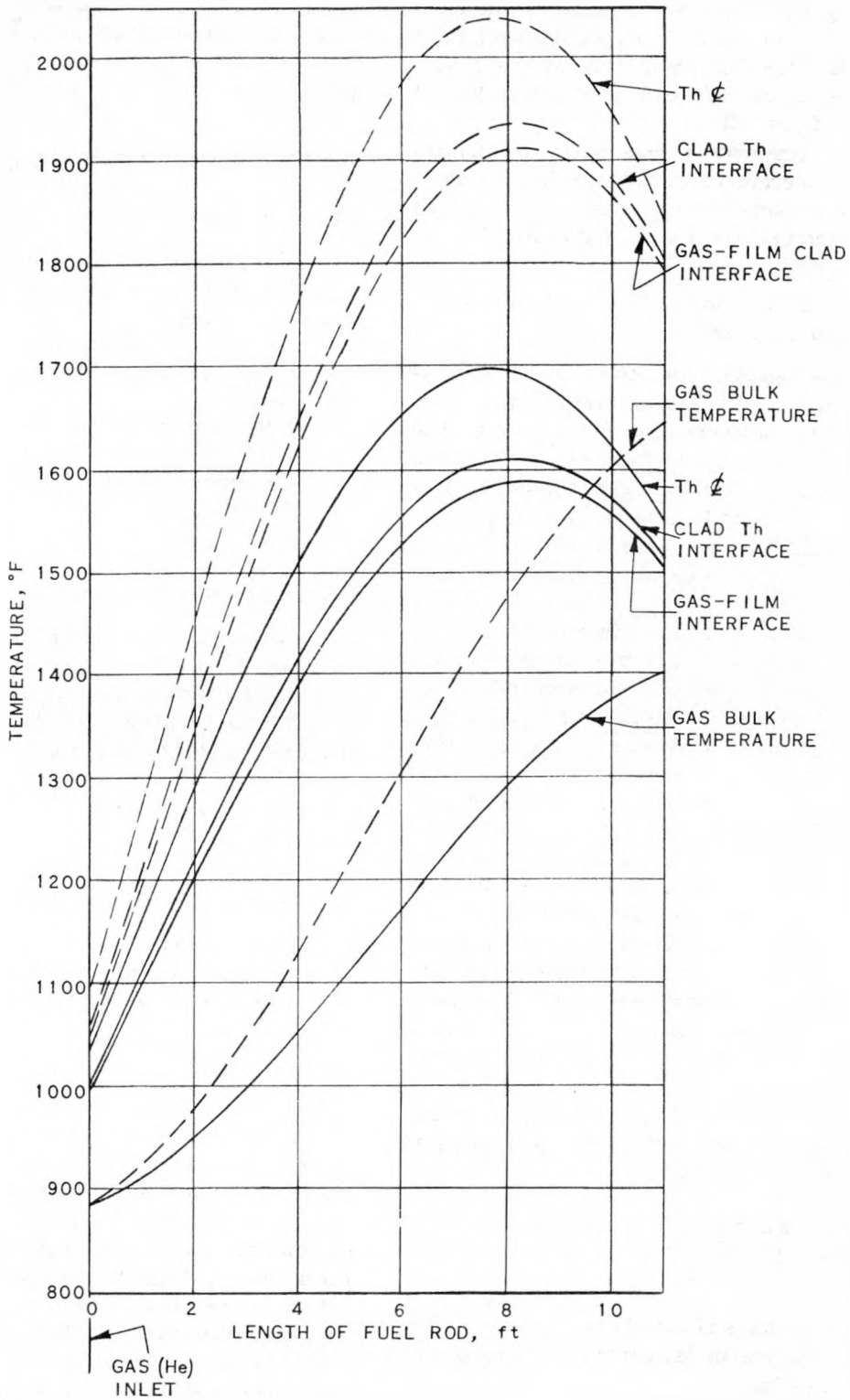

Fig. 5—Calculations for the 500-Mw helium-cooled reactor. ——, no hot-channel factors. ----, with hot-channel factors.

4. Using a thermal conductivity for thorium of 313.6 Btu/hr/sq ft/°F/ft, the temperature drop through the thorium fuel rod without a hot-channel factor is 85°F and with a hot-channel factor of 1.21 is 102°F.

The gas temperature rise along the channel and the temperatures at the gas-jacket interface, the jacket-thorium interface, and the center of the thorium are plotted in Fig. 5.

3.3 Thermal Stresses in Thermal Shield and Pressure Vessel

In calculating heat generation outside the reflector, only the leakage of gamma rays from the core was considered for this first try. The core was replaced by a sphere of equal volume in calculating this leakage. It was assumed that ten 2.4-mev gamma rays were emitted per fission and that they were attenuated according to laws of slab penetration, with a $1/R^2$ factor and a build-up term included. This resulted in a heat production, q_0, at the inner surface of the thermal shield of 0.16 watt/cm^3 for the 500-Mw reactor. The 189-Mw reactor was not calculated but is assumed to be the same value.

The analysis of temperature drops and thermal stresses in the thermal shields and pressure vessel was made for the designs illustrated in Fig. 2. The configuration of the cooling-gas passages was not set but was assumed to allow a gas-film coefficient of 50 Btu/hr/sq ft/°F to gas-cooled surfaces; i.e., both sides of the thermal shields and the outside of the pressure vessel. The inside of the pressure vessel was assumed to be perfectly insulated. The temperatures were calculated from the equation of heat conduction, assuming the above film coefficient and an exponentially attenuating heat source, as differences from coolant stream temperature and were converted into thermal stresses by the relation

$$\sigma_{Th} = \frac{E\alpha\,\Delta T'}{1-\mu_p}$$

where E = modulus of elasticity
$\Delta T'$ = maximum temperature difference in metal
μ_p = Poisson's ratio
σ_{Th} = thermal stress

The maximum thermal stresses are of the order of 1500 psi in either the thermal-shield sections as illustrated or the reactor-vessel walls.

4. OTHER ENGINEERING CONSIDERATIONS

4.1 Properties of Helium

The properties of helium are obtained from formulas developed in reference 13. The values thus obtained are:

Inlet specific volume, $\overline{V}$	= 3.596 cu ft/lb
Density	= 0.278 lb/cu ft
Average specific volume, $\overline{V}$	= 4.312 cu ft/lb
Density	= 0.232 lb/cu ft
Outlet specific volume, $\overline{V}$	= 5.041 cu ft/lb
Density	= 0.198 lb/cu ft

4.2 Pumping Horsepower

The horsepower required to circulate the helium in the reactor only is established by the expression given in reference 14 and amounts to 15,095 hp (11,269 kw) for the 500-Mw reactor and 5696 hp (4252 kw) for the 189-Mw reactor. Assuming 32.5 per cent net efficiency, this amounts to 7 per cent of the net electrical output of the reactor.

4.3 Pressure Drop

The expressions for pressure drop, outlined in references 15, 16, and 17, total 18 psi and apply to the 500-Mw reactor only.

4.4 Piping

The inlet gas from the recuperator or heat exchanger is carried downward, by means of two risers located 180 deg apart, to a doughnut-shaped collector duct. The collector duct contains a series of openings which pass the inlet gas into the low plenum chamber. Similar ducting at the upper end of the reactor receives the hot gas from the reactor for transmittal to the high-pressure turbine. The collector ducts and their associated risers are the same size. The outlet ducting contains 2.50-in.-thick internal thermal insulation, which is secured by a perforated metal membrane. The duct material is

Table 5 — Piping Data

Reactor size, Mw	No. of Radial ducts	Size of radial ducts, Inlet O.D.	Inlet Wall	Outlet O.D.	Outlet Wall	Velocity in radial ducts, ft/sec Inlet	Outlet	Size of collector ring, in. Inlet O.D.	Inlet Wall	Outlet* O.D.	Outlet* Wall	Velocity in collector rings, ft/sec Inlet	Outlet
500.0	10	14.00	0.438	20.00	0.625	339	309	31.25	0.968	38.00	1.187	339	311
189.0	6	12.75	0.406	18.00	0.563	257	260	22.00	0.688	27.25	0.844	259	260

* Contains 2.5-in.-thick internal thermal insulation.

the same as the pressure vessel, i.e., Carilloy T_1 or equivalent.

The piping data are outlined in Table 5.

5. PHYSICS

5.1 General

Calculations were made for several reactors with lattice spacing as parameter, using thorium-U^{233} fuel elements. Finally it was decided to flatten the radial flux and subdivide the fuel in order to increase the power density. Flattening is effected by properly adjusting the enrichment of the fuel. Studies are made of an 8-ft-diameter core and an 11-ft-diameter core reactor with a diameter vs. length ratio of one. The nuclear characteristics of these reactors are shown in Table 3.

The fuel is subdivided into 19-rod clusters of thorium and U^{233} in the flat region and 7-rod clusters in the buckled region, the assemblies in both regions being located on a 6-in. lattice. In order to avoid complications in fuel fabrication, the enrichment in the buckled region is unchanged from that of the flat region. However, in order to increase k_∞ in the buckled region as compared with k_∞ in the flat region, the number of rods in the buckled-region assemblies is reduced to 7 from 19 in the flat region. This increases the volume ratio of moderator to thorium, which in turn increases the resonance escape probability. Thermal utilization decreases but not at a rate sufficient to overcome the increase in resonance escape. Such a device to obtain a flat flux offers only a temporary advantage since the changes in fuel and poison concentrations during operation change the critical properties of each region. Since virtually no time was spent in the study of reactor dynamics, no solution is presented for maintaining this condition.

5.2 Cross Sections

Neutron energies are assumed to be 0.083 ev, which corresponds to the mean graphite temperature of 700°C. Cross sections are for this energy. Helium density is based on Akin's formula.[13] In order to accommodate the high temperatures to which the clad is subjected, 310 stainless steel is used in spite of its poor nuclear qualities. The cross section of graphite is taken as 0.0032 barn at 0.025 ev. This is, perhaps, an unrealistically low value which presumes an exceedingly high purity graphite. Hence, to some extent the results of the calculation are optimistic. Graphite age at 1025 ev is taken as 375 cm^2 for a graphite density of 1.60 g/cm^3. Allowing for density decrease when at operating temperature, τ is estimated to be 400 cm^2 for graphite.

The thermal diffusion length for graphite is taken as 2600 cm^2 at 0.025 ev. The protactinium absorption cross section is taken as 62 barns at 0.025 ev.

The thorium resonance cross section is taken to be

$$\sigma_{res}^{Th} = \frac{10}{3.07}\left[1 + \frac{0.55}{(M/S) + 0.08}\right]$$

where M is the mass of thorium in a cluster of rods and S is the surface of thorium in a cluster of rods. In order to account for self-shielding, the surface is assumed to be the circumference of a circle circumscribing the fuel cluster. It is assumed that any resonance-energy neutron

entering the circumscribing circle is captured.

To allow for the resonance disadvantage factor in calculating the resonance escape, p, Σ_{res}^{Th} is decreased by a factor 1/1.10 over the formula just given.

5.3 Equilibrium Protactinium

It is desired to load the reactor with a sufficient amount of U^{233} to override the presence of equilibrium Pa^{233}. The concentrations of Pa^{233} were calculated for the flat region and the buckled region, assuming $\overline{\phi} = 6 \times 10^{13}$ in each region. Time-dependent concentrations of other isotopes are not considered in this analysis; in other words, it is assumed that an equilibrium concentration of Pa^{233} is present as a poison in the virgin reactor.

The fraction of U^{233} atoms tied up as Pa^{233} was taken from the steady-state equation

$$\frac{N_{Pa}}{N_{U^{233}}} = \frac{ICR\ \sigma_{U^{233}}}{\sigma_{Pa} + (\lambda_{Pa}/\overline{\phi})}$$

where ICR = initial conversion ratio
$\sigma_{U^{233}}$ = microscopic cross section of U^{233}
σ_{Pa} = microscopic cross section of protactinium
λ_{Pa} = the decay constant of protactinium, measured in sec^{-1} and taken from a half life of 27.4 days
$\overline{\phi}$ = mean flux

The U^{233} requirements for criticality were multiplied by $[1 + (N_{Pa}/N_{U^{233}})]$ to obtain fuel feed requirements.

5.4 Migration Area

Because of the helium coolant channels, there is a considerable amount of streaming. Hence, according to Report CL-697, page 20 of Chapter IVE, perpendicular and parallel components of M^2 are calculated.

$$M_{\perp}^2 = f_{mod}\, L^2 \left[1 + \phi\left(1 + \frac{a}{\lambda_{thermal}}\right)\right] + \tau\left(1 + \frac{V_0}{V_1}\right)\left[1 + \phi\left(1 + \frac{a}{\lambda_{fast}}\right)\right]$$

$$M_{\parallel}^2 = f_{mod}\, L^2 \left[1 + \phi\left(1 + \frac{2a}{\lambda_{thermal}}\right)\right] + \tau\left(1 + \frac{V_0}{V_1}\right)\left[1 + \phi\left(1 + \frac{2a}{\lambda_{fast}}\right)\right]$$

where f_{mod} = thermal utilization of moderator
L^2 = diffusion length of moderator
ϕ = fraction of reactor taken up by empty parallel cylindrical channels
a = radius of the empty channels
τ = age of moderator
V_0 = volume of fuel
V_1 = volume of moderator
$\lambda_{thermal}$ = thermal transport mean free path of moderator
λ_{fast} = fast transport mean free path of moderator

In computing f_{mod} a poison factor of 0.045 $\Sigma_a^{U^{233}}$ was used to allow for the cross sections of xenon and samarium, and a thermal disadvantage factor of 1/1.25 in the fuel element was taken. This value may be optimistic.

5.5 Miscellaneous

The axial reflector saving was computed to be in the 40-cm range and was assumed to be 40 cm in all cases.

The radial reflector savings and buckled-zone thickness were computed by one-group diffusion theory and cylindrical geometry. The average flux in the system was computed from the total power and the flux shapes derived from this computation.

The initial conversion ratio was computed for each zone and power-weighted in averaging. The equilibrium protactinium was included as a poison in this case.

6. DISCUSSION

6.1 Design Method

The foregoing designs were arrived at by working around aiming points of 500 and 200 Mw heat output, exit bulk gas temperatures of 1400°F, and maximum central metal temperatures of 2000°F.

The fuel-rod diameter and assembly configurations were adjusted until a specific power was reached which indicated the possibility of a reasonable size for the pressure vessel. The flow passages in the fuel lattices were computed to allow an equivalent diameter whereby the mass flow, pressure drop, gas velocity, and coefficient of heat transfer are adjusted to optimum values. The high degree of radial flux flattening gives an excellent power distribution across the reactors. The resultant maximum to average heat flux ratio varies slightly between reactors and between the flat and buckled zones in each reactor. The ratio is about 1 to 0.745 for the 500-Mw reactor and about 1 to 0.773 for the 189-Mw reactor.

6.2 Fuel Elements

One of the primary problems is to develop a fuel element capable of withstanding high pressures and temperatures. Including the hot-channel factors, the curves of Fig. 5 indicate that both thorium and jacket temperatures are above acceptable values. These conditions may be adjusted by:

1. Using molybdenum tubes.[19]
2. Developing a cermet or ceramic fuel element capable of withstanding these temperatures.
3. Using smaller diameter fuel rods.
4. Using a lower heat flux and accepting a reduction in the power level.

Of these alternatives the use of a ceramic or cermet material is the most promising long-range approach, although it may be possible to have almost as good performance at a lower heat flux.

To get onto the Th^{232}-U^{233} cycle, it is necessary to begin with a fuel material of Th^{232} enriched with U^{235}. The problems thus entailed in fabrication, processing, separation, etc., must be reviewed. The thermal bond in the fuel assembly in the reference reactors is sodium. A review of other mediums, such as NaK or lead, should be made.

6.3 Pressure Vessel

One of the problems in the design of the pressure vessel is to maintain a wall temperature below that of the coolant. This might be accomplished by using either Monobloc or stainless-steel wool insulation contained in a perforated membrane of high-temperature material such as Inconel X. Refractory type insulations might also be effective since degradations of the insulation from radiation effects and abrasions from thermal expansions and contractions are factors to consider. Temperature gradients in the pressure-vessel wall from gamma radiation also must be considered. The reference design, Fig. 2, shows a number of thermal shields between the thermal insulation and the graphite reflector. These sizes are estimates and have not been computed.

The third major problem in the pressure vessel is to develop a gastight closure. The high-temperature high-pressure closure problem is now being actively worked on by a number of firms and will probably be carried on to a successful solution.

6.4 Shielding

No attempt was made to compute the shielding requirements. The problem of streaming also must be considered.

6.5 Shutdown Cooling

Time limitations prevented a study of this problem.

6.6 Thermodynamic Properties of Helium

The only data available in the high-temperature high-pressure range are the General Electric reports[13] which end in the temperature range of 600°F. These data should be extended into the 1000 to 2000°F range and the 1000 to 2000 psi pressure range. The equations in these reports were used to determine specific volume, density, and viscosity. The value for specific heat was not computed; the conventional value of 1.250 Btu/lb/°F at constant pressure was used, although the computed value would appear to be slightly less. The value for thermal conductivity of helium was not computed, although in the expression for the Prandtl number, i.e., $C_p\mu/K_c$, the value of thermal conductivity K_c is stated in the General Electric report as $\mu C_v \epsilon$, where ϵ is the proportionality constant of 2.44. The Prandtl number 0.78, used in the expression for h in reference 18, the coefficient of heat transfer, results in a more unfavorable value than if the computed value of

0.688 for the Prandtl number were used. The resulting increase in the value of h would reduce the film-temperature drop by approximately 17°F.

6.7 Machinery

An over-all study should be made on the effect of a helium coolant on the efficiency of the compressors, turbines, and heat exchangers. These subjects are discussed in more detail in the American Turbine Company report.[4]

7. CONCLUSIONS

The high efficiency of a closed-cycle nuclear system plus the advantages of a nonradiative coolant certainly indicate that this type of plant merits further consideration. To prove this system at a minimum of cost, a pilot reactor-turbine plant may be engineered and built. If a pilot reactor with a heat power size of 55,000 kw is used as a basis, at 27.5 per cent, 30.0 per cent, and 32.5 per cent efficiencies, the electrical output would be 15,125, 16,500, and 17,875 kw, respectively. These sizes closely span some of the sizes of gas-turbine power units now in operation[12] and would afford some excellent comparative data. The reference reactors show a volume vs. heat power ratio of 2.1 cu ft of core per megawatt of heat. On this core volume vs. heat power ratio, as a very rough approximation, the core volume for the pilot reactor would then be about 115 cu ft or about 5.25 ft in diameter by 5.25 ft long. The pressure vessel to contain this reactor would be approximately 9 ft in diameter. These figures, it must be emphasized, are very rough approximations.

ACKNOWLEDGMENTS

The assistance of the following people is gratefully acknowledged: W. S. Flinn, ANL, for information on stress in the pressure vessel from heating; M. Grotenhuis, ANL, for information on gamma heating; L. E. Link, ANL, for assistance in calculations on maximum fuel temperatures and temperature drop in pressure-vessel wall; J. F. Schumar, ANL, and K. F. Smith, ANL, for metallurgical assistance and advice; and N. Balai, ANL, for helpful suggestions regarding choice of pressure-vessel materials.

REFERENCES

1. C. Keller, The Escher Wyss-AK Closed Cycle Turbine, Trans. Am. Soc. Mech. Engrs., 68(8): 791-812 (1946).
2. C. Keller, Closed Cycle Gas Turbine — Escher Wyss-AK Development, Trans. Am. Soc. Mech. Engrs., 72(6): 835 (1950).
3. S. T. Robinson, The Closed-cycle Gas-turbine Power Plant, ASME Preprint 52-A-137.
4. S. T. Robinson, Design Study 60-Mw Closed-cycle Gas-turbine Nuclear Power Plant, American Turbine Company Report ATC-54-12.
5. Claude Seippel, Gas Turbines in Our Century, Trans. Am. Soc. Mech. Engrs., 75(2): 121-234 (1953).
6. J. C. Carter, A Closed-cycle Gas-turbine Installation, Report ORNL-55, June 1, 1948.
7. C. T. Evans, Materials for Power Gas Turbines, Trans. Am. Soc. Mech. Engrs., 69(6): 601 (1947).
8. A. Amorosi, Heat Transfer in Gas-cooled Power Piles, Report Mon-N-299, May 29, 1947.
9. Farrington Daniels, Suggestion for an Experimental Power Reactor, Report ANL-4448, April 1950.
10. Wright Aeronautical Corp., Analysis and Design of a Helium Compressor-Turbine Unit, Report NEPA-1563, Aug. 31, 1950.
11. Wright Aeronautical Corp., Bibliography on Gas Turbines — 1896–1948, published by the American Society of Mechanical Engineers.
12. L. N. Rowley and B. G. A. Skrotski, Gas Turbines, Power, 96(12): 79-110 (December 1952).
13. S. W. Akin, Thermodynamic Properties of Helium, G.E. Report 55141, ASME Preprint 49-A-96.
14. O. W. Eshbach, editor, "Handbook of Engineering Fundamentals," 2d ed., pp. 8-42, John Wiley & Sons, New York, 1952.
15. W. H. McAdams, "Heat Transmission," 2d ed., p. 122, Eq. 13; p. 128, Eq. 23, McGraw-Hill Book Company, Inc., New York, 1942.
16. W. H. McAdams, "Heat Transmission," 2d ed., p. 128, Eq. 22c, McGraw-Hill Book Company, Inc., New York, 1942.
17. W. H. McAdams, "Heat Transmission," 2d ed., p. 128, Eq. 124, McGraw-Hill Book Company, Inc., New York, 1942.
18. W. H. McAdams, "Heat Transmission," 2d ed., p. 174, Eq. 4j, McGraw-Hill Book Company, Inc., New York, 1942.
19. J. J. Harwood, Molybdenum: Our Most Promising Refractory Metal, Product Eng., 23: 121 (January 1952).

ABOUT THE AUTHORS

Robert H. Armstrong, a member of the Reactor Engineering Division, Argonne National Laboratory, received his training as a mechanical engineer at the Armour Institute of Technology. Before joining ANL in 1948, he was an engineer for the Tucker Corporation and prior to that, a cost consultant in the Engineering Division of Carrier Corporation.

Adolf Lovoff, an electrical engineer with the Reactor Engineering Division, Argonne National Laboratory, is on loan from the Vitro Corporation of America. He received the B.S. degree in 1936 from the University of Michigan and the M.S. degree in 1940 from the California Institute of Technology. Before joining Vitro in 1952, he was associated with the Navy Department and was in charge of the Nuclear Radiation Instrumentation Program.

Lyman J. Templin is a physicist with the Reactor Engineering Division, Argonne National Laboratory. He received the B.S. degree in 1935 from the Illinois Institute of Technology and the M.S. degree in 1937 from Loyola University. Prior to joining ANL in 1949, he taught mathematics at Loyola University.

BUILDING REACTOR COMPONENTS

Fabrication of Zircaloy-2 Core Vessel for the Homogeneous Reactor Test

The Homogeneous Reactor Test (HRT) is the second homogeneous reactor experiment to be constructed by the Oak Ridge National Laboratory. It will be the first step in development of the two-region thorium breeder reactor. One of the requirements of the ultimate breeder type reactor is a core-vessel material with a low total absorption cross section for thermal neutrons. This requirement is met by hafnium-free zirconium. The best available alloy of zirconium for this purpose is Zircaloy-2, which contains approximately 1.5 per cent tin, 0.12 per cent iron, 0.1 per cent chromium, and 0.05 per cent nickel. However, up to the spring of 1954 all welding of zirconium had been done in dry boxes containing completely inert gas atmospheres because of the high affinity of zirconium for oxygen and nitrogen, which have detrimental effects on zirconium properties.

The HRT core vessel is the first pressure vessel of its size constructed of a zirconium alloy and is the first reactor-grade zirconium welded outside a dry box. It was fabricated by the Newport News Shipbuilding & Dry Dock Co. under a development contract with the Carbide and Carbon Chemicals Company for the AEC. The plate material and forgings were produced by the Crucible Steel Co. of America according to procedures outlined by Newport News, from ingots supplied by the AEC.

Fabrication of the vessel required development of techniques for rolling, forming, forging, welding, heat-treatment, and inspection of Zircaloy-2. All techniques used were tested and proved to produce satisfactory results before production of any part of the vessel was attempted. Jigs and fixtures were designed, built, and tried on dummy operations before being used. Even the rolling procedure was used first on an experimental billet.

The fabricator's welding engineers felt from the beginning that a practical method of localized gas control could be developed for use in welding the alloy. The figures presented here show how this method was applied in joining the various sections of the vessel.

[Editors' Note: The Editors are indebted to W. R. Gall and G. E. Elder of the Oak Ridge National Laboratory for this item.]

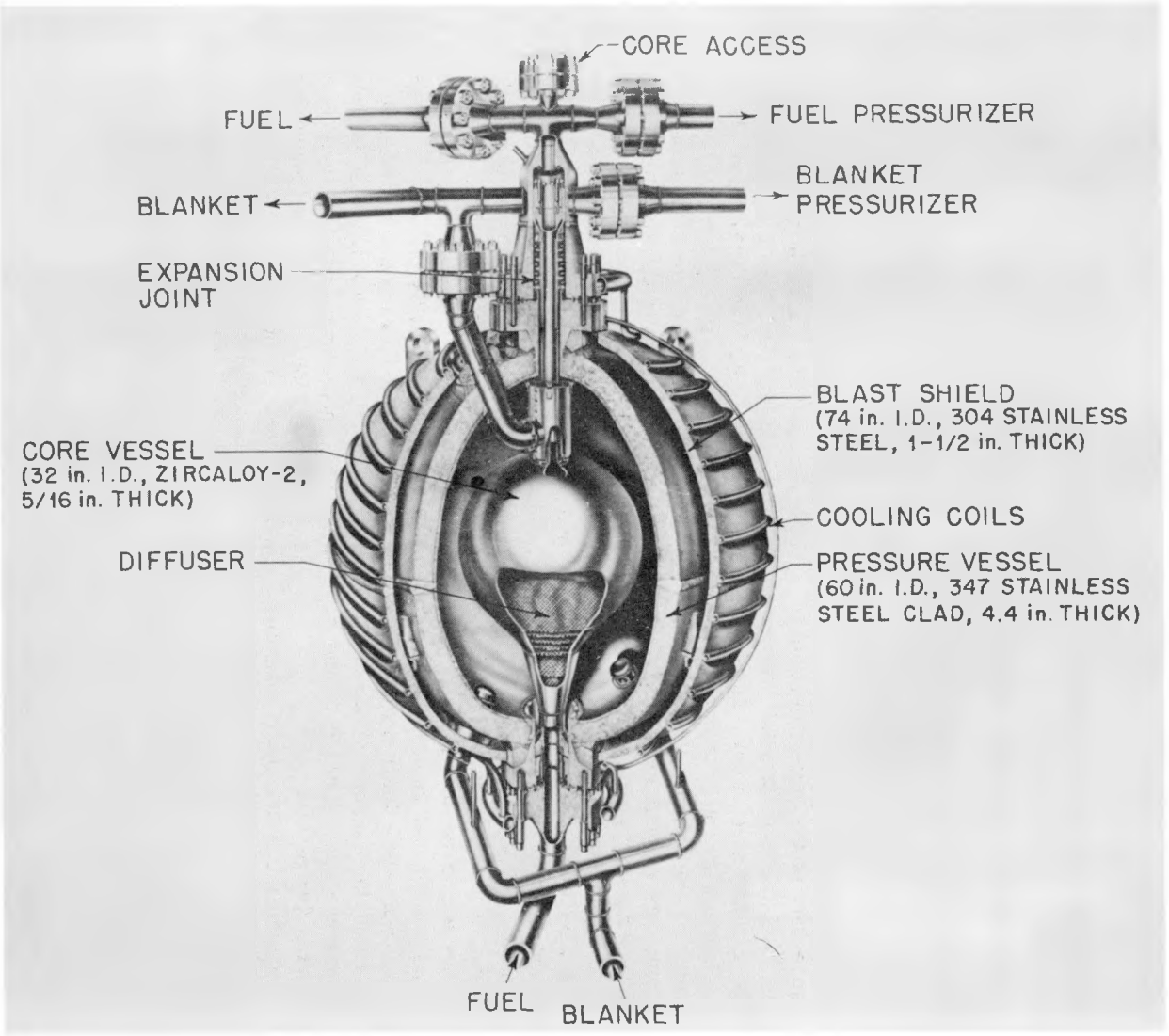

Fig. 1—HRT reactor vessel assembly. The core vessel is contained inside the larger diameter pressure vessel, which contains the blanket fluid. Flow is diffused through two conical sections, containing diffuser screens, into the spherical section of the core.

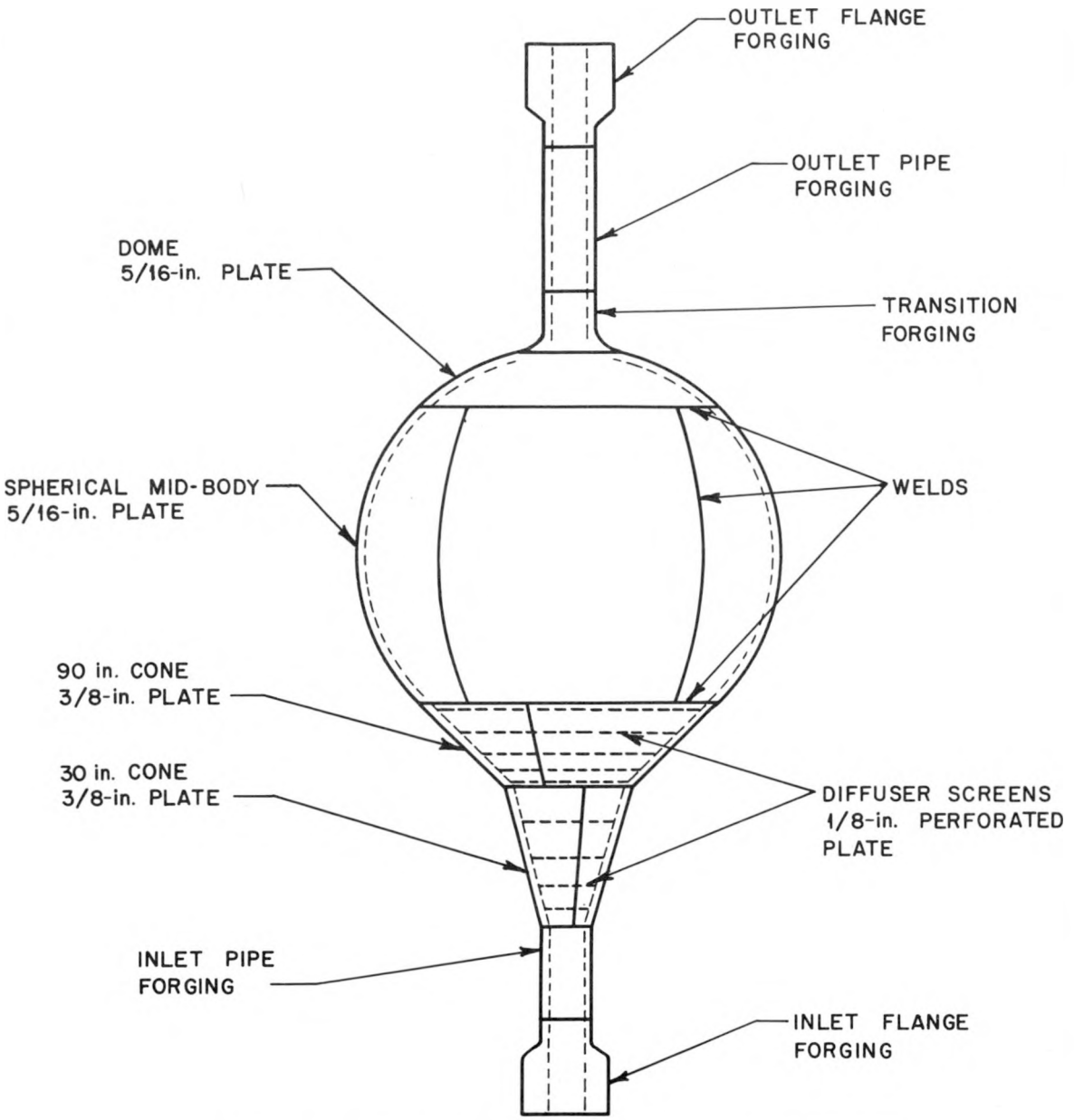

Fig. 2—Sketch of vessel, showing breakdown into fabrication components.

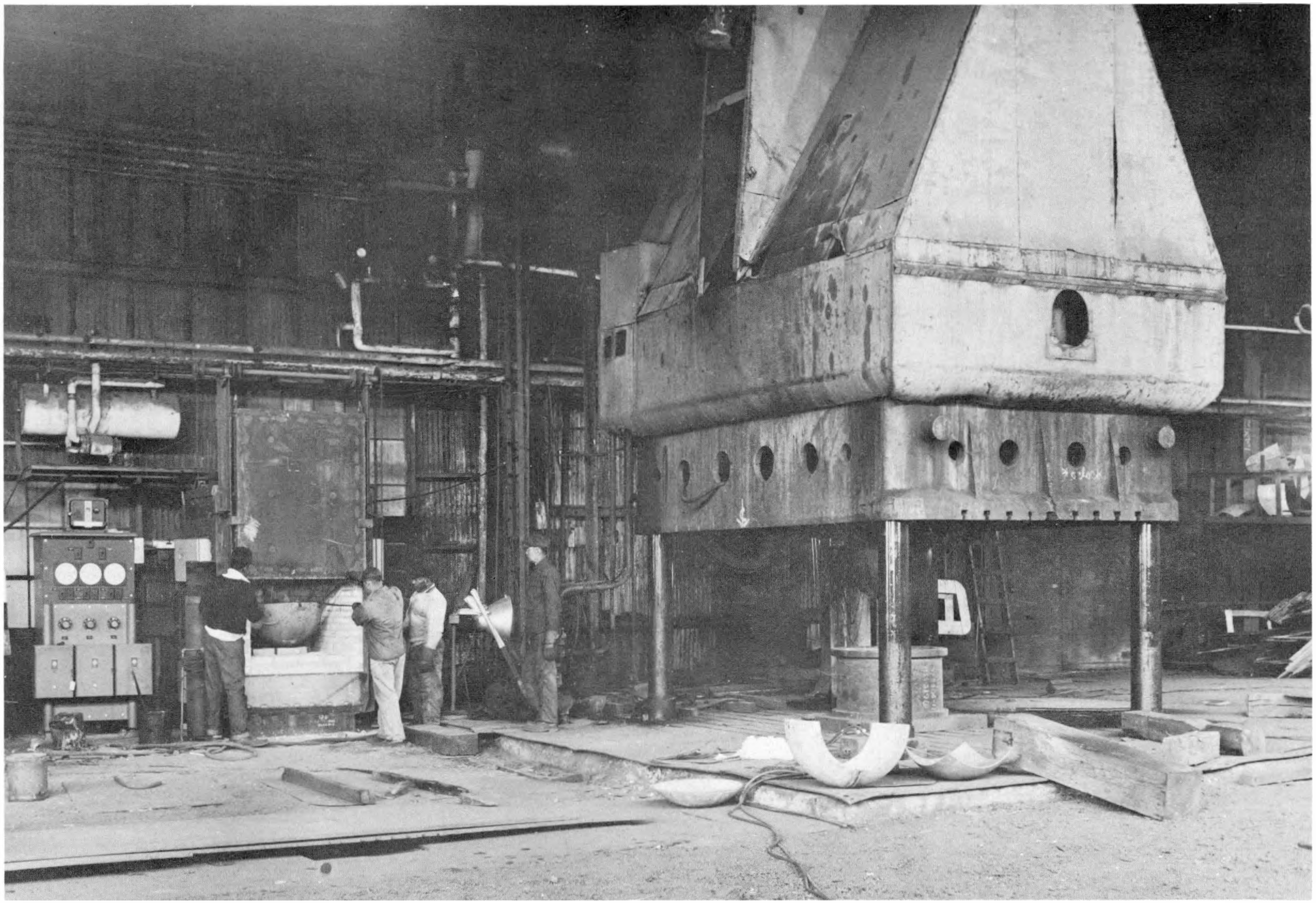

Fig. 3—General view of a forming operation on the mid-body section. The electric furnace and controls are in the left background. To the right is the press with a half and a quarter of the mid-body section and the dome section. All forming was done in air with the plate temperature between 750 and 1225°F. After final forming, the shaped plate was held at 1200 to 1225°F for 20 min and then cooled in the die to 200°F.

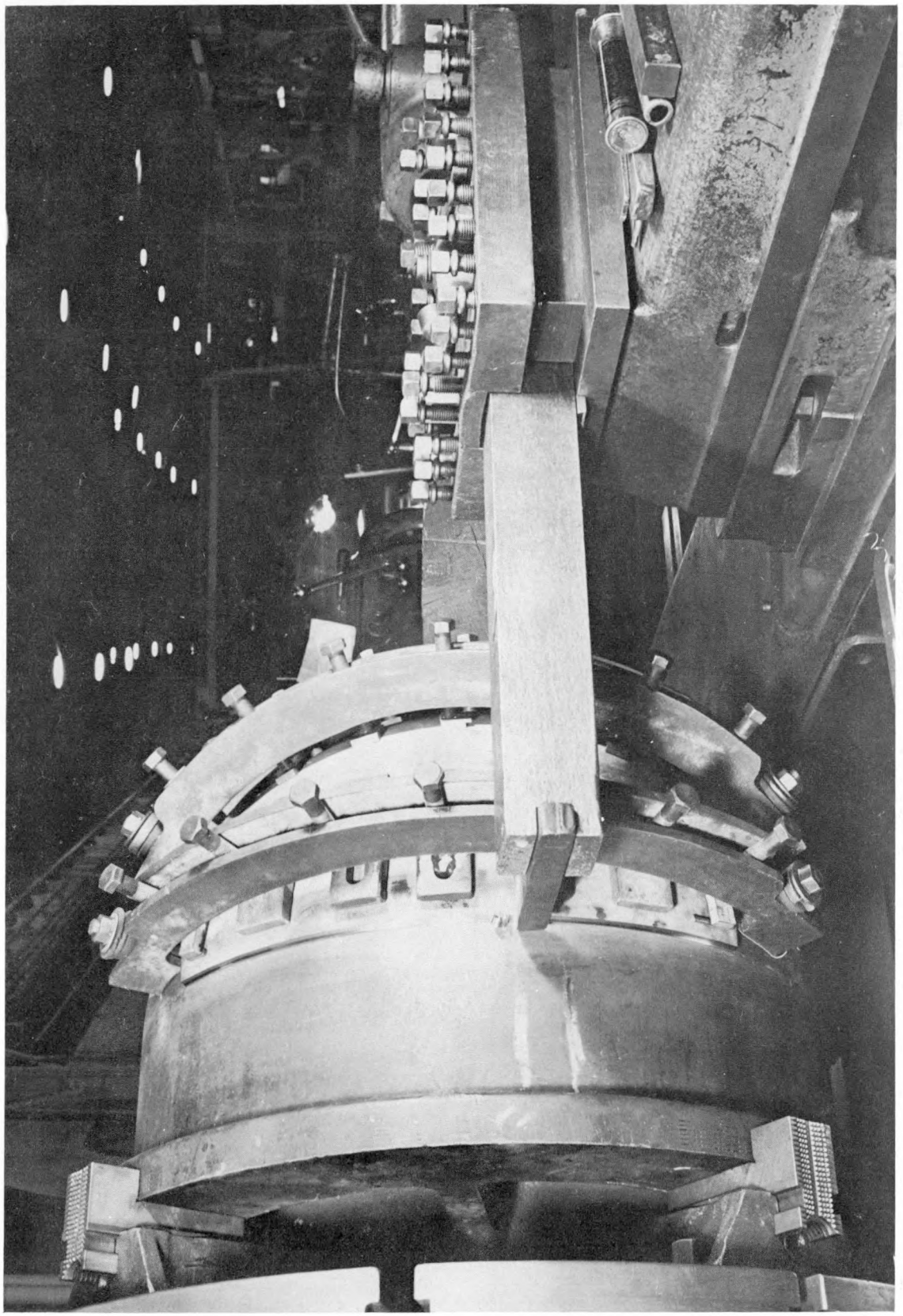

Fig. 4 — View showing the method of holding and machining spherical sections of plate. The material being machined is supported by male portion of forming die. All edges were machined before welding.

Fig. 5 — Preliminary forming of half of 30-deg cone.

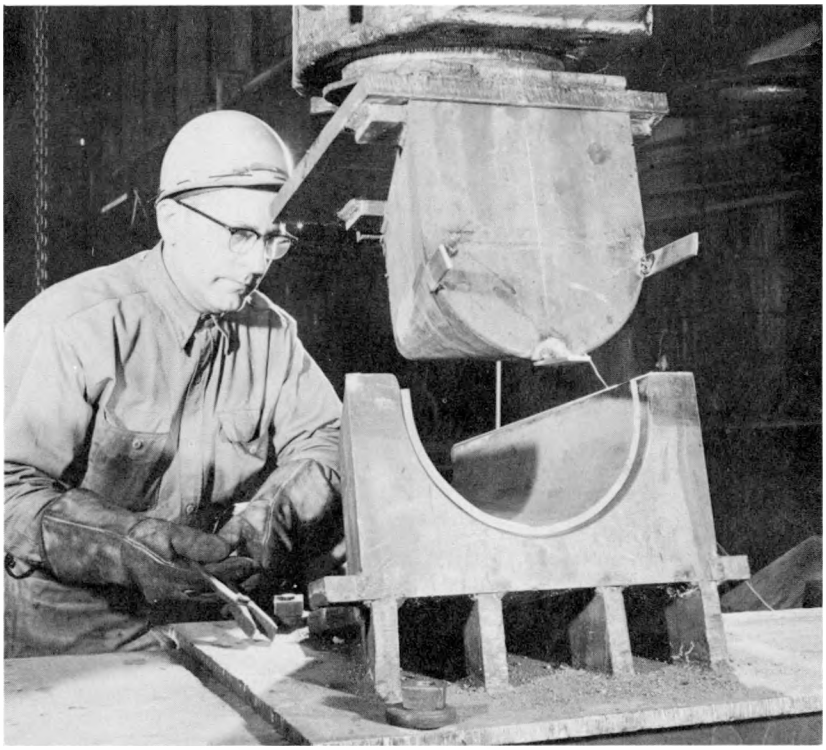

Fig. 6 — Final forming of half of 30-deg cone prior to welding halves together.

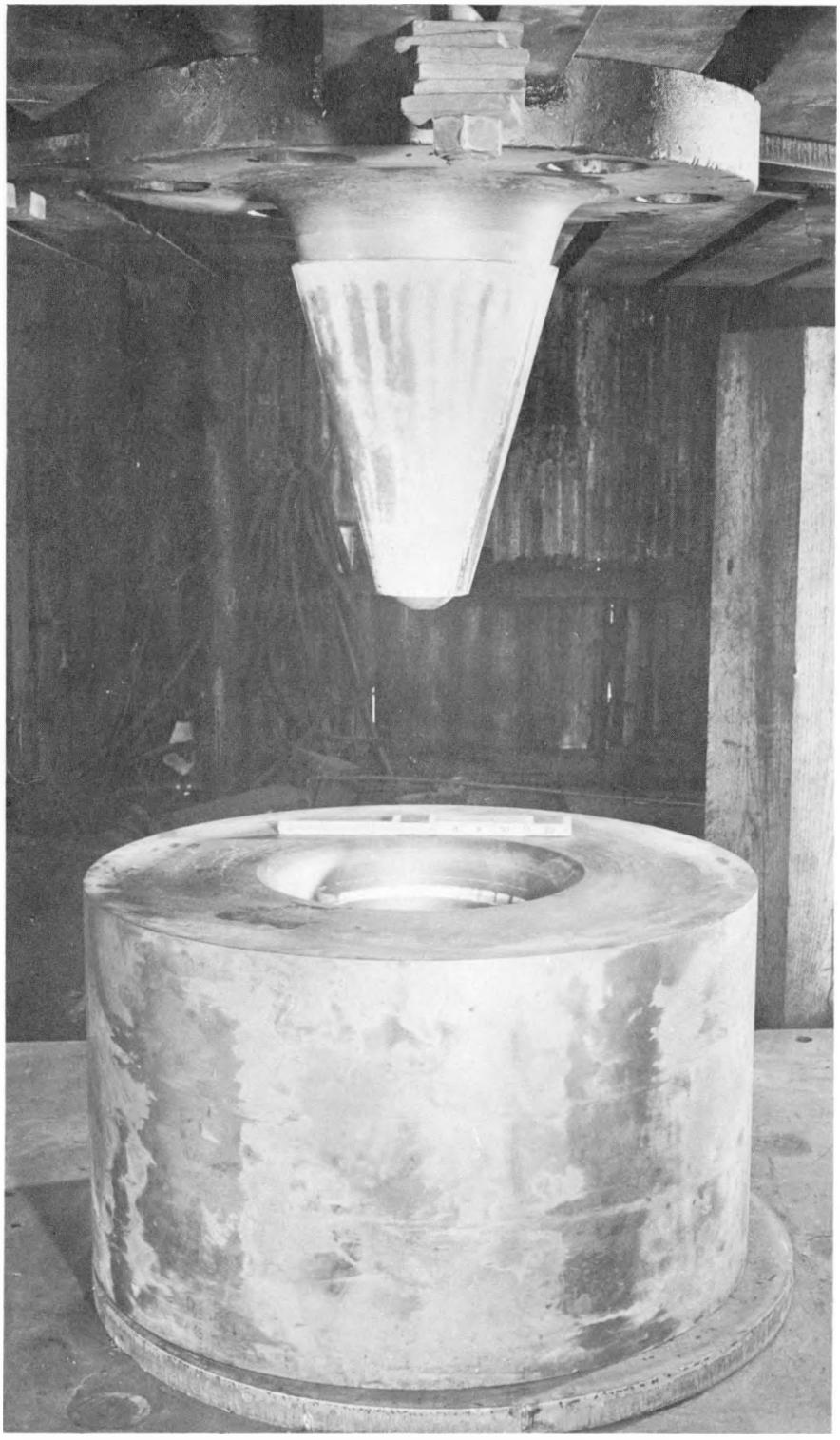

Fig. 7 — Final forming operation on 30-deg cone. The cone halves have been welded together and can be seen stuck to the upper die.

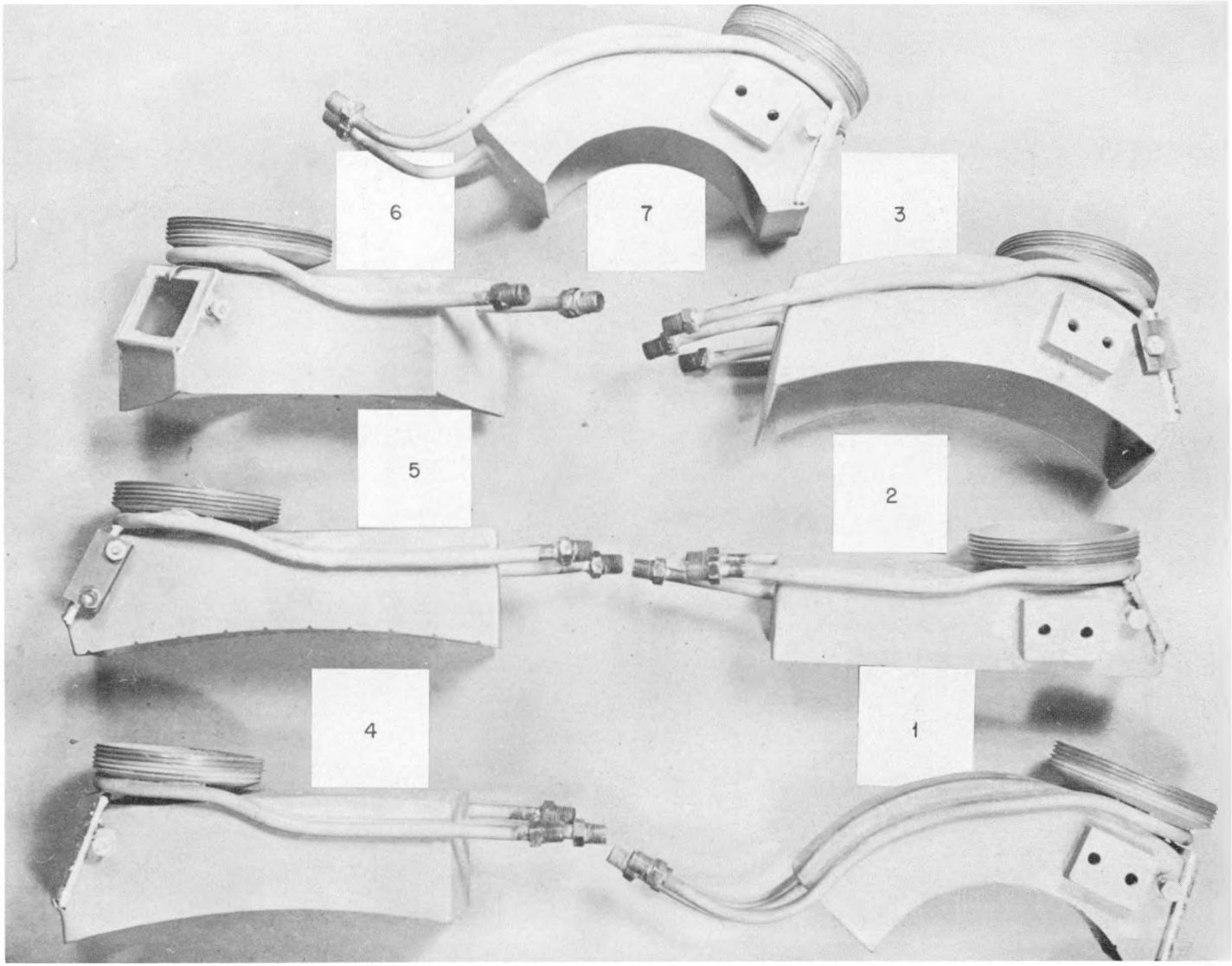

Fig. 8—Side view of the seven different welding shields used in welding. The shield was attached to a standard heliarc torch. Inert gas entered the shield via the torch and also through the copper tube inside the shield. Each shield is shaped to conform to the geometry of a particular joint. Outer tube provides cooling.

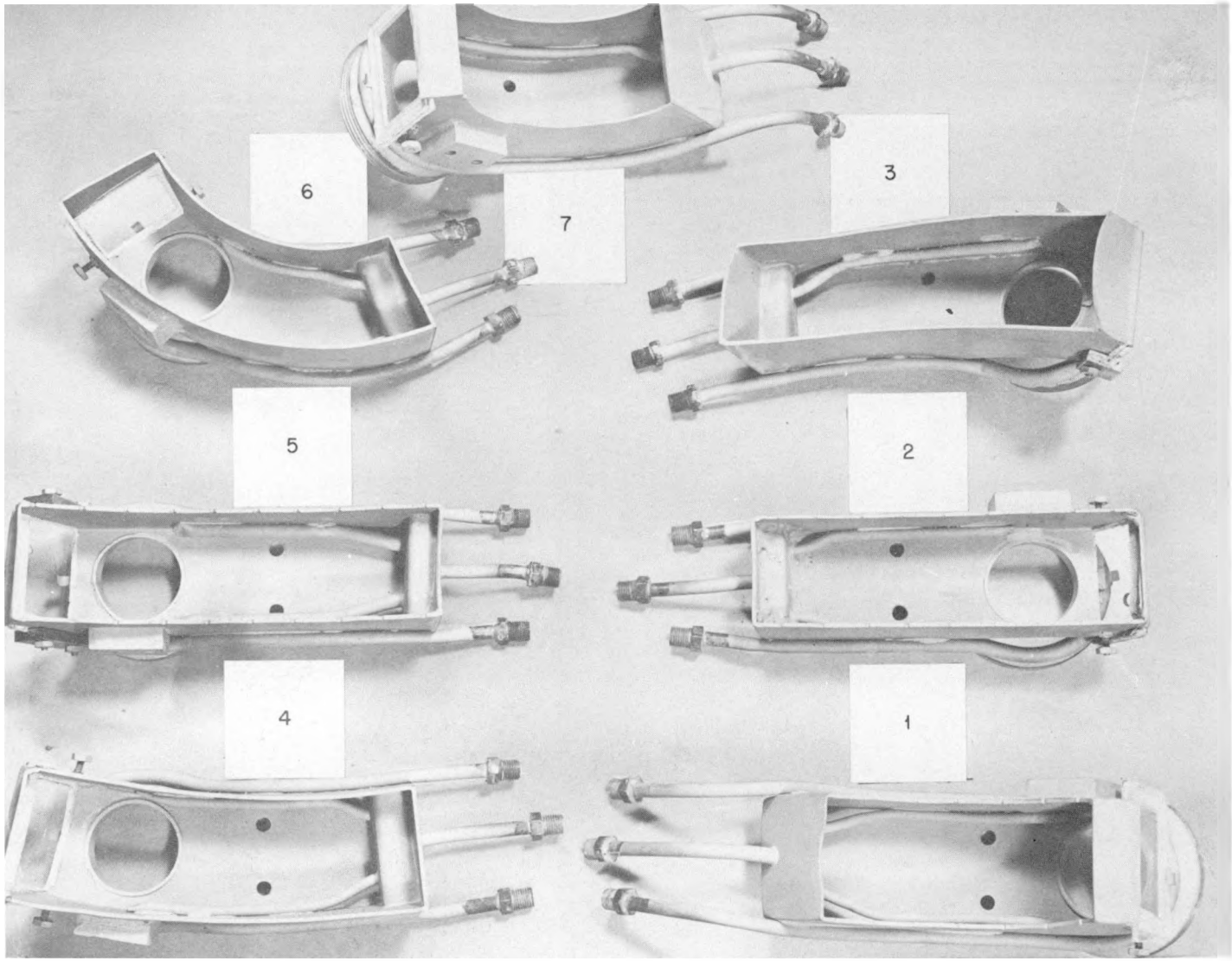

Fig. 9—Bottom view of seven welding shields. The opening in the forward end of each shield is for a glass window. Filler metal wire is inserted through a hole in the window.

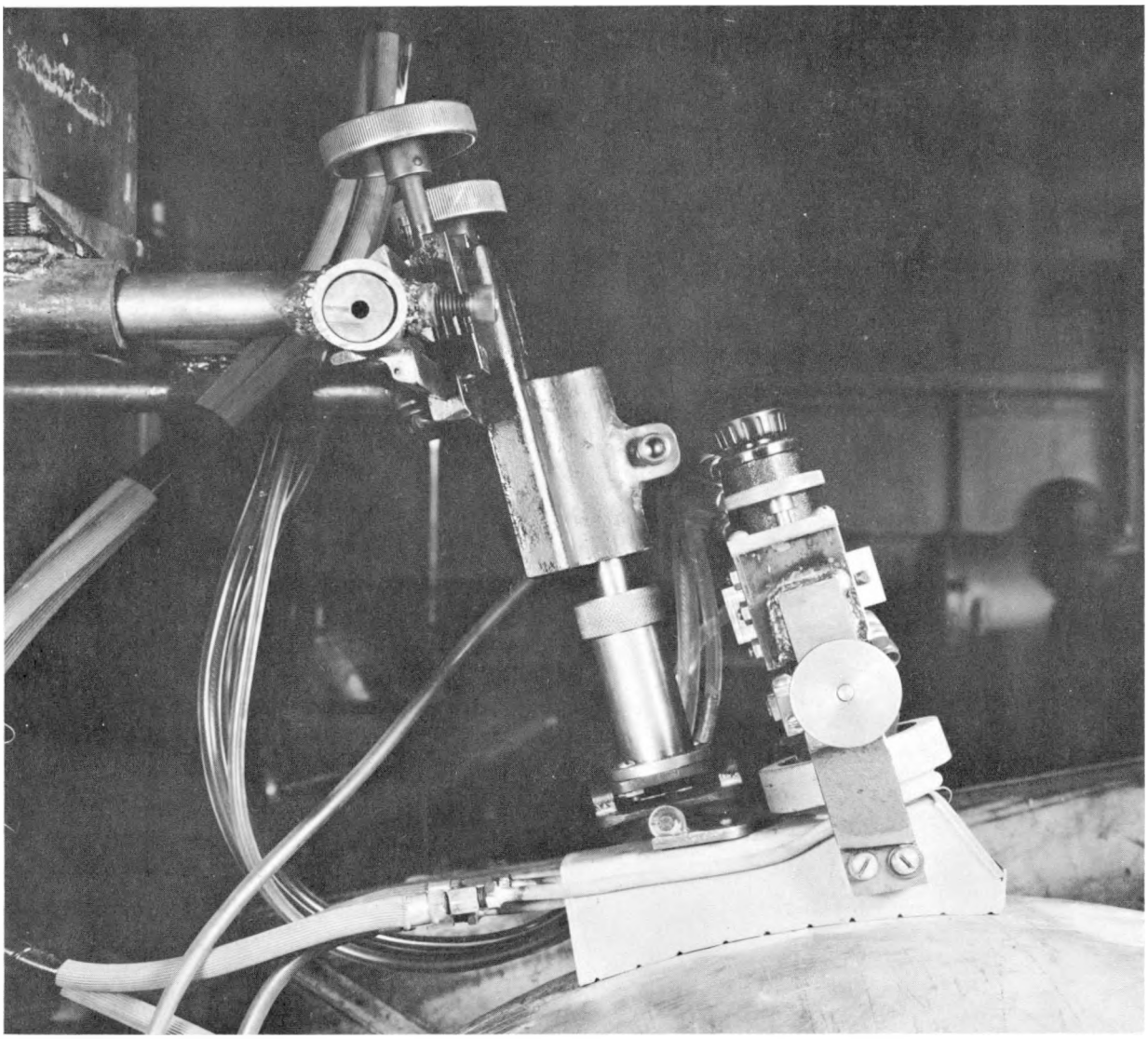

Fig. 10—Side view of torch and shield set up to weld spherical joint. Notches in the shield at the surface of the sphere allow the escape of gas.

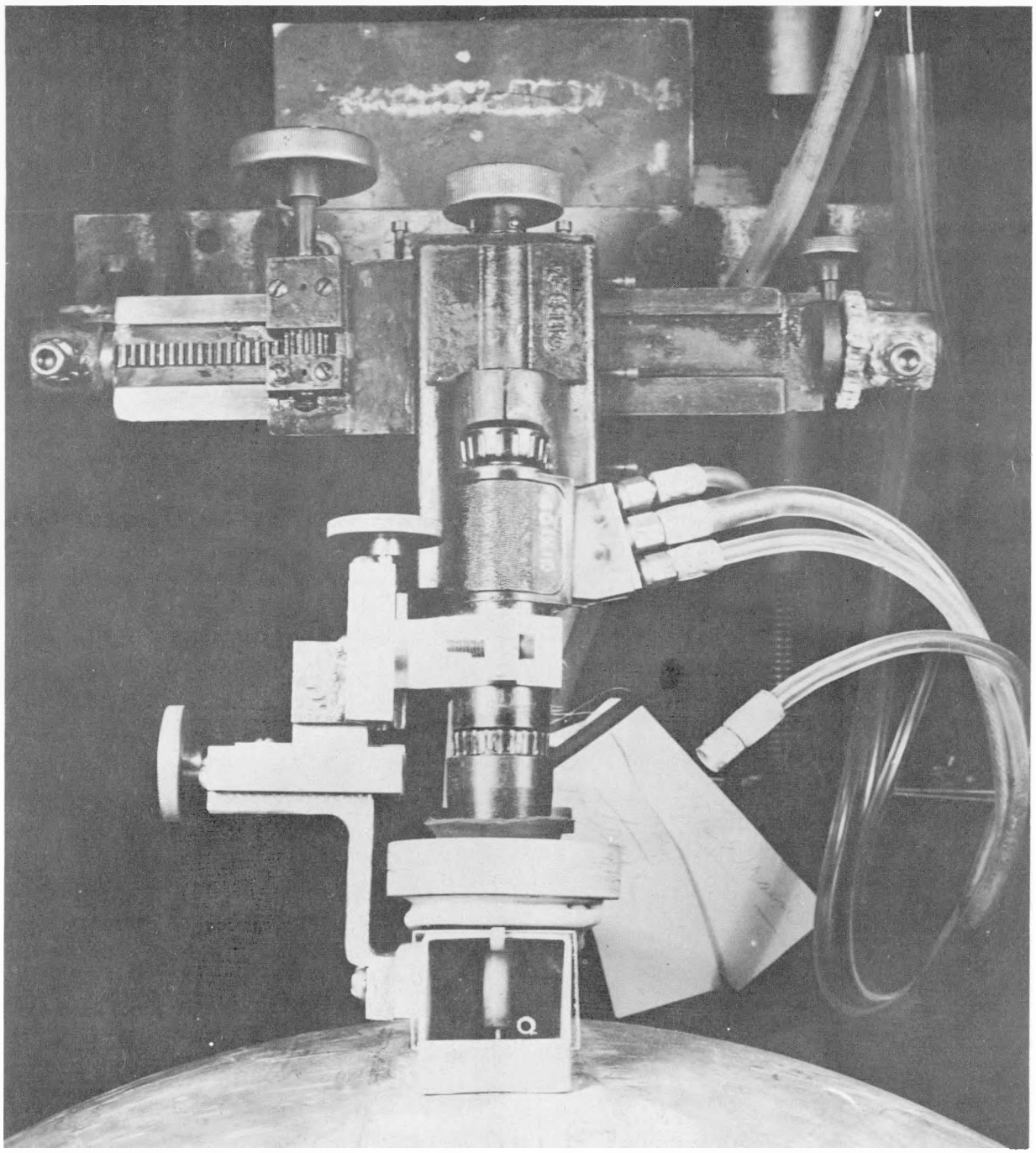

Fig. 11 — Front view of torch and shield set up to weld spherical joint. The two knobs on the left of the shield were used to adjust the arc length and to center the head on the weld. Welding was done by two operators. One operator manually fed filler wire into the weld puddle through the small hole in the glass window. He also controlled the transverse position of the electrode and the welding-current foot switch. The second operator controlled the arc voltage by adjustment of arc length, the welding current by a remote switch connected to the welding machine, and the movement of the work by a start-stop switch.

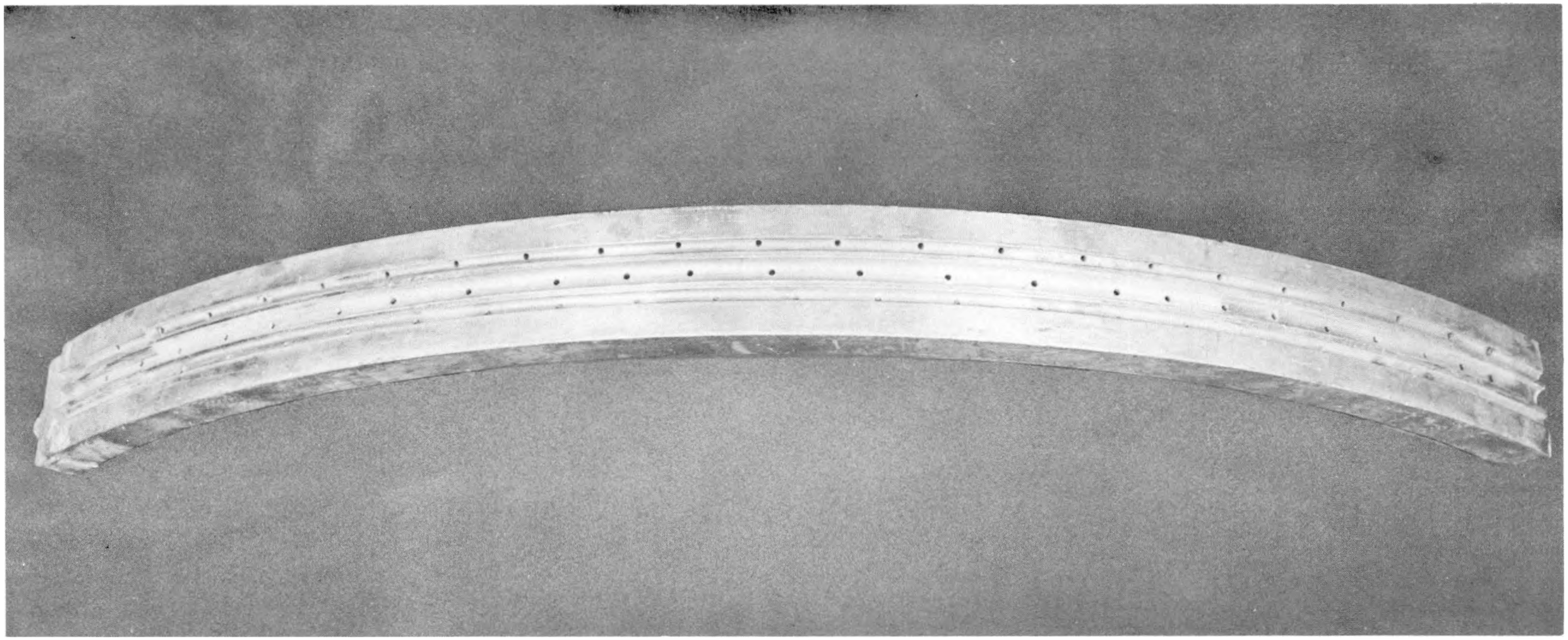

Fig. 12—Copper bar used for gas shielding on the back side of mid-body joints. A positive pressure of inert gas was maintained inside passages in the bar with gas flowing over the weld area from regularly spaced holes. In some cases back shielding was accomplished by closing both ends of the assembly and filling with inert gas.

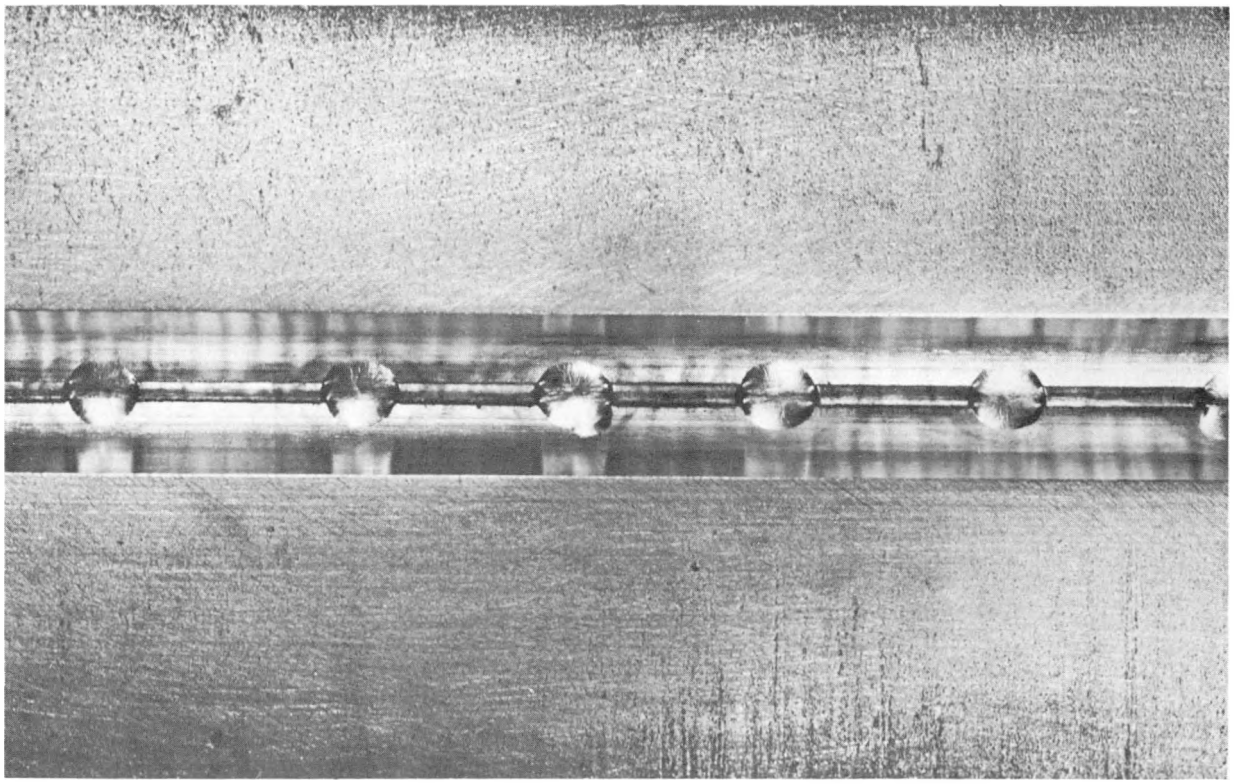

Fig. 13—Typical joint fitted up for welding. A $^{5}/_{32}$-in. E. B. type consumable insert is tack welded in place at about 1-in. intervals using a heliarc hand torch. Insert is fused into root pass without additional filler metal by moving joint under shielded torch.

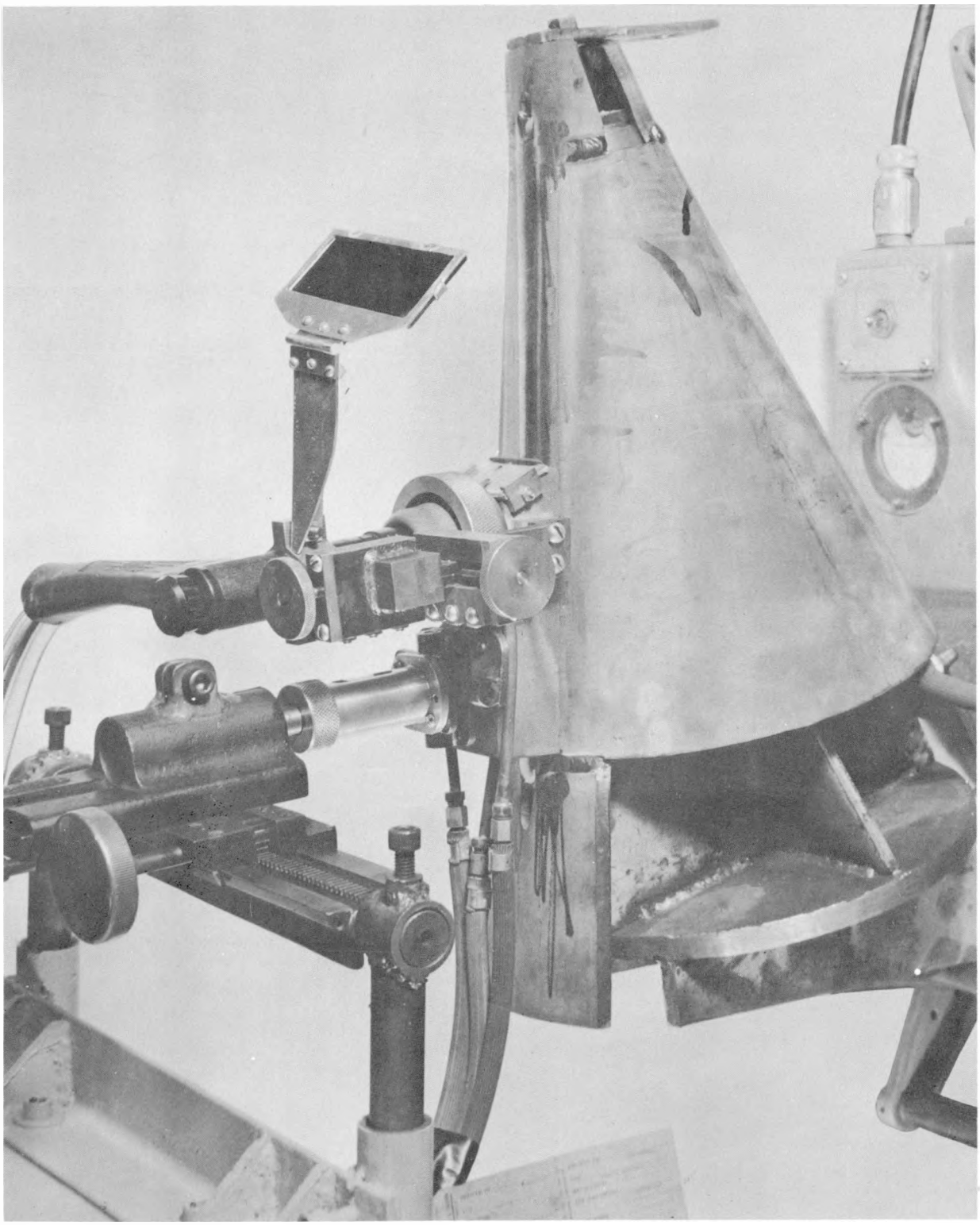

Fig. 14—Arrangement for making longitudinal joints in 30-deg cone section. Note the end tabs and completed weld.

Fig. 15—Arrangement for joining two spherical pieces of mid-body section. The assembly is rotated about the center of curvature, and the copper backing bar is held in place by the inner supporting structure.

Fig. 16—Setup for joining inlet cylinder to 30-deg cone. Back shielding is accomplished by closing the ends and feeding inert gas into the flange end of the assembly.

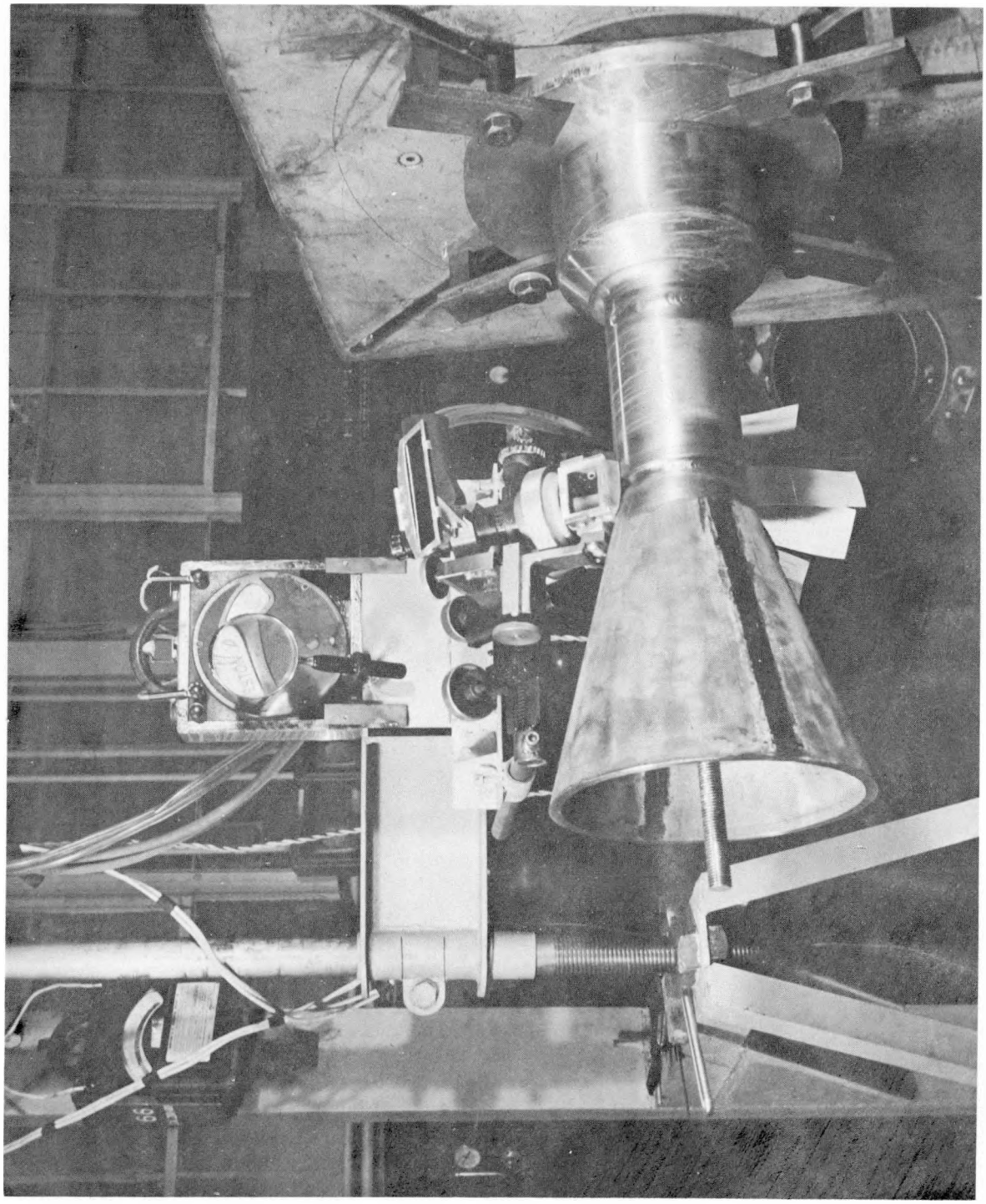

Fig. 17—Another view of setup for joining inlet cylinder to 30-deg cone.

Fig. 18—Arrangement for joining 90-deg cone to spherical mid-body.

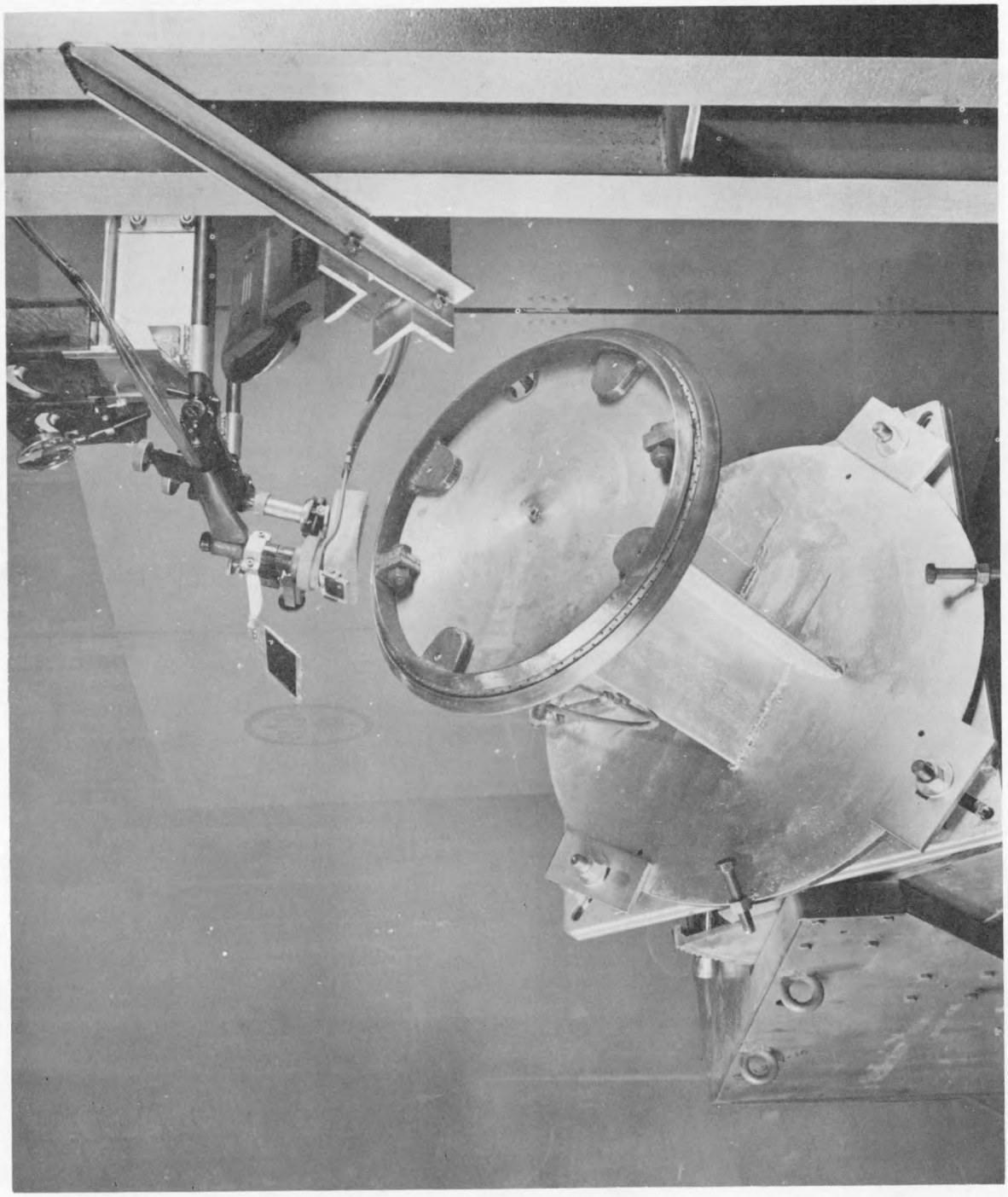

Fig. 19—Arrangement for providing inert gas backing in the setup in Fig. 18.

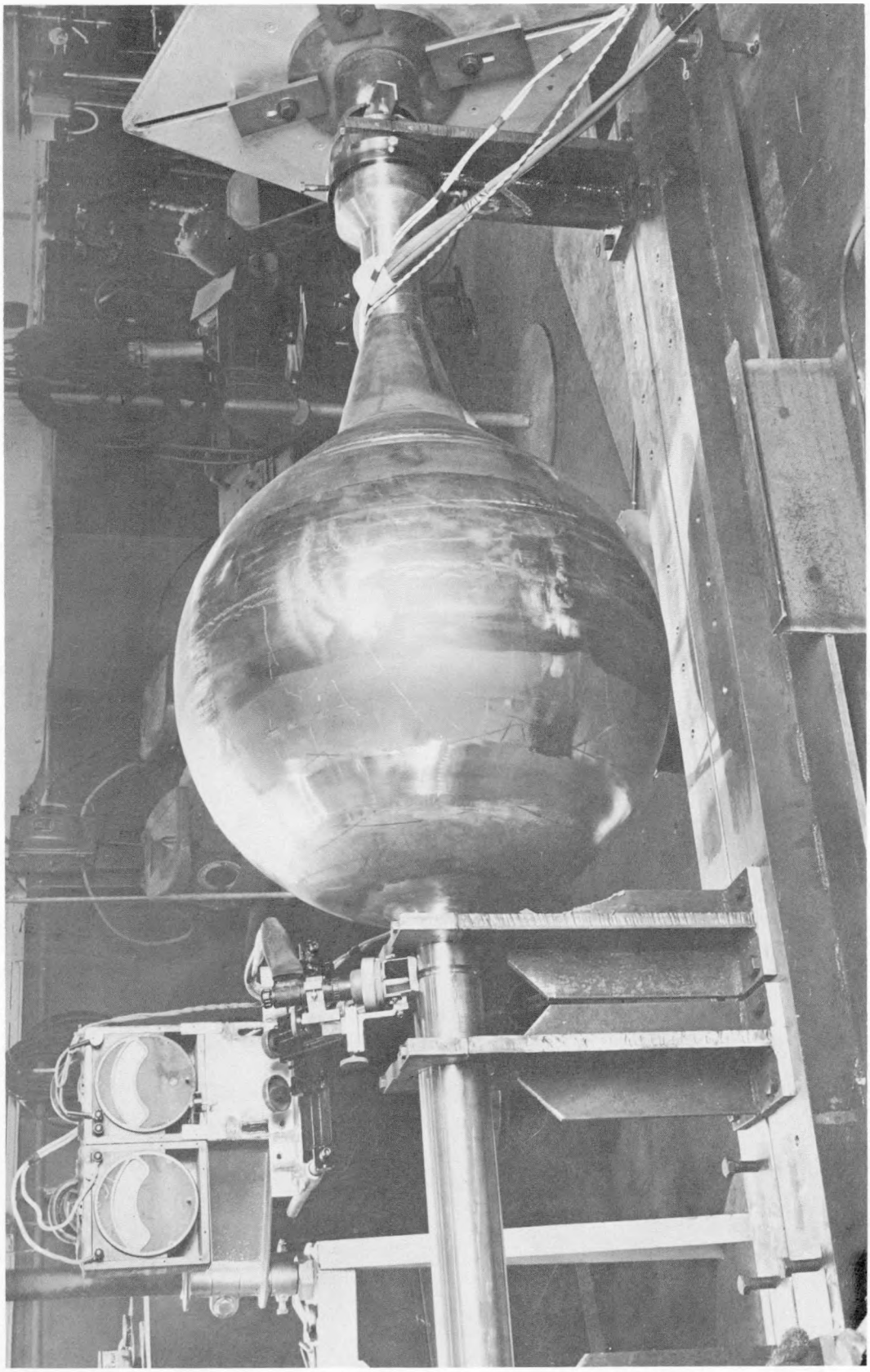

Fig. 20—Joining transition piece to outlet cylinder.

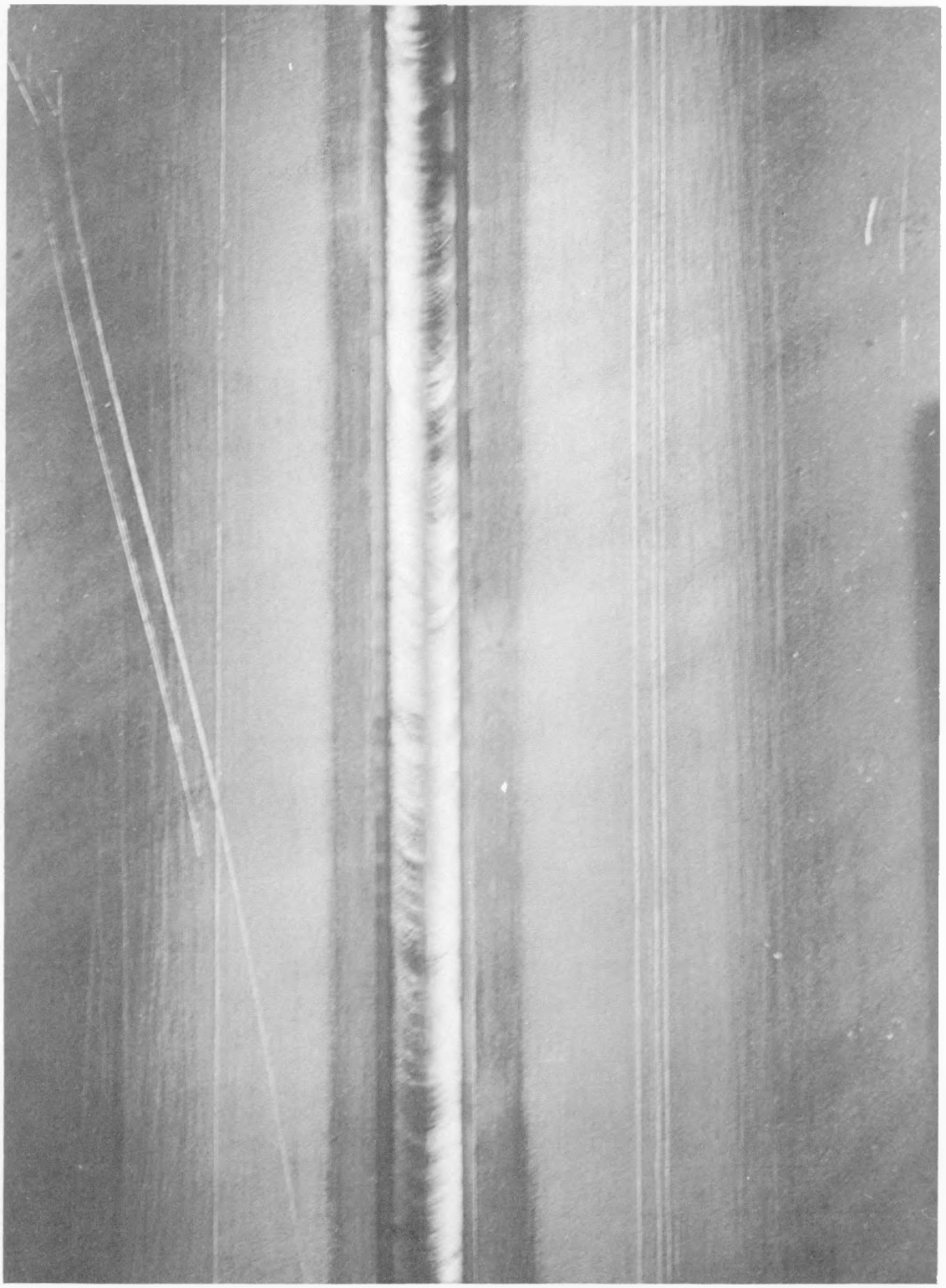

Fig. 21—Groove side of typical joint after fusing consumable insert in $\frac{5}{16}$-in. material.

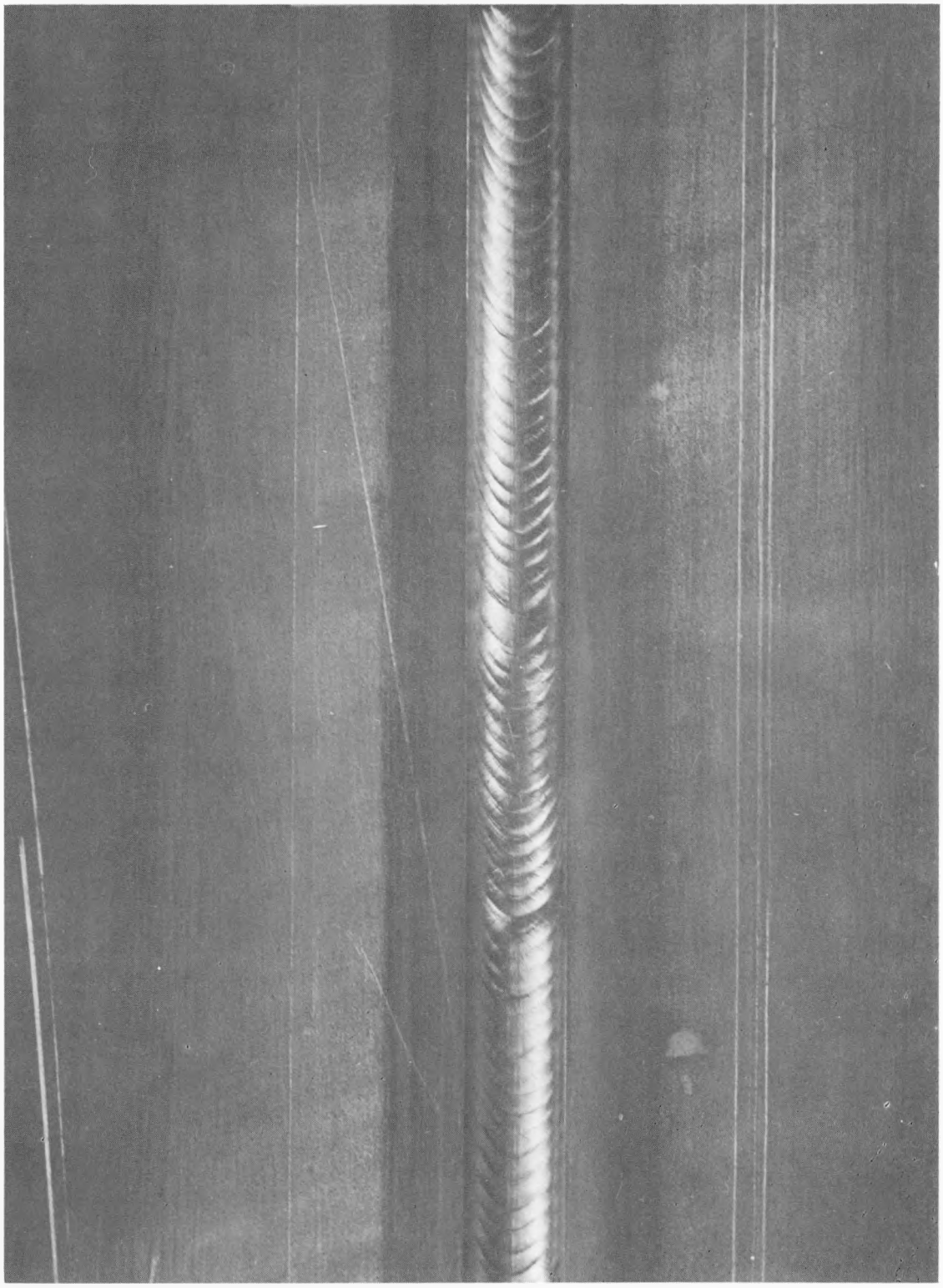

Fig. 22—Groove side of typical joint after second pass.

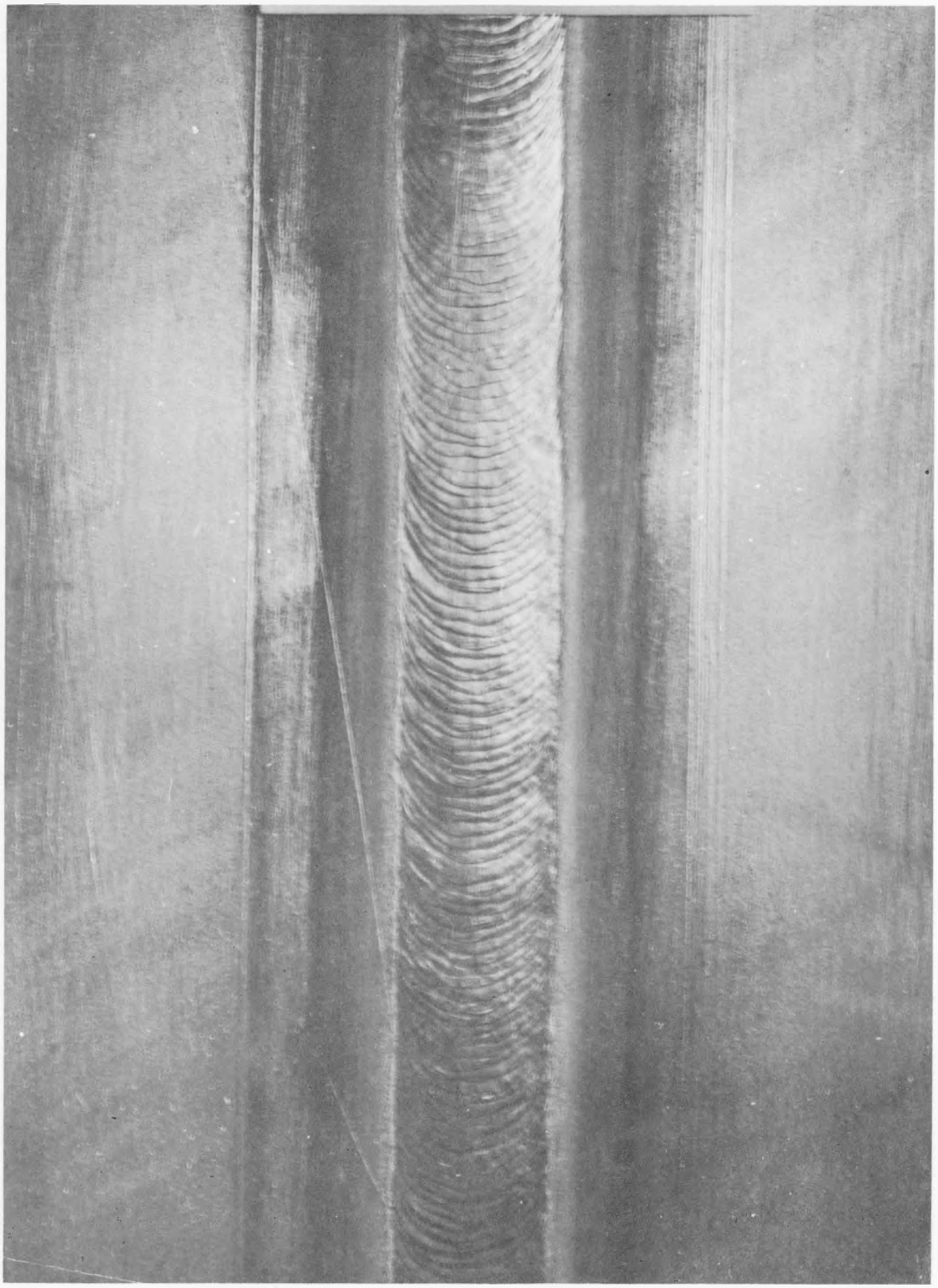

Fig. 23—Outside of typical joint after fifth pass (final) in $^{5}/_{16}$-in. material.

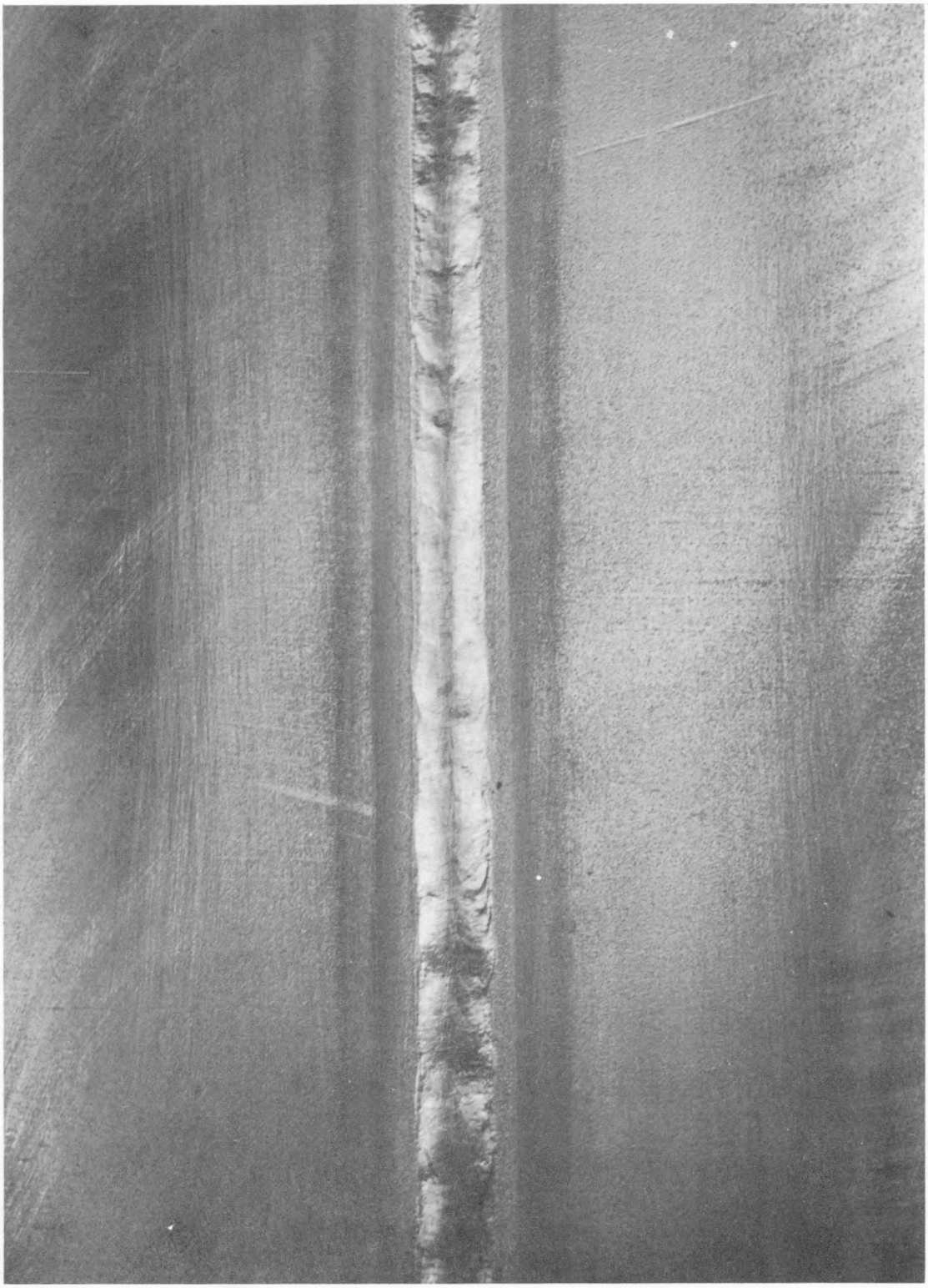

Fig. 24 — Back side of joint with fused consumable insert in $\frac{5}{16}$-in. plate.

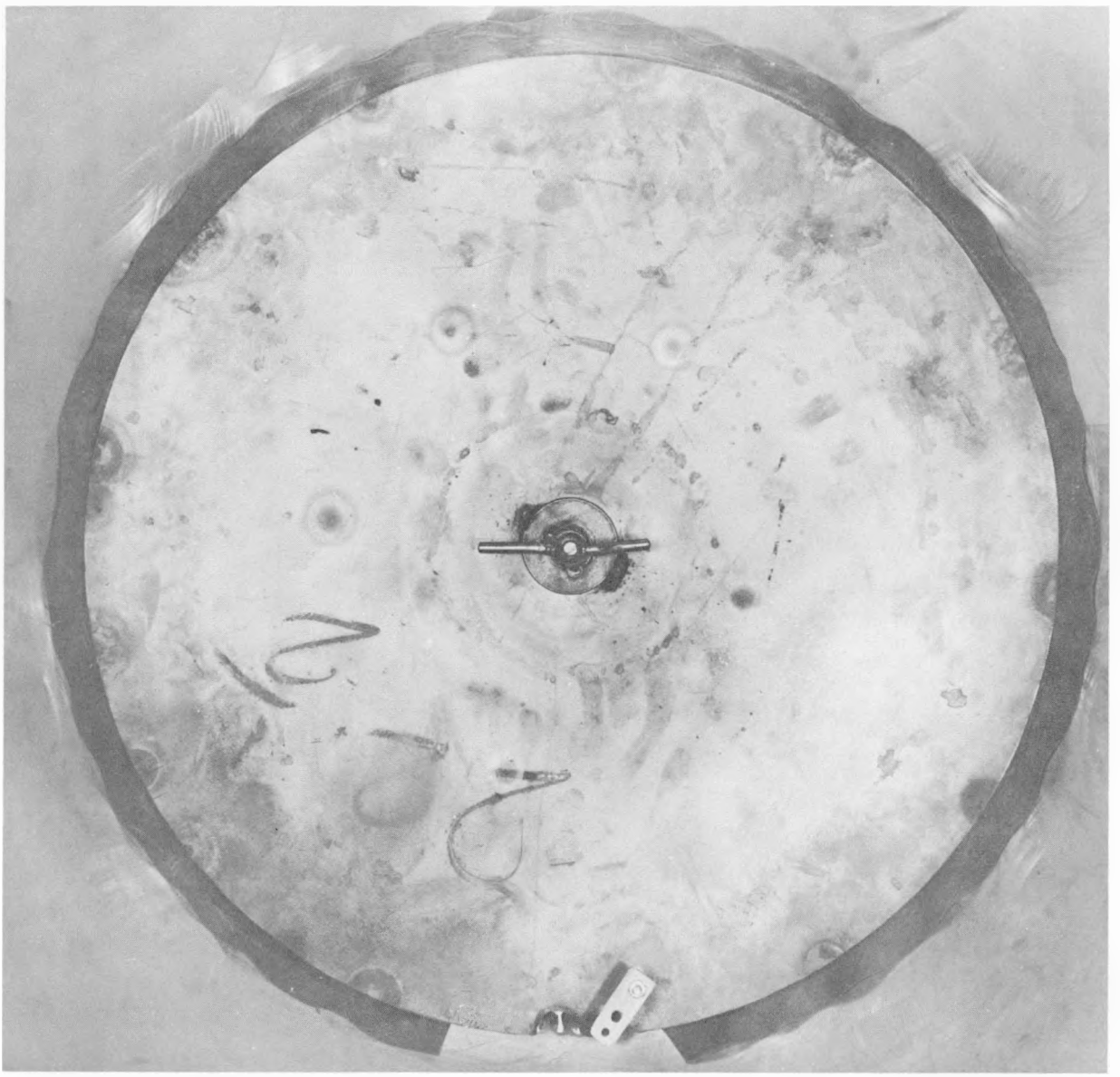

Fig. 25—Blanking arrangement for welding No. 9 diffuser screen in place. These were hand welded to the inner surface of the cone through the small hole in the blank at the bottom of the picture.

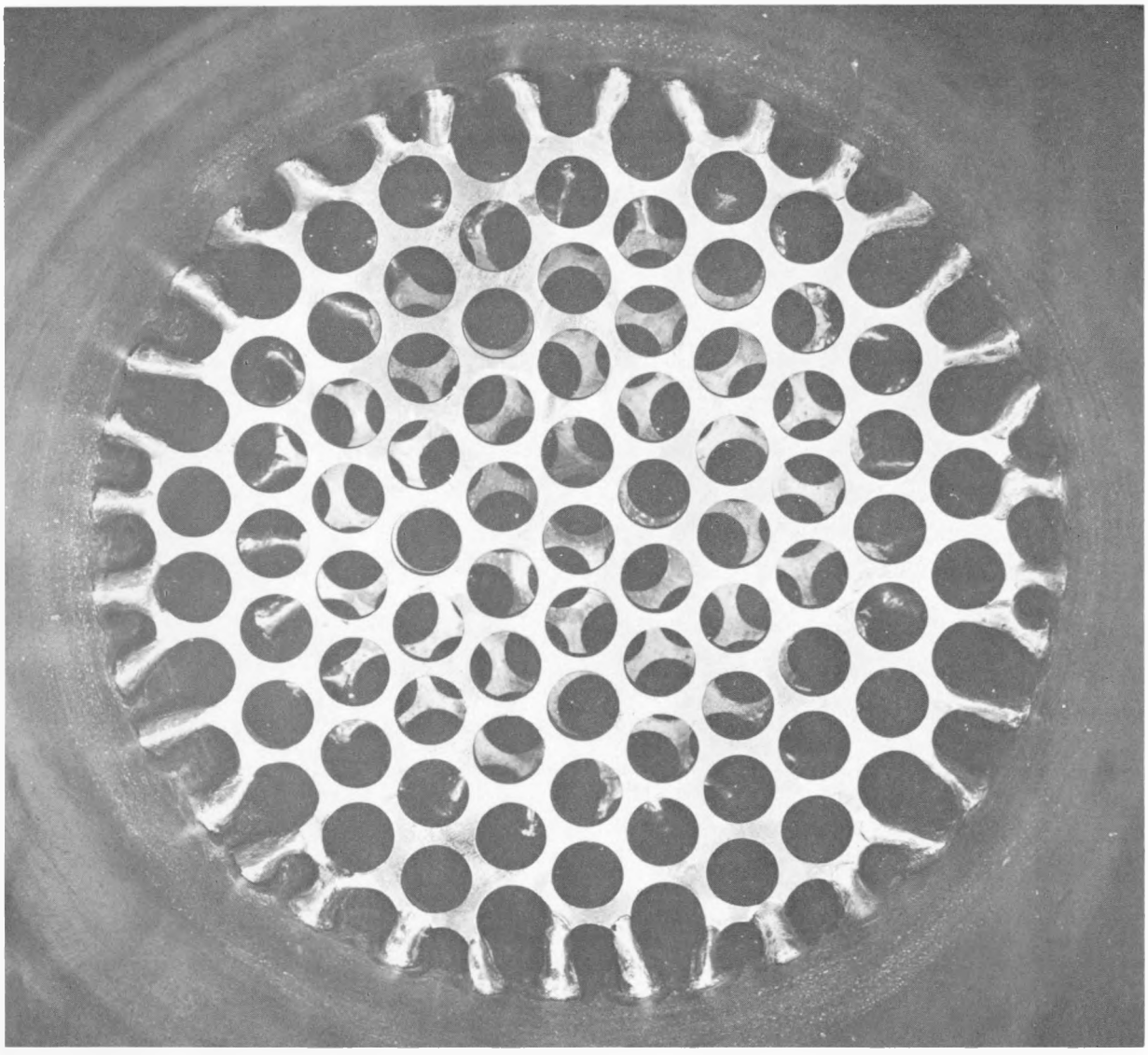

Fig. 26—Interior view of diffuser screen attached to 30-deg cone.

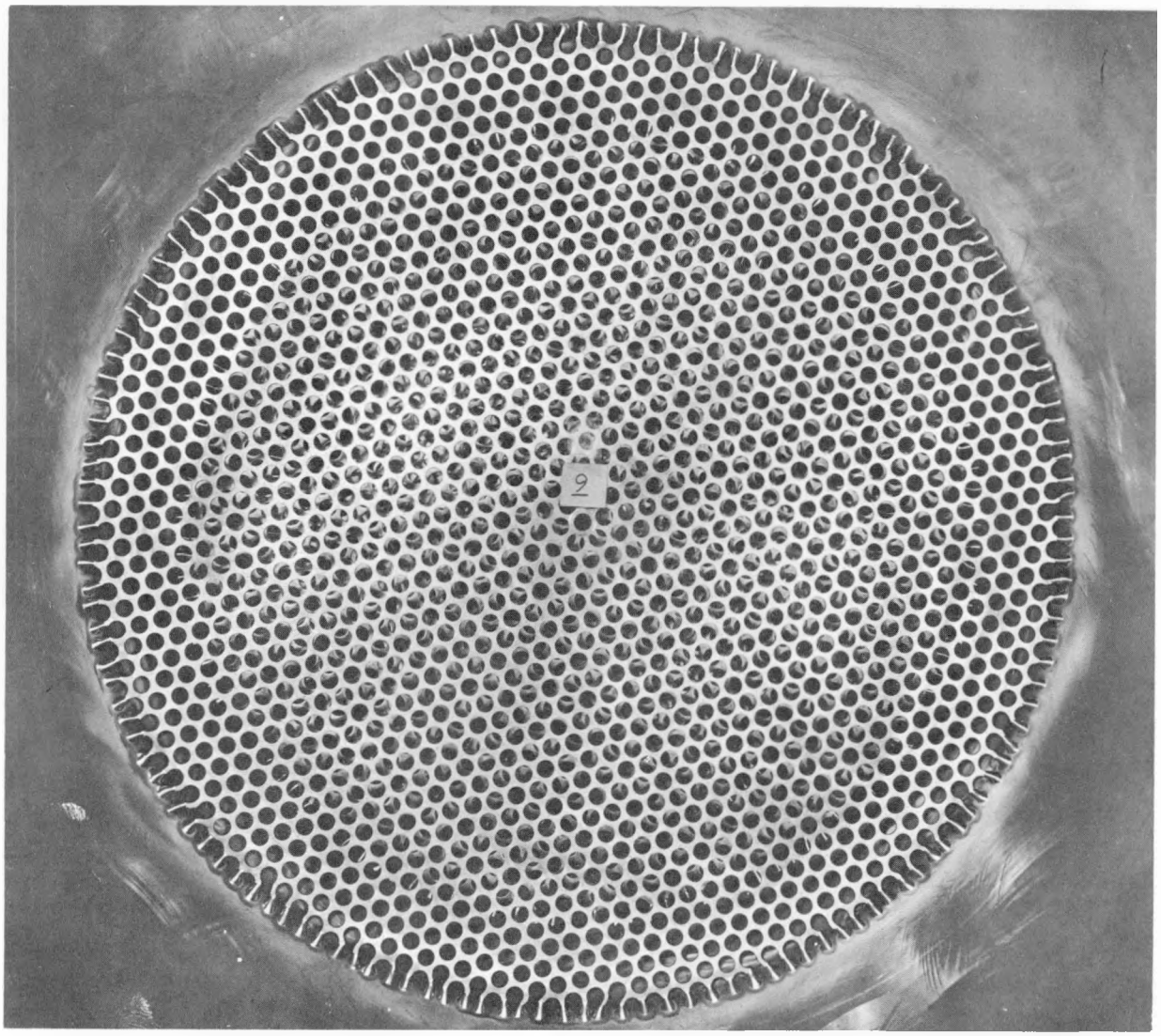

Fig. 27 — View looking down into vessel with all screens in place.

Fig. 28—Making dimensional check of outside of vessel. Measurements of both radius and thickness were made and recorded every 15 deg. Thickness measurements were made by a calibrated audigauge. Radius readings were taken before and after the hydrostatic test.

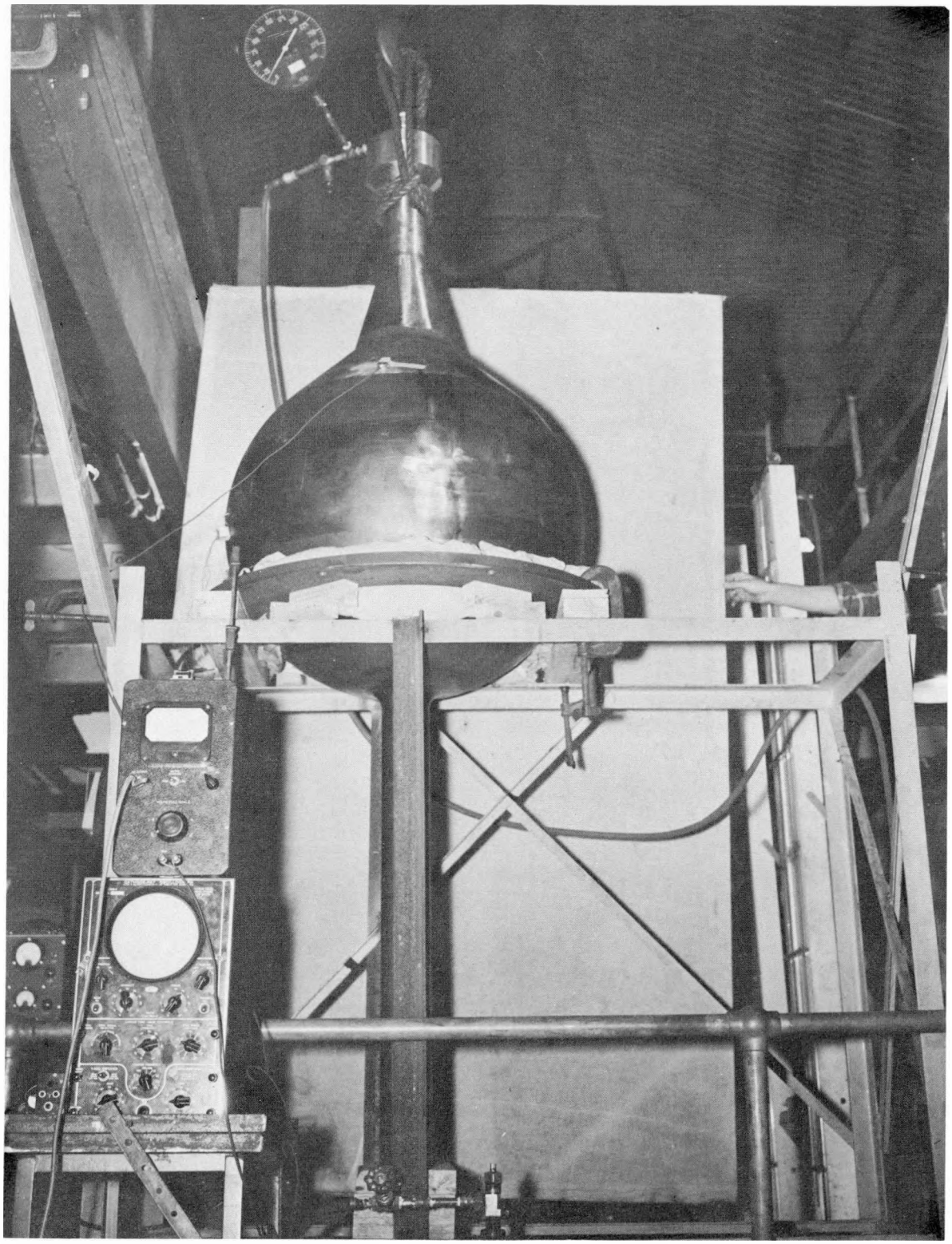

Fig. 29—Hydrostatic test of completed vessel at 775 psi. The membrane stress for this pressure is 20,000 psi. The yield at 0.2 per cent offset for the material is at 44,000 psi.

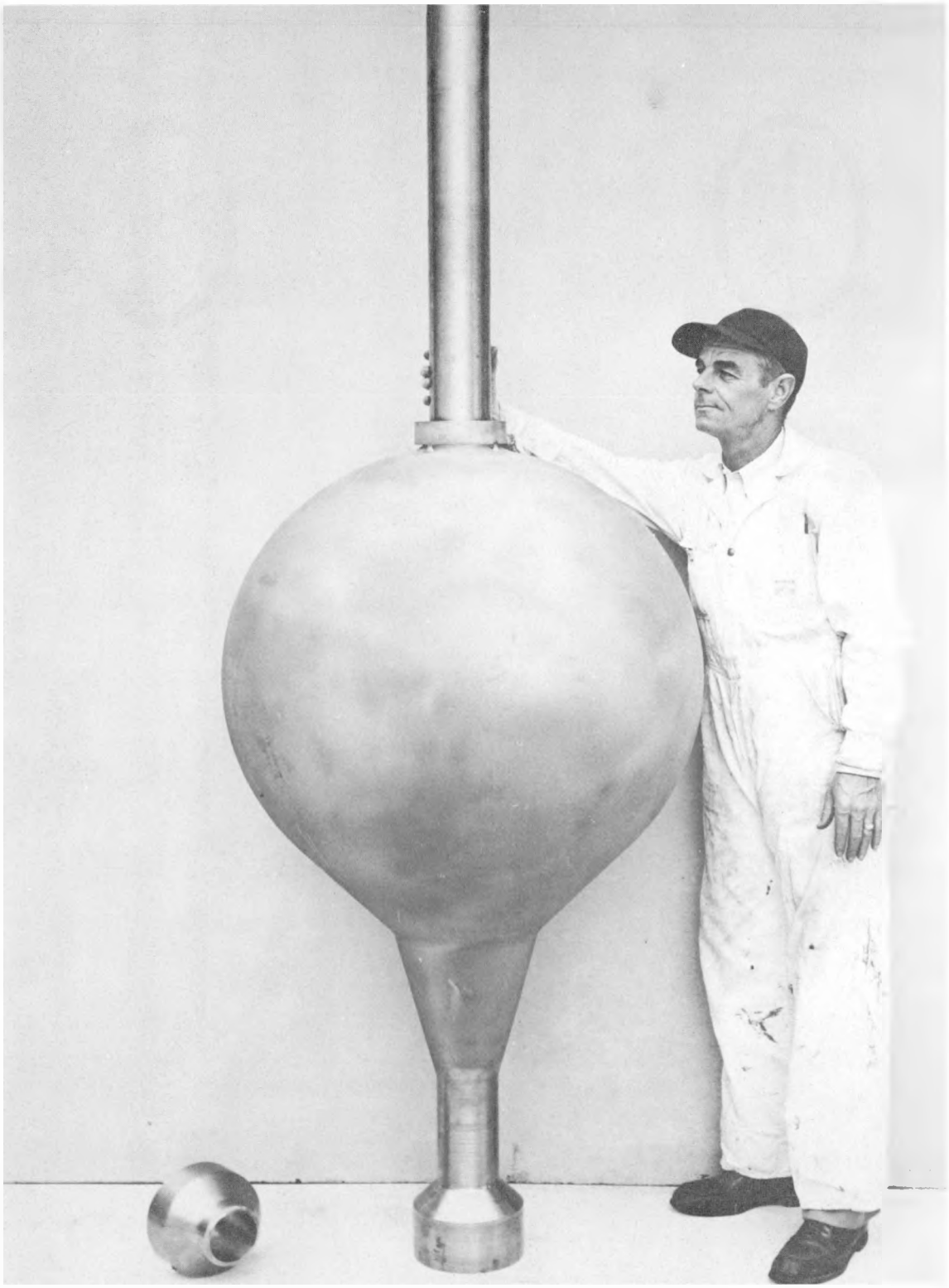

Fig. 30 — Completed Zircaloy-2 vessel prior to installation inside the outer pressure vessel. The outlet flange shown on the floor was welded to the outlet cylinder after installation in the top portion of the pressure vessel.

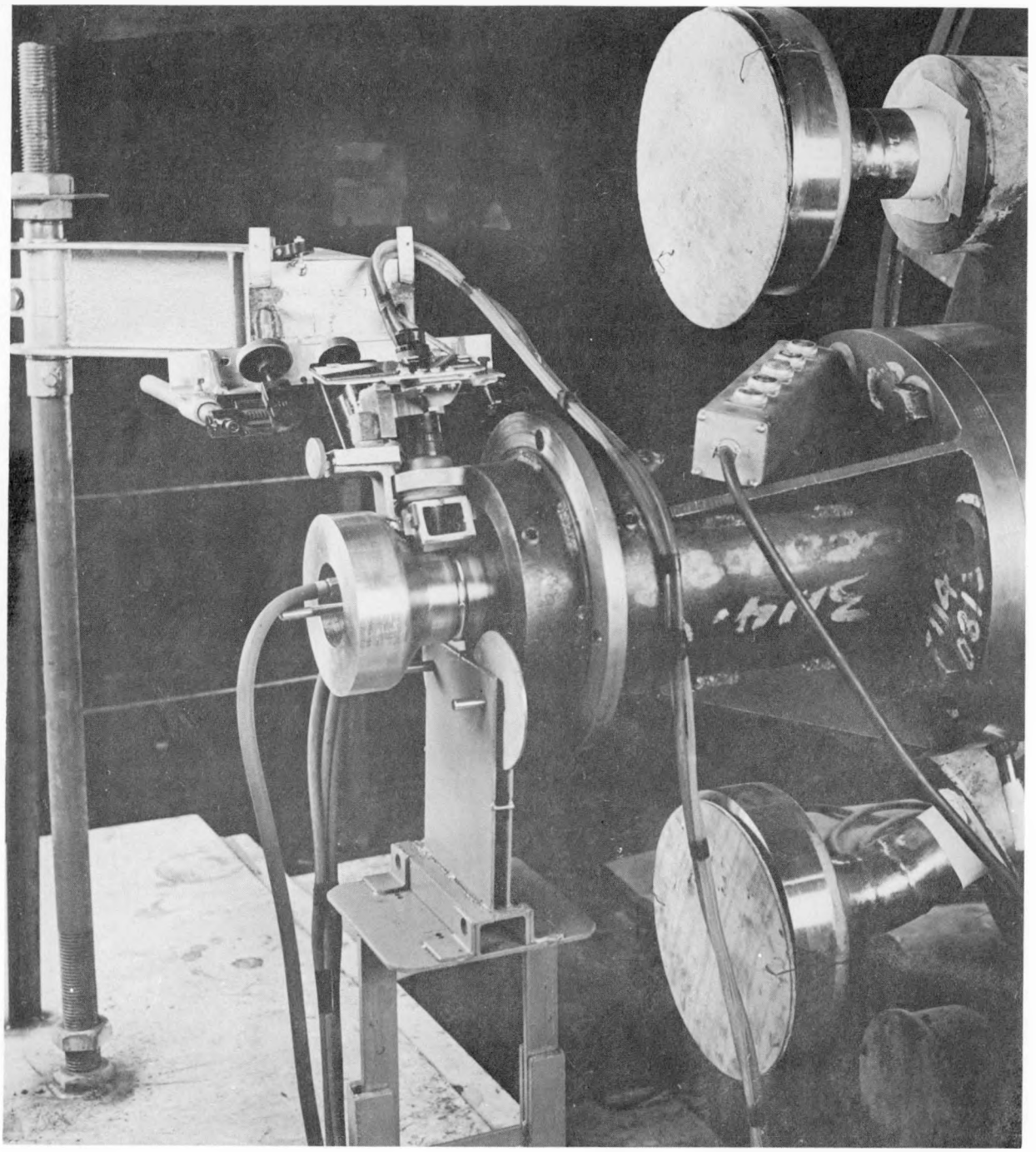

Fig. 31 — Final weld of Zircaloy-2 material. The core vessel is inside the pressure vessel to the right.

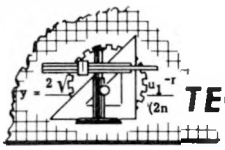

TECHNICAL NOTES

Spontaneous Ignition of Highly Irradiated Fuel

J. H. KITTEL

Argonne National Laboratory

September 19, 1950

Occasionally, routine handling of highly irradiated fuel specimens at Argonne National Laboratory (ANL) has been complicated by an observed tendency of such material to ignite spontaneously and to burn to oxide. An incident of this nature not only is an incendiary hazard but also has been observed to cause large amounts of fission-product activity to become air-borne. In order that those who are contemplating the handling of highly irradiated fuel for purposes such as experimental measurements or metallurgical reprocessing may become more familiar with this phenomenon, the following account is given regarding a number of such occurrences that have been observed during hot-cell operations at ANL.

The first metal that was observed to ignite was a 2.8-g specimen, No. AA-15, of uranium–0.52 wt. % zirconium alloy which had been irradiated to 1.7 per cent total atom burn-up (14,000 Mwd/ton). It was being examined in October 1953, after having been removed from an irradiation capsule containing NaK for heat transfer.[1] About 5 min after the specimen was chemically cleaned of adhering NaK and dried, it was picked up with a pair of forceps. When touched, the specimen briefly flashed and a few seconds later was a flowing cherry-red. After an additional few seconds the specimen was white hot and began to disintegrate, and during this stage tiny flakes of burning metal were observed to occasionally spall off the specimen, one of which ignited some paper about 18 in. away. Within a minute the specimen was completely converted into a small heap of black oxide. The conditions under which the specimen was irradiated are shown in Table 1, and a photograph of a similar specimen that did not burn is shown in Fig. 1.

Fig. 1 — An irradiated gamma quenched uranium–0.52 wt. % zirconium alloy specimen similar to specimen AA-15, which ignited before being photographed. (Magnification 2×.)

Table 1 — Irradiation Conditions for Specimens Which Have Ignited

Specimen	Composition	Fabrication and heat-treatment	Preirradiation dimensions, in.		Weight, g	Calculated burn-up		Max. irradiation temp.,* °C	Approx. ignition time,† min.
			Length	Diameter		Total at. %	Mwd/ton		
AA-15	U–0.52 wt. % Zr 10% enriched	Swaged at 300°C; 1 hr at 800°C; water quenched; 2 hr at 575°C	0.750	0.125	2.8	1.7	14,000	620	5
G-16	U, 10% enriched	As-cast	1.00	0.16	6.5	0.99	8,400	790	10
G-17	U, 10% enriched	Swaged at 300°C; 20 min at 725°C; water quenched; 2 hr at 575°C	1.00	0.16	6.5	1.2	10,000	720	15
G-20	Natural U	Powder compact; pressed at 600°C	1.00	0.375	33.6	0.53	4,500	770	40
BG-5	U–10 wt. % Pu	Extruded at 500°C; 2 min at 645°C; 1 hr at 500°C; furnace cooled	0.750	0.120	2.8	0.45	3,800	520	5

* Calculated for central metal conditions at beginning of exposure.
† Elapsed time between removal of specimen from cleaning solution and its ignition.

Fig. 2 — Specimen G-16, as-cast unalloyed uranium, with a total atom burn-up of 0.99 per cent (8400 Mwd/ton). The hazy appearance of the right end of the specimen resulted from the ignition of the specimen at that point during photographic exposure. (Magnification 2×.)

Fig. 3 — Specimen G-17, beta quenched unalloyed uranium, with a total atom burn-up of 1.2 per cent (10,000 Mwd/ton). Shortly after this photograph was taken the specimen ignited at the left end. (Magnification 2×.)

Subsequently, the four other specimens of various types listed in Table 1 have also been observed to ignite and to burn to oxide under similar circumstances, although all these specimens ignited without being touched at the time by another object. The ignition time, or elapsed time between removal of the specimens from the cleaning solution and their ignition, ranged from about 5 to approximately 40 min. The ignition time of all the specimens appeared to depend on their weights. Photographs of these specimens, or of identical specimens that did not burn, are shown in Figs. 2 to 5. The dependence of ignition time on the weights of the specimens is shown in Fig. 6.

It can be noted from the photographs that all the specimens have had their surface to mass ratios greatly increased by extensive roughen-

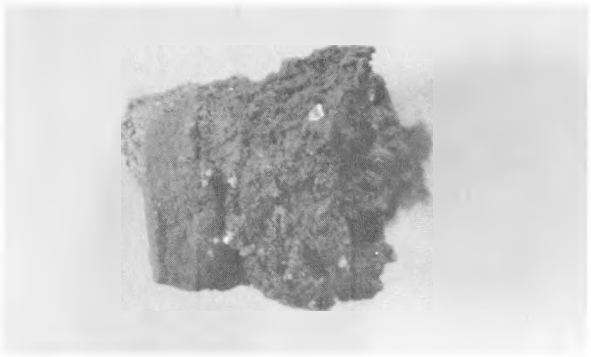

Fig. 4 — Specimen G-20, a hot-pressed unalloyed uranium compact, with a total atom burn-up of 0.53 per cent (4500 Mwd/ton). The specimen ignited about 35 min after this photograph was taken. (Magnification 2×.)

Fig. 5 — An irradiated uranium–10 wt. % plutonium alloy specimen cooled slowly through the beta-alpha transformation. This specimen is similar to specimen BG-5, which ignited before being photographed. (Magnification 2×.)

ing. However, several dozen other specimens with similar surfaces and burn-ups have not burned but have oxidized slowly in a normal manner; thus at present it is possible to predict from the appearance of a specimen only that it could ignite. Based on the information obtained thus far, there appears to be a critical time for any specimen of this type of material, after exposure to air, when it is most apt to ignite.

This critical time is largely dependent on the mass of the specimen. If the specimen survives this period without igniting, the chances are that it will then slowly oxidize in the same manner

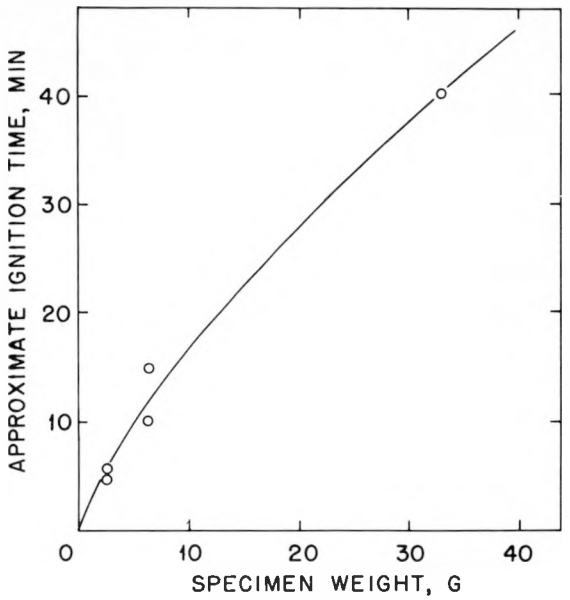

Fig. 6 — Dependence of ignition time on specimen weight.

as unirradiated fuel. Specimens of this nature can be handled safely if they are always under surveillance when exposed to air. If one does ignite, there is a period of several seconds after the specimen has begun to glow during which it can be moved to auxiliary ventilation or covered with sand before it begins to disintegrate.

REFERENCE

1. J. H. Kittel and P. Tedeschi, A Capsule Design for Experimental High-flux Irradiation of Fuel Materials, Report ANL-4900, Oct. 6, 1952.

ABOUT THE AUTHOR

J. H. Kittel is an associate metallurgist in the Metallurgy Division at Argonne National Laboratory (ANL). He received the B.S. degree in metallurgical engineering in 1943 from the State College of Washington. After graduation he was employed as a metallurgical engineer in the High-temperature Materials Section of the National Advisory Committee for Aeronautics (NACA), Lewis Flight Propulsion Laboratory, until 1947, when he was employed by ANL, on loan from NACA. Returning to NACA in 1950, he rejoined the ANL staff in 1951, and since that time he has been a member of the Irradiation Effects Group in the Metallurgy Division.

EDITORIAL POLICY AND SUGGESTIONS TO CONTRIBUTORS

Nuclear Science and Technology publishes research and development papers of the type which would appear in the established scientific and engineering journals were they not classified. The circulation of the journal to persons who may receive this classified information is over 1000, and its readers are estimated to number over 5000. Engineers and scientists who publish in the journal are thus assured of a large and critical group of readers for their papers.

In the interest of those planning to submit papers, it is advisable to summarize existing editorial policies with regard to the various types of articles that are acceptable for publication. These are described in the following paragraphs.

ARTICLES

The editors endeavor to supply in each issue a balance of review articles and articles reporting new results and presenting new ideas. Classified papers in any field of interest to the atomic energy program are acceptable, with emphasis placed on physics, chemistry, chemical engineering, and metallurgy.

Review Articles. Reviews of given subjects or a phase of a particular development are encouraged and are published as review articles in *Nuclear Science and Technology*. Such reviews serve to collect and summarize results that would otherwise be available only by an extensive search of the classified literature.

New Results. The desirability of reporting new results of a specific research problem in the journal should be emphasized. Acceptable articles may be either condensed versions of very detailed reports or a reporting of results that have not been disseminated elsewhere. This category may include results that have received only cursory inclusion in quarterly reports or information that will later be published in greater detail in laboratory reports. Articles reporting theoretical studies, as well as the results of research and development projects, are acceptable.

Arguments and New Ideas. Readers are encouraged to use the journal as the medium: (1) for exchanging new ideas, (2) for stimulating thought by airing personal opinions, (3) for pointing out discrepancies in data, (4) for presenting the arguments for or against controversial issues, and (5) for the early dissemination of partially developed ideas.

TECHNICAL NOTES

This department includes short articles on specific techniques, new measurements, gadgets, or ideas. These notes will be accepted essentially as written (or will be rejected *in toto*) by the editorial staff. Emphasis is on an informal and speedy presentation of information which is not extensive enough for an article.

REACTOR FUTURES

The department of the journal entitled "Reactor Futures" has been established as a medium for the presentation of new and novel reactor systems, technical features associated with reactors, or new ways to utilize atomic energy. Readers are encouraged to present for consideration new schemes, ideas, concepts, designs, or studies in an informal way. Contributions will be considered for publication even though somewhat fragmentary in nature and not subjected to rigorous examination. Old project

ideas should be reexamined in light of new knowledge and new interest of recent years. The editors feel sure that, to date, the response to and use of the Reactor Futures department have not been indicative of the productivity of project personnel with regard to potential future reactor ideas.

LETTERS TO THE EDITORS

"Letters to the Editors" are used: (1) to present brief technical items, (2) to criticize or commend articles in the journal, (3) to report on classified and other meetings covering nuclear technology, and (4) to make the wants of individual readers known. Such letters will be accepted and published as received or will be rejected entirely, depending upon the decision of the editors.

BUILDING REACTORS, CHEMICAL PLANTS, ETC.

Various phases in the construction of major reactor, chemical-processing, and other installations are presented in a series of actual on-the-spot photographs. Readers are invited to indicate their interest in possibilities for future "picture stories" of this kind.

MATERIAL NOT ACCEPTABLE

The following types of material are not acceptable for publication:

1. Classified documents that have been given project-wide distribution, either as reports or as part of a single quarterly report almost identical in context to the submitted paper, if such distribution has occurred prior to, or almost simultaneously with, the publication of the journal.
2. Classified documents that will be declassified at about the time of publication.
3. Unclassified information.
4. Sensitive information, i.e., information from which actual or projected production costs or production rates can be derived is normally distributed on a need-to-know basis only and cannot be included in journal articles. Also, manuscripts on weapons development and technology, as well as related subjects having a security sensitivity such as to prevent wide distribution, are not acceptable. In fact, all contributions are carefully examined and reviewed for such information.

DEADLINES FOR SUBMISSION OF ARTICLES

With a four month's lead time (processing time) for articles, the deadlines for receipt of the manuscripts must be honored. Manuscripts received after the deadlines indicated will automatically be scheduled for the following issue.

The deadline for manuscripts to be published as articles is the first day of even-numbered months (with publication scheduled the first day of the even-numbered month four months later).

The deadline for Technical Notes and Reactor Futures is three weeks later than the date specified for articles. Letters to the Editors may be received up to six weeks after the deadline date for articles.

Manuscripts should be addressed to:

J. A. Lane
Oak Ridge National Laboratory
Post Office Box P
Oak Ridge, Tennessee
Attention: Code NST

PREPARATION OF MANUSCRIPT

In order to ensure the best possible quality in the ultimate appearance of the material in the journal, contributors are requested to submit manuscript that is (1) clean and entirely legible and (2) complete in every detail. If the manuscript can be read easily by the production editors, compositors, and make-up personnel, a saving of processing time—and expense—will be effected. The complete contribution to the journal should contain the following:

1. Original and three copies of the manuscript.
2. Original illustrations (linens, glossy photographs, etc.).
3. Abstract of not more than 200 words.
4. Author's laboratory address.
5. Brief biographical sketch of the author.

In the following paragraphs suggestions are given which, if followed, will contribute materially to the expeditious processing of the journal.

Typing. The textual material (abstract, body of the paper, tabular material, and references) should be typewritten double spaced with wide

margins on a durable white paper. Each page should be numbered, and the main and subordinate headings should be numbered.

Equations. In complicated mathematical expressions care should be used to distinguish between zero (0) and the capital letter (O), the number (1) and the letter (l), the degree sign (°) and the lower-case letter (o), the letter (x) and the times sign (×), and Greek and English letters of similar form (τ, t, X, χ). Distinctions should be made between the lower-case and capital form of the same letter, e.g., S(s) and X(x). Subscripts and superscripts should be clearly marked. All symbols should be defined in text. The solidus (/) should be used for all fractions that are run into the line of text. Built-up fractions should be used in equations that stand alone. Enclosures are usually assigned thus: ( ), [ ], {}. If more than three are needed, the sequence is repeated in a larger size. However, there are exceptions to this rule, e.g., functions, crystal indices, etc. These exceptions should be noted. Centered dots and times signs used for scalar and vector products, respectively, should be identified. The abbreviations ln ($\log_e$) and log ($\log_{10}$) should be followed consistently.

References. The bibliographical references throughout the text should be designated by superscript numbers, and the references should be grouped at the end of the article, numbered consecutively. The preferred form is: author's surname with forename or initials, title or work cited, facts of publication (including date), and page number or numbers. *Chemical Abstracts* should be followed for journal abbreviations.

Tables. Tables should be numbered consecutively and references to each cited in numerical sequence in text. All tables should be given a caption; it is also preferred that all columns be given a heading along with the appropriate unit of measurement, if one is needed. Symbols are acceptable as column heads, provided they have been defined in text.

Illustrations. All photographs should be clear glossy black and white prints (not photostats) with good detail, preferably 8 by 10 in. in size. They should be unmounted and identified by figure number and classification on the reverse side. Labels and call-outs should be indicated on tissue overlay, using extremely light pressure on the overlay to prevent indention on the photograph which may reproduce. Never use cellulose tape to fasten overlays in place, and never roll photographs for mailing.

Line drawings must be in black ink on white paper or tracing cloth. If possible, these should be either 4 or $8\frac{3}{8}$ in. wide and not more than $9\frac{3}{4}$ in. high. Whenever possible, illustrations should stand vertically on the page. On full-page illustrations, allow space for printing the figure legend. Lettering should be all capital, Gothic style, of such size that when reduced 25 per cent it will be about $\frac{1}{16}$ in. high. For example, drawings prepared in the widths mentioned above should be lettered with a No. 100 Leroy Guide using a 00 pen. If in doubt, leave lettering for Technical Information Service at Oak Ridge to perform. Legends should be supplied with all figures. Never fold line drawings for mailing.